Aalto University
School of Chemical
Technology

School of Chemical Technology
Degree Programme of Chemical Technology

Fanny Henriksson

EFFECT OF IMPURITIES ON HYDROGENATION OF CO_2

Master's thesis for the degree of Master of Science in Technology submitted for inspection, Espoo, 30 September, 2016.

Supervisor **Professor Ville Alopaeus**

Instructor **D.Sc. Matti Reinikainen**

D.Sc. Reetta Karinen

Aalto University
School of Chemical
Technology

Aalto University, P.O. BOX 11000, 00076 AALTO
www.aalto.fi

Abstract of master's thesis

Author Fanny Henriksson

Title of thesis Effect of impurities on hydrogenation of CO_2

Department Department of Biotechnology and Chemical Technology

Professorship Industrial Chemistry **Code of professorship** KE-40

Thesis supervisor Professor Ville Alopaeus

Thesis advisor(s) / Thesis examiner(s) D.Sc. Matti Reinikainen, D.Sc. Reetta Karinen

Date 30.9.2016 **Number of pages** 85+8 **Language** English

Abstract

The literature survey of this thesis deals with capture and separation technologies for CO_2, impurities found in industrial CO_2 streams and impurity effect on CO_2 hydrogenation catalysts. In addition, impurities originating from CO_2 separation have been discussed. The experimental part studied the effect of impurities on four different CO_2 hydrogenation catalysts by temperature programmed desorption (TPD) and reaction tests in a fixed bed plug flow reactor (PFR). The catalysts studied were two in-house Fe-based FT catalysts (one impregnated and one precipitated), a commercial Ni-based methanation catalyst and a commercial Cu-based methanol synthesis catalyst. Special emphasis was given to studying the effects of monoethanolamine (MEA), a commonly used absorbent for CO_2 separation, and hydrogen sulphide (H_2S) on the catalysts. MEA was chosen due to a lack of earlier research on the effects of MEA on catalytic processes, while H_2S was chosen as it is a typical catalyst poison and a common impurity in separated CO_2. Furthermore, previous researches studying the effect of H_2S on catalytic processes have been rather contradictory.

The effect of MEA was studied by pulse reaction experiments in the TPD apparatus with a constant H_2 flow by pulsing CO_2 and following the formation of methane. During poisoning experiments, the concentration of MEA in the carrier gas was approximately 570 ppm. Interestingly, the CH_4 formation increased after MEA poisoning for precipitated in-house catalyst 100Fe/4.6Si/2.0Cu/1.5K (atomic ratio composition) and commercial CuO/ZnO catalyst. The reason for increase in CH_4 formation is proposed to be a modification in selectivity of the catalysts caused by MEA and its degradation products. For the other studied catalysts, the formation of CH_4 was drastically decreased during MEA poisoning without catalyst recovery. For the precipitated in-house catalyst 5Fe/5Mn/Al_2O_3 (weight ratio composition), the formation of CH_4 was decreased by 61% without catalyst recovery. It is suggested that MEA's degradation products, e.g. NO_x, oxidizes the active carbide sites on the catalyst to inactive magnetite.

The effect of H_2S on catalysts was studied in TPD and reaction tests in PFR. However, the TPD tests were only indicative and thus the PFR tests were considered to be more reliable. The CuO/ZnO catalyst maintained its activity surprisingly well. After 60 ppm H_2S poisoning the catalyst recovered almost completely (initial conversion 17.5% compared to 15.6% during recovery). However, during the poisonings the selectivity of CO was increased on the expense of methanol. The impregnated Fe catalyst deactivated completely at 30 ppm, while the precipitated Fe catalyst recovered from 1 ppm H_2S, but deactivated completely at 60 ppm. However, the selectivity of the catalyst remained unaffected.

Keywords CO_2 hydrogenation, CO_2 utilization, catalysis, Fischer-Tropsch synthesis, methanol synthesis, H_2S, monoethanolamine, MEA, catalyst poisoning, TPD, PFR

Aalto-universitetet
Högskolan för
kemiteknik

Aalto-universitetet, PB 11000, 00076 AALTO
www.aalto.fi

Sammandrag av diplomarbetet

Författare Fanny Henriksson

Titel Föroreningars inverkan på CO_2 hydrering

Institution Högskolan för kemiteknik

Professur Teknisk kemi **Kod för professuren** KE-40

Övervakare Professor Ville Alopaeus

Handledare / Granskare TkD Matti Reinikainen, TkD Reetta Karinen

Datum 30.9.2016 **Sidantal** 85+8 **Språk** Engelska

Sammandrag

Diplomarbetets litteraturdel har undersökt CO_2 avskiljnings- och separeringstekniker, förekomsten av föroreningar i industriströmmar samt föroreningarnas inverkan på CO_2 hydrering. Dessutom har föroreningar som härstammar från CO_2 separering diskuterats. I arbetets experimentella del har föroreningars inverkan på fyra olika katalysatorer (en kommersiell Ni-, en kommersiell Cu- samt två interna Fe-katalysatorer, varav en var impregnerad och en utfälld) undersökts. Den experimentella delen bestod av TPD-test (*Temperature Programmed Desorption*) och reaktionstest i en packad bädd tubreaktor. Inverkan av svavelväte (H_2S) och monoetanolamin (MEA), som är en vanlig absorbent i separering av CO_2, undersöktes. Valet att studera MEA berodde på brist av tidigare utförda studier i ämnet, medan H_2S valdes eftersom det är ett typiskt katalysatorgift och en vanligt förekommande förorening i separerad CO_2. Dessutom är tidigare forskningar i H_2S:s inverkan på katalytiska processer något motstridiga.

MEA:s inverkan på katalysatorerna undersöktes genom pulsreaktionsexperiment, där CO_2 pulserades med ett konstant väteflöde. Därmed följdes mängden producerad metan upp. MEA-halten i bärgasen var under förgiftningsexperimenten ca 570 ppm. Under MEA-förgiftningen för den utfällda 100Fe/4.6Si/2.0Cu/1.5K-katalysatorn (komposition enligt atomförhållande) och den kommersiella CuO/ZnO-katalysatorn producerades intressant nog mer metan i jämförelse med före förgiftningen. Orsaken till detta föreslås vara att MEA eller dess sönderfallsprodukter leder till modifiering i katalysatorns selektivitet. För de övriga katalysatorerna hade MEA en negativ inverkan på CH_4 formation, från vilken katalysatorn inte återhämtade sig. Den impregnerade 5Fe/5Fe/Al_2O_3-katalysatorn (komposition enligt viktförhållande) förlorade 61 % av sin aktivitet under MEA-förgiftning och återhämtades inte. Orsaken tros vara att MEA:s sönderfallsprodukter, t.ex. NO_x, oxiderar aktiv karbid till inaktiv magnetit, vilket leder till att aktiva säten på katalysatorn förlorades.

Svavelvätes inverkan på katalysatorerna undersöktes i TPD- och tubreaktorstesten. TPD-resultaten var endast antydande och därför sattes större vikt vid resultaten från reaktionstesten i tubreaktorn. CuO/ZnO-katalysatorn upprätthöll sin aktivitet förvånande väl under förgiftningen av H_2S. Efter att ha utsatts för 60 ppm återhämtades katalysatorn nästan fullständigt (jämför konversion 17.5% före förgiftning med 15.6% efter förgiftning). Dock förändrades katalysatorns selektivitet under förgiftningsstadierna genom att öka CO-selektiviten på bekostnad av metanolselektiviten. Den impregnerade Fe-katalysatorn deaktiverades av 30 ppm, medan den utfällda Fe-katalysatorn återhämtade sig från 1ppm:s förgiftning, men deaktiverades av 60 ppm.

Nyckelord CO_2 hydrering, CO_2 utnyttjande, katalys, Fischer-Tropsch-syntesen, metanolsyntesen, H_2S, monoetanolamin, MEA, förgifting av katalysatorer, TPD, PFR

Preface

The master's thesis has been conducted from March 2016 to September 2016 at VTT Technical Research Centre of Finland for the Neo-Carbon project.

I wish to thank Pekka Simell for giving me the opportunity to write my master's thesis at VTT. I thank especially Matti Reinikainen who has selflessly given me excellent guiding and support throughout this process. I am also very grateful for all the input and comments from professor Ville Alopaeus, Reetta Karinen and Juha Lehtonen. I also extend my deepest of gratitude towards all my colleagues at VTT who have helped me with everything from lab guidance to Excel assistance. It has been a joy working with you! And last but not least, I would like to thank my friends and family, for supporting and encouraging me not only during this project, but throughout my studies as well.

Espoo, September 30, 2016

Fanny Henriksson

Table of contents

Nomenclature

Abbreviations

AGR	Acid Gas Removal
ASU	Air Separation Unit
BET	Brunauer-Emmett-Teller isotherm
CCS	Carbon Capture and Storage
CCUS	Carbon Capture, Utilization and Storage
COFs	Covalent organic frameworks
DeNOx	Denitrogenation of flue-gas
DMEA	Dimethylethanolamine
DMDS	Dimethyl disulphide
DMS	Dimethyl sulphide
FGD	Flue-gas desulphurization
FID	Flame ionization detector
FT	Fischer-Tropsch
FTS	Fischer-Tropsch synthesis
GC	Gas Chromatograph
GSTC	Gasification & Syngas Technologies Council
HRST	Heat Recovery Steam Generator
IGCC	Integrated gasification cycle
MEA	Monoethanolamine
MeSH	Methyl mercaptan
MFC	Mass flow controller
MOFs	Metal-organic frameworks
PFR	Plug flow reactor
PG	Poisoning gas
ppbv	parts per billion by volume
ppbw	parts per billion by weight

ppm	parts per million
ppmv	parts per million by volume
ppmw	parts per million by weight
PSA	Pressure swing adsorption
RG	Reactant gas
RWGS	Reverse water-gas shift
TCD	Thermal conductivity detector
TIC	Temperature Indicator and Controller
TPD	Temperature programmed desorption
TRS	Total reduced sulphur
TSA	Temperature swing adsorption
UCG	Underground coal gasification
VSA	Vacuum swing adsorption
WGS	Water-gas shift
WHSV	Weight hourly space velocity
WWTP	Wastewater treatment plant
XANES	X-ray absorption near edge structure
XPS	X-ray photoelectron spectroscopy
XRD	X-ray diffraction

Symbols

A	Peak area
C	Concentration [ppm]
ΔH	Enthalpy [kJ/mol]
I	Ion current [A]
M	Molar mass [g/mol]
m	Mass (g and µg)

$\dot{m}$	Mass flow [g/dm^3]
N	Amount of carbon atoms
n	Moles [mol, mmol or µmol]
$\dot{n}$	Molar flow [mmol/h]
p	Pressure [bar]
ρ	Density [g/dm^3]
RF	Response factor
S	Selectivity [%]
T	Temperature [^{o}C]
T.o.s.	Time on stream [h]
V	Volume [dm^3 or cm^3]
$\dot{V}$	Volume flow [dm^3/h]
V_m	Molar volume [dm^3/mol]
V%	Volume percentage [vol-%]
WHSV	Weight hourly space velocity [1/h]
X	Conversion [%]
Y	Yield [%]

Subscripts

0	Inlet conditions
i	Component index
meas	Measured condition
OUT	Outlet
tot	Total

1 Introduction

The increase in global temperatures is already an accepted reality. One of the main reasons to the threat of climate change is the increased level of carbon dioxide (CO_2) in the atmosphere. The concentration of CO_2 in the atmosphere has climbed from 280 ppm before the industrialization to 390 ppm in 2010. The concentration is predicted to increase even further to 570 ppm in the end of the century (Xu & Moulijn 1996). Therefore, reducing CO_2 emissions is a top priority if climate change is to be stopped.

This master's thesis will focus on utilizing CO_2 that can be captured from industrial sources. Figure 1 illustrates the principals of CO_2 utilization by hydrogenation of CO_2. Thus, CO_2 can be captured from industrial sources and separated from flue gas. The separated CO_2 gas is then purified and utilized by e.g. hydrogenation of CO_2, which through catalytic processes produces products such as methanol, methane and Fischer-Tropsch (FT) products which can be used as fuels (Wang et al. 2011). When the fuels are burned they emit CO_2, which then again can be captured.

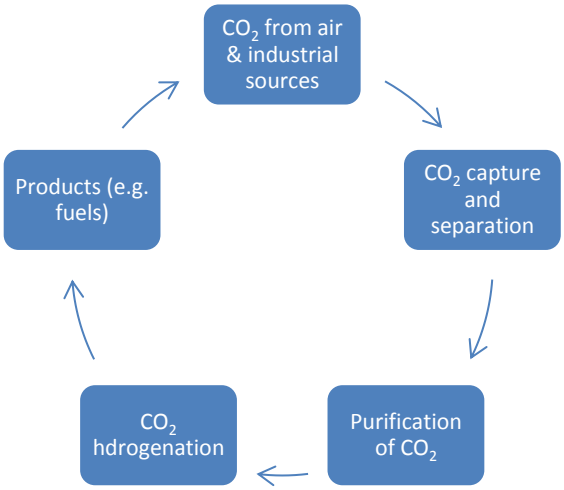

Figure 1. CO_2 utilization by hydrogenation of CO_2.

The purification step is a costly and demanding process, and therefore some contaminants are expected to remain in the purified CO_2 stream. Even small concentrations of e.g. hydrogen sulphide (H_2S) have been shown to deactivate catalysts completely (Ma et al. 2016). Thus, to be able to rely on utilizing captured CO_2 in the

future, the real effects of all contaminants present in CO_2 streams must be fully known. Therefore, this thesis will focus on studying the effect of impurities in CO_2 hydrogenation and its catalysts.

A commonly used method for separating carbon dioxide from flue gas is by absorbing carbon dioxide to a solvent, typically monoethanolamine (MEA) (Rochelle 2009). Studies covering the effect of MEA on catalytic processes are lacking, and thus will this thesis give special emphasis to studying the effect of MEA on CO_2 hydrogenation catalysts. Special emphasis will also be given to hydrogen sulphide, which has been vastly discussed in several studies as it is a typical catalyst poison and common impurity in syngas. However, some studies are quite contradictory and in order to understand its full effect on catalysts, further studies are required. The aim of the thesis is thus to find out 1) whether MEA is affecting CO_2 hydrogenation and its catalysts and 2) what kind of effects MEA and different poisoning levels of H_2S has on the catalysts.

LITERATURE REVIEW

2 CO_2 capture and separation technologies

The removal of carbon dioxide from the gaseous streams can be managed by several different separation methods. The most researched methods include absorption, adsorption, membrane separation and cryogenic distillation, from which absorption is the most common industrially used method. All approaches are shortly presented below.

2.1 Absorption

Absorption is the most commonly used carbon dioxide separation technology in industries. In this method, the flue gas is generally cooled down and led to the absorber column (scrubber) where CO_2 is absorbed in the solvent. The solvent-CO_2 solution is then fed into a heater and a stripper column, where CO_2 is released and the solvent is regenerated (Gupta et al. 2003). This method can be further divided into a) chemical absorption and b) physical absorption.

In chemical absorption, CO_2 is chemically reacting with the liquid solvent. Typically amines, such as monoethanolamine (MEA) and dimethylethanolamine (DMEA) (Rochelle 2009), are used in chemical absorption. Figure 2 presents a typical amine scrubbing system for CO_2 capture. In the model presented by Yeh et al. (2001), CO_2 is recovered from a flue gas originating from a fossil fuel power plant. The flue gas is cooled down before entering the absorption chamber, where CO_2 is selectively absorbed in MEA at a temperature between 38 ^{o}C and 50 ^{o}C. After the absorption, the CO_2-MEA solution is passed through a heat exchanger and into the regenerator where it is heated to desorb CO_2. If pressure is involved in the process, it is lowered at the regenerator in order to enhance desorption of CO_2. MEA is then pumped back to the absorber for reuse while the captured CO_2 is led to a flash chamber where contaminants are removed. Absorption of CO_2 by amine scrubbing is considered the most suitable option for CO_2 removal from flue gases when the CO_2 concentration is between 5 and 15 vol-% (Walspurger & Dijk 2012).

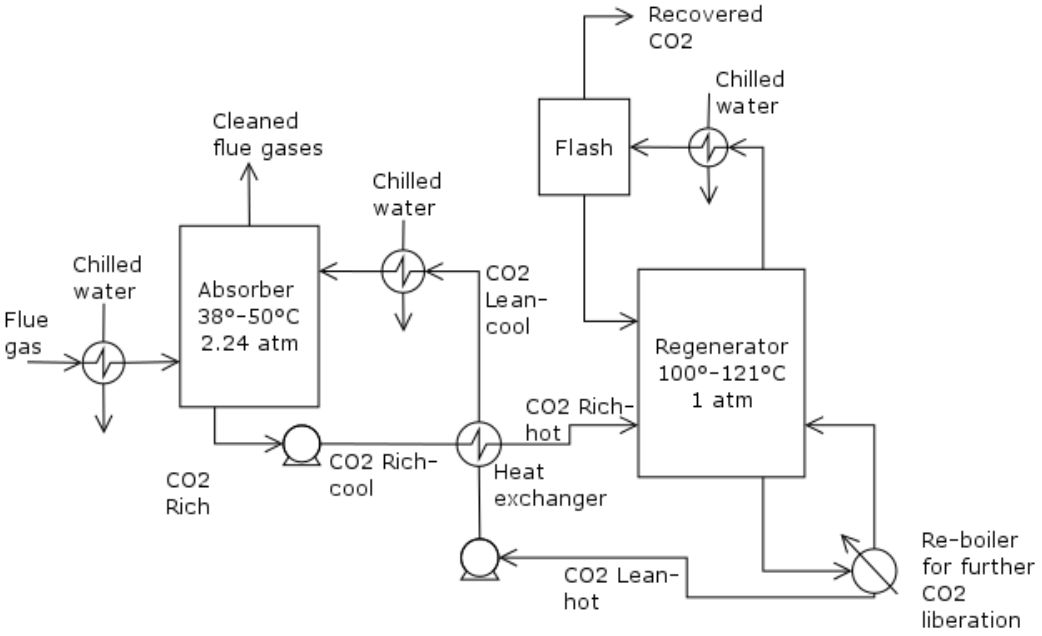

Figure 2. Typical chemical absorption system based by the model of Yeh et al. (2001).

In physical absorption, the solvent only interacts physically with CO_2, i.e. CO_2 is dissolved in the absorbent. An example of a physical absorbent is methanol in the Rectisol® process (Kargari & Takht Ravanchi 2012). The Rectisol® process removes H_2S, CO_2 and other trace contaminants from a gas stream by physically absorbing them to methanol. By lowering the pressure, CO_2, H_2S and the other contaminants are released from methanol, which is regenerated for reuse simultaneously (White et al. 2003). Rectisol is the preferred purification process for coal, heavy oils and waste gas produced by gasification. Another examples of a physical absorbent is the mixture of dimethyl ethers of polyethylene glycol in the Selexol™ process (White et al. 2003).

2.2 Adsorption

CO_2 can be separated by adsorbing the compound on a solid sorbent. In chemical adsorption CO_2 is adsorbed by a chemical reaction on the surface of the sorbent. For example metal oxides, such as CaO and MgO, can be used for this purpose. In physical adsorption carbon dioxide is attached to the sorbent by weak van der Waals' forces. Sorbents used are typically activated carbon, zeolites or molecular sieves. (Li et al. 2013; Songolzadeh et al. 2014)

The regeneration strategies include pressure swing adsorption (PSA), temperature swing adsorption (TSA) and vacuum swing adsorption (VSA). In PSA, CO_2 is adsorbed from the gas mixture on the solid adsorbent at a relatively high pressure in a packed column. The adsorbed CO_2 is then desorbed by lowering the pressure, and the sorbent can thus be reused (Sircar 2002). TSA and VSA function in similar approaches, but are relying on a shift in temperature (TSA) and by swinging to vacuum pressure (VSA).

2.3 Membrane separation

Separating carbon dioxide by membrane technology is an attractive concept considering the fact that it is a continuous, steady-state process, which would be ideal as an energy saving approach for CO_2 capturing. The membrane works as a selective barrier, which allows CO_2 in the gas stream to pass through the membrane faster than other components. The driving force of gas separation is related to partial pressure of the component (Walspurger & Dijk 2012). Hence, membrane separation is most suited for CO_2-gas streams at higher concentrations (above 10 vol-%) and at higher pressures (Songolzadeh et al. 2014). This makes membrane separation unsuitable for e.g. post combustion (further discussed in section 3.1), due to the low partial pressure of CO_2. The performance of the membrane is dependent on two characteristics; a) permeability, which is the flux of a specific gas through the membrane and b) selectivity, which is the preference on gas species that the membrane passes through (Scholes et al. 2009). The major disadvantage with membrane technology for CO_2 separation is the lack of membranes with simultaneous high permeability and selectivity. (Songolzadeh et al. 2014; Kargari & Takht Ravanchi 2012)

There are various types of different membranes used for separation of gases, including polymeric-, ceramic-, metallic- and gas absorption membranes. Polymeric membranes are interacting with the target molecule, and allow it to diffuse across the membrane, thus separating it from the remaining compounds. Ceramic and metallic membranes are porous, and the principle is based on that only a certain size of molecules is able to pass through the pores. Finally, gas absorption membranes are solid microporous membranes that are impregnated with a liquid absorbent. The molecule being separated diffuses over the membrane, followed by being trapped and removed by the liquid solvent. (Aaron & Tsouris 2005)

2.4 Cryogenic separation

Carbon dioxide can be separated from a gas mixture at low temperatures. This mechanism is called cryogenic separation, and it enables direct production of liquid CO_2, which is an advantage for e.g. transportation (Xu et al. 2014). However, cryogenic separation is limited to gaseous streams with an already high CO_2 concentration, with a preferred concentration of over 90 vol-%. Cryogenic separation is most suitable to be implemented for high-pressure gaseous streams, such as streams obtained from pre- and oxy-fuel combustion. This technology requires an excessive amount of energy for refrigeration, and additionally compounds such as water and heavy hydrocarbons need to be removed from the stream prior to cooling in order to avoid freezing and blockage of heat exchanges. (Kargari & Takht Ravanchi 2012)

3 Impurities in industrial CO_2 streams

The amount and type of impurity in separated CO_2 streams is mainly dependent on the source, combustion capture technology and separation technology. The sequestrated CO_2 can be further used in several different industries and products such as fire extinguishing systems, food industry, enhanced oil recovery and alkaline water treatment (Last & Schmick 2011). Therefore, the purification quality of the CO_2 stream is highly dependent on the end use.

This chapter focuses on impurities found in industrial CO_2 streams with special emphasis on the use of CO_2 in catalytic processes. In sections 3.1-3.4 compositions of CO_2 streams from different sources are presented. In addition, section 3.5 examines impurities that originate from the separation process itself. Notable impurities present in most streams are carbon monoxide (CO), hydrogen sulphide (H_2S), nitrogen oxides (NO_x) and sulphur dioxide (SO_2). Sass et al. (2005) presented possible trace level impurities present in CO_2 streams by source types (Table 1).

Table 1. Possible trace level impurities in CO_2 source streams by source type. Table adapted from Sass et al. (2005).

Component	Combustion	Fermentation	Hydrogen/ Ammonia	Coal Gasification
Aldehydes	X	X	X	X
Amines	X		X	
Benzene (C_6H_6)	X	X	X	X
Carbon monoxide (CO)	X	X	X	X
Carbonyl sulfide (COS)		X	X	X
Cycloaliphatic hydrocarbons	X		X	X
Dimethyl sulfide ($(CH_3)_2S$)		X		X
Ethanol	X	X	X	X
Ether		X	X	X
Ethyl acetate ($CH_3COOCH_2CH_3$)		X		X
Ethyl benzene ($C_6H_5CH_2CH_3$)			X	X
Ethylene oxide (C_2H_4O)				X
Halocarbons	X			X
Hydrogen cyanide (HCN)	X			X
Hydrogen sulfide (H_2S)	X	X	X	X
Ketones	X	X	X	X
Thiols	X	X	X	X
Mercury	X			X
Nitrogen oxide (NO_x)	X	X	X	X
Sulphur dioxide (SO_2)	X	X	X	X
Toluene (C_7H_8)		X	X	X
Vinyl chloride (C_2H_3Cl)	X			X
Volatile hydrocarbons	X	X	X	X
Xylene ($C_6H_4C_2H_6$)		X	X	X

3.1 Combustion processes

In order to capture CO_2 from flue and fuel gas, three different combustion principles can be applied. These carbon capturing processes are called post-, pre- and oxy-fuel combustion, and are presented in Figure 3, which is a modification of a model presented by Thiruvenkatachari et al. (2009). In post combustion technologies, the fuel is burned for energy conversion, followed by a CO_2 separation from the flue gas. In pre combustion processes sources of carbon are separated prior to the burning of the fuel. By gasifying the fuel, a CO and H_2 rich syngas is produced, followed by a catalytic shift reactor, which converts CO to CO_2. The carbon is then separated from the mixture and

H_2 is burned for energy purposes. In oxy-fuel combustion, oxygen is first separated from air by an air separation unit (ASU), whereupon the fuel is burned in an oxygen rich environment, resulting in an exhaust gas that is almost pure CO_2. (Lin et al. 2010; Kargari & Takht Ravanchi 2012)

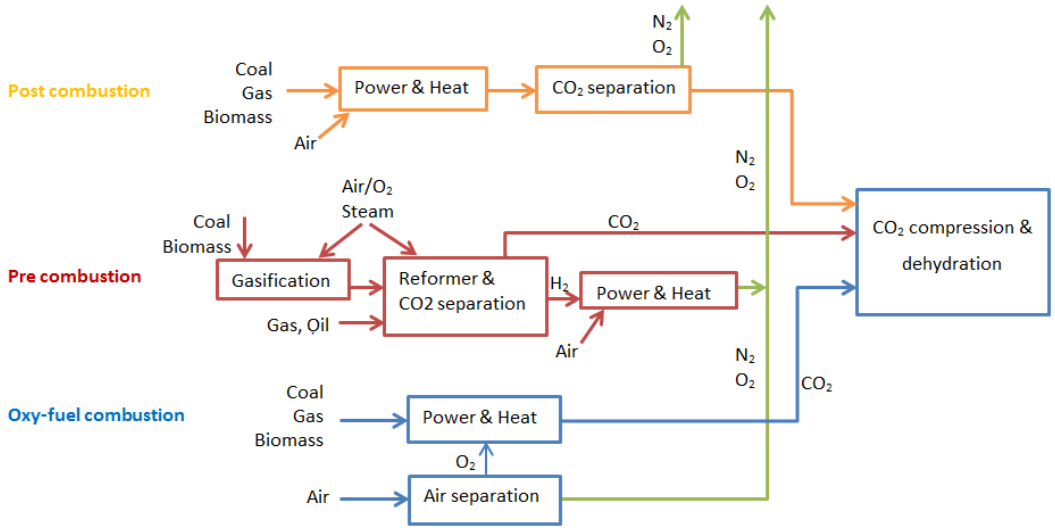

Figure 3. Three basic routes of CO_2 capture based upon Kargari & Ravanchis (2011) model.

The advantage of post combustion is that it can be implemented on already running facilities. For this reason, it has been the most researched of the above mentioned technologies. Nevertheless, in post combustion processes, the treatment stream has been diluted by combustion air, which results in higher cost for separation. The advantage of pre- and oxy-fuel combustion is that the gas stream has a higher concentration of CO_2, which is beneficial in further separation (see section 2) of CO_2. The oxy-fuel combustion technology produces a nearly pure CO_2 stream, thereby often avoiding the need for further CO_2 separation. However, the separation of oxygen from air is an energy demanding process, which drastically increases the costs. The pre combustion technology produces a stream with a CO_2 content of 15-40 vol-%. (Last & Schmick 2011; Feron & Hendriks 2005; Kargari & Takht Ravanchi 2012)

Combustion processes are by far the most significant and widely used source from where CO_2 streams can be separated, due to the fact that combustion of fossil fuels and biomass are extensively used for power generation. As mentioned earlier, pre- and oxy-fuel combustion result in higher CO_2 containing streams, while post combustion streams

have a lower concentration of CO_2. Usually streams from post combustion tend to generate a flue gas where the CO_2 concentration is as low as 10-15% (Last & Schmick 2011). The major impurities originating from combustion processes include SO_2, NO_x and H_2O. Compounds originating from air (i.e. N_2, O_2 and Ar) are considered inert in the sense of separation techniques by some authors. Nevertheless, high levels of especially oxygen can still result in unwanted reactions. Thus, the air originating compounds are still considered as impurities in CO_2 streams.

As indicated earlier, the impurities in the separated stream are highly dependent on the raw material. As an example, coal is not purely consisting of hydrocarbons, but comprises heteroatoms and inorganic compounds as well (Drage et al. 2012). Therefore, the gas from the combustion will include a range of gaseous and solid components. The composition of the flue gas will also differ based on the location of flue gas treatment units in the process chain. Thus, the location of e.g. the flue gas desulfurization and NOx reduction has an impact on the composition of the stream. Table 2 presents a compilation of composition of flue gas from coal and gas combustion by Drage et al. (2012). It is noted that flue gas originating from coal has a higher concentration of CO_2 (12-15%) than flue gas originating from natural gas (3-5%), since the C/H ratio of coal is considerably higher than for natural gas. The main impurities (excluding the compounds of air), are H_2O, SO_2 and NO_x. Trace impurities found in combustion processes include carbon monoxide (CO), Mercury (Hg), Arsenic (As) and particulate matter. When separating the CO_2 of the flue gas, many of the impurities will follow.

Table 2. Typical flue gas composition from coal and natural gas post combustion. The values are quoted as vol-% unless otherwise stated. Table adapted from (Drage et al. 2012).

Component	Coal[a] (no FGD/DeNO$_x$)	Coal (after FGD/DeNO$_x$)	Natural Gas
N_2	75-80%	75-80%	74-80%
CO_2	12-15%	12-15%	3-5%
SO_2	1800 ppm	10-70 ppm	<10 ppm
NO_x	500 ppm	50-100 ppm	50 ppm
H_2O	5-7%	5-14%[b]	7-10%
O_2	3-4%	3-4%	12-15%
CO	<100 ppm[c]	<100 ppm[c]	<5 ppm
Hg/As	ppb	ppb	0
Particulates	10-20 mg/Nm^3	10-20 mg/Nm^3	not present

FGD= Flue-gas Desulphurization. DeNOx= Denitrogenation of flue-gas.
[a]Based on a medium to high sulfur coal. [b]The moisture content of post FGD flue gas will depend on whether a wet or dry technology is used. Wet FGDs typically produce a flue gas at outlet with between 10-14 vol-% H_2O. [c]Occasionally 5000 ppm.

Porter et al. (2015) classified impurities in three different categories (see Table 3) based on their origin; i) fuel oxidation, ii) excess oxidant/air ingress and iii) process fluids. Impurities originating from fuel oxidation are the complete or partial oxidation products of e.g. coal and biomass. The partial oxidation products (e.g. CO, COS) arise from fuel-rich conditions. Other impurities belonging to this category are volatiles, trace metals and particulates. Volatile compounds, such as hydrogen and light hydrocarbons originate from fuel devolatilization, while trace metals in the fuel may be released on combustion and end up in the CO_2 stream. The second category; excess oxidant and air ingress impurities include oxygen, nitrogen and argon, which are considered as non-condensable species (or as inert compounds in the sense of separation technique). The final category is impurities from process fluids, which are the species used for separation of CO_2. This will be further discussed in section 3. Commonly used process fluids are monoethanolamine (MEA) and Selexol™ solvent, which is a mixture of dimethyl ethers of polyethylene glycol. All categories of impurities are presented in Table 3. (Porter et al. 2015)

Table 3. Classes of potential impurities by origin (adapted from Porter et al. 2015).

Fuel oxidation	Complete oxidation	H_2O, SO_x, NO_x, HCl, HF
	Partial oxidation	CO, H_2S, COS, NH_3, HCN
	Volatiles	H_2, CH_4, C_2H_6, C_3+
	Trace metals	Hg ($HgCl_2$), Pb, Se, As, etc.
	Biomass alkali metals	KCl, NaCl, K_2SO_4, KOH, etc.
	Particulates	Ash, PAH/soot
Excess oxidant/air ingress		O_2, N_2, Ar
Process fluids		Glycol, MEA, Selexol, NH_3, etc.

In oxy-fuel combustion, the fuel is burned with oxygen instead of air, which results in higher concentrations of SO_2 and NO_x when compared to an air-coal combustion plant. This is because the total volume of the flue gas is lower (<20% of an equivalent air-coal combustion plant) when nitrogen is excluded from the combustion. However, the total amount of NO_x in oxy-fuel combustion is lower than post combustions streams, since recirculated NO_x can be reduced in the furnace. Other impurities in oxy-fuel combustion are N_2/Ar (as the ASU also lets a small amount of N_2/Ar through), O_2 (in excess to ensure a complete combustion) and H_2O. (Liu & Shao 2010)

3.2 Gasification processes

Gasification is a well-established process that is gaining increasing popularity all over the world. In 2016, more than 272 operating gasification plants are found worldwide, with another 74 plants under construction (Gasification & Syngas Technologies Council 2016b). During gasification processes, the fuel is gasified, producing a syngas mixture of CO and H_2. Before cleaning the gas mixture also contains CO_2 and other impurities. Since gasification is conducted in a controlled amount of oxidation medium, the amount of nitrogen is lower in the product gas from gasification than from combustion. The syngas can be further used for several applications. According to data provided by Gasification & Syngas Technologies Council (GSTC), the most significant application of the produced syngas is for chemicals production, followed by production of gaseous fuels, liquid fuels and power (e.g. gasification used in pre combustion, as was described in section 3.1) (Higman 2014).

The most dominant feedstock of gasification is coal. Other sources of carbonaceous material include petroleum, gas, petroleum coke, biomass and waste (Higman 2014).

There are several environmental benefits of gasification, compared to traditional combustion systems. For instance, capturing CO_2 is more efficient for gasification plants than for coal-fired power plants, since CO_2 can be captured prior to combustion. Inert materials in the gas can easily be transformed to marketable materials. Mineral materials separate from the gaseous feedstock and other inert materials (e.g. ash) melt and fall to the bottom of the gasifier. Furthermore, up to 99% of the sulphur can easily be removed and utilized, since sulphur impurities in the gas mixture are in the form of hydrogen sulphide (H_2S) and/or carbonyl sulphide (COS) and can be removed by e.g. absorption processes or a Claus process, which turns H_2S into marketable sulphur or sulfuric acid. In addition, water use is significantly lower than for other coal-based technologies. Additionally, waste can be transformed to energy and other products, which would result in a decrease of methane emissions. (Gasification & Syngas Technologies Council 2016a)

Impurities in CO_2 streams from gasification processes are highly dependent on the feedstock used (Walspurger & Dijk 2012). The preferred final separation and purification technology used with gasification is physical absorption, using processes such as Rectisol®, which is able to separate HCN, aromatics, organic sulphur and gum forming hydrocarbons from the gas. The gas composition is also highly dependent on the oxidation medium, i.e. air or oxygen. Air results in a N_2-rich gas, while oxygen produces more concentrated CO-, H_2- and CO_2-gas. This is presented in Table 4 (Oasmaa et al. 2010).

Biomass gasification is considered an environmental friendly and renewable source of energy. The cleaned syngas can be used for power or be converted to fuels, such as Fischer-Tropsch products, and several chemical products (de Jong et al. 2012). The syngas produced contain impurities such as particulates, tar, alkali metals, and nitrogen- and sulphur compounds. Table 4 presents the composition of coal and biomass gasification gases. It can be noted that gasification of coal with oxygen produces the most concentrated CO_2- and H_2 gas. (Oasmaa et al. 2010)

Table 4. Composition of coal and biomass gasification gas (adapted from Oasmaa et al. 2010).

Process	Fluidised bed (U-GAS)	Fluidised bed (Lurgi CFB)	Fluidised bed (Battelle)	Fluidised bed (VTT PDU tests)	Reformed fluidised bed gas (VTT PDU tests)
Method	Oxygen	Oxygen	Indirect	Air	Air
Fuel	Coal	Biomass	Biomass	Biomass	Biomass
CO	22.8	33.5	29	12.6	18.1
H_2	42.9	33.4	31.6	9	17.1
CO_2	29.8	26.6	23.1	10.8	7.9
H_2O	-	-	-	19.3	15.5
CH_4	3.7	4.9	13.6	3.4	0.2
Residue	0.8	1.7	2.7	44.7	41.3

Gasification processes can be combined with e.g. combustion processes. For example in pre combustion methods, gasification of the fuel is a fundamental part of the process. Pre combustion carbon capture is often combined with the integrated gasification combined cycle (IGCC). IGCC is a power generation technology where the solid raw material, e.g. biomass or coal, is partially oxidized with oxygen and steam to produce syngas mainly consisting of carbon monoxide and hydrogen. The syngas is then shifted by the WGS reaction in order to produce more concentrated CO_2 and H_2, followed by an Acid Gas Removal (AGR) unit, which captures H_2S and CO_2. The hydrogen-rich gas is then burned in gas turbine for energy generation, and the hot flue gases are used in a Heat Recovery Steam Generator (HRSG) to raise steam and simultaneously generate extra electricity. There are several benefits with IGCC plants, one being the very low SO_x, NO_x and particulate emissions (Cormos 2011). The main impurities found in CO_2 streams from IGCC processes comprise H_2O, H_2S, COS, NH_3 and the non-condensable species (N_2, O_2, Ar). (Cormos 2012)

Another example of gasification processes is underground coal gasification (UCG), which is a process where coal is gasified *in situ* underground by igniting the coal and injecting air/oxygen and water by injection wells into the coal bed. This produces a syngas that easily can be transported to ground level and be directly used as a fuel for power generation (Riet 2008). The process has been researched over the past 80 years and has several advantages compared to traditional mining. E.g. UCG is considered as a healthier, safer and more environmentally friendly solution to the conventional mining technologies. In addition, UCG reduces sulphur oxides to very low levels since roughly half of the sulphur, mercury, tar, ash and particulates from the used coal remain below grounds. Furthermore, any sulphur or metals that reach the surface are in a chemically

reduced state, which makes them relatively simple to remove (Fennerty et al. 2009). UCG can be applied to carbon capture technology, which significantly reduces the emissions of carbon dioxide. The major impurities found in separated CO_2 streams are methane (CH_4), CO, NH_3, H_2S, tar, water and particulates. (Imran et al. 2014)

By comparing the impurities found in gasification processes with combustion processes, it can be concluded that the amount of sulphur- and nitrogen oxides is reduced in streams originating from gasification processes, since oxygen is not in excess, which is the case for combustion processes. However, hydrocarbons, such as methane and tar, and H_2S are more abundant in gasification streams.

3.3 Metallurgical processes

Metallurgical processes include the manufacturing of iron and steel, which generates a large quantity of emissions, such as CO_2 and CH_4. Iron and steel manufacturing is a large industry emitter of CO_2, accountable for approximately 1% of the total amount of CO_2 emissions in the U.S. 2013 (Olivier, Jos et al. 2013; U S Environmental Protection Agency 2015). A central component in the process is metallurgical coke, which is used for reducing iron ore to iron. (Last & Schmick 2011)

The most common iron production process is the integrated steel mill. This process is based on blast furnace and basic oxygen furnace. Metallurgical coke is utilized in a blast furnace, resulting in a side product that is a CO-rich gas that can be utilized as an energy carrier on the steel mills site. The blast furnace gas is the source of the majority of the CO_2 emissions. The carbon dioxide can be captured from either the combustible process gases or flue gases coming from combustion of process gases and other fuels. Hence, the most feasible technology for carbon capturing of iron and steel processes is post combustion. (Romano et al. 2013)

The impurities in CO_2 streams captured from iron and steel plants vary significantly. Last & Schmick (2011) estimated that the composition of CO_2 gas captured from iron and steel mills are similar to those of flue gas from coal-fired power plants. Table 5 shows the estimation of impurities from captured CO_2 gas from iron and steel plants. Technologies used for recovery of CO_2 from the iron and steel production are pressure swing adsorption and alkanolamine scrubbers. Japanese JFE Steel corporation has been

able to capture relatively high CO_2 quantities (up to 70%) by a 2-stage vacuum swing process for blast furnace gas (Walspurger & Dijk 2012).

Table 5. Estimated composition of captured CO_2 gases from iron and steel plants (adapted from Last & Schmick 2011).

Component	Relative proportions in flue gas [% (v)]	Relative proportions in separated CO_2 stream without wet flue gas desulfurization scrubber [% (w)][a]	Relative proportions in separated CO_2 stream with wet flue gas desulphurization scrubber [% (w)][a]	Relative proportions in separated CO_2 stream with low NO_x burners, selective catalytic reduction and wet flue gas desulphurization scrubber[% (w)] [a]	Estimated concentrations in separated CO_2 stream, assuming amine adsorption [% (v)] [b]
CO_2	13.5	97.45	99.8	99.8	93.2
SO_2	0.016	2.3	0.12575	0.12575	Trace
SO_3	0.00325	0.0295	0.01535	0.01535	Trace
N_2	74.7				0.17
NO_2	0.0025	0.00585	0.0046	0.0046	
NO_x	0.06				Trace
HCl	0.00525	0.0422	0.000575	0.000575	
O_2	4				0.01
H_2O	7.7				6.5
Hydrocarbons	Trace [b]				Trace [b]
Metals	Trace [b]				Trace [b]
Hg (2+)	Trace	0.0000142	0.00000145	0.00000145	

[a.] Estimated values (except mercury) include both with and without salt formation. [b.] After Sass et al. (2005).

Metallurgical coke is often produced co-located with iron and steel production plants, since it is an essential part of the production of iron and steel. The coke is produced by destructive distillation of metallurgical coal in oxygen-free coke ovens until volatile components are removed.

Table 6 presents the impurities of combustion flue gas emissions from metallurgical coke production. Thus, Table 5 describes the estimated impurities from the main steel and iron production, while Table 6 describes the impurities from the indirect production, i.e. the production of metallurgical coke. (Last & Schmick 2011)

Table 6. Impurities of combustion flue gas emissions from coke production, adapted from Last & Schmick (2011). The unit is expressed as kg emissions per Mg (1000 kg) of coal charged.

Component	Emissions (kg/Mg)	Relative proportion [% (w)]
CO_2[a]	482	99,37313
SO_x[b]	1.47	0.003
NO_x	0.82	0.002
CO	0.34	0.0007
Total organic compounds	0.19	0.0004
Methane	0.1	0.0002
Volatile organic compounds	0.047	0.0001
Acetone	0.0295	0.00006
HCl[b]	0.013	0.00003
Extractable organic matter	0.012	0.00002
Benzene	0.0075	0.000016
Ethane	0.005	0.000010
Toluene	0.0033	0.000007
Chloromethane	0.0032	0.0000066
Benzoic acid	4.14E-05	0.0000001
Diethyl phthalate	9.90E-06	0.00000002
2,4-Dimethylphenol	4.17E-06	0.00000001
Bis(2-ethylhexyl)phthalate	3.40E-06	0.00000001
Phenol	2.56E-06	0.00000001

[a]Blast furnace gas. [b]Desulfurized coke oven gas.

Hence, it can be concluded that the impurities originating from metallurgical processes are similar to those from combustion processes. The main impurities in these processes are thus sulphur- and nitrogen oxides.

3.4 Biogas and biotechnical processes

Biogas is produced by anaerobic digestion of organic substrates, which include manure, sewage sludge, waste streams from food processing and energy crops. Landfill gas is biogas that is produced by anaerobic degradation in landfills (Petersson & Wellinger 2009). Biogas and landfill gas are gas-mixtures mainly comprising methane (CH_4) and CO_2. The content of energy in the gas correlates to the CH_4 concentration of the gas. Thus, by removing carbon dioxide, the energy content of the gas can be increased (Oasmaa et al. 2010). Typically landfill gas has a lower content of methane compared to biogas, and a higher content of nitrogen. Landfill gas tends to contain a great number of trace gases, which are not as present in biogases. The gas composition has great

variations, which are dependent on factors such as source (Table 7), time and weather conditions. Table 7 presents gas compositions originating from different sources. (Oasmaa et al. 2010)

Table 7. Biogas composition, adapted from Oasmaa et al. (2010).

Typical values [a]	Municipal WWTP sludge digestion	Industrial waste digestion	Animal manure digestion	Landfill gas
Methane (CH_4)	50-70%	60-80%	50-70%	45-60%
Carbon dioxide (CO_2)	30-45%	20-40%	30-50%	35-40%
Water vapour (H_2O) [b]	1-4%	1-4%	1-4%	1-2%
Hydrogen sulphide (H_2S) and total reduced sulphur (TRS)	150-3000 ppmv	Up to 30000 ppmv	Up to 5000 ppmv	10-1000 ppmv
Siloxanes (HCSi)	10 ppmv	negligible	negligible	10 ppmv
Hydrocarbons (HC)	negligible	negligible	negligible	<2500 ppmv
Halogenated hydrocarbons (HCX)	negligible	negligible	negligible	<100 ppmv
Nitrogen (N_2)	<5%	negligible	<5%	<10%
Oxygen (O_2)	<1%	negligible	<1%	<3%

[a] May be exceeded at specific sites treating unique wastes. [b] Saturated at digester temperature.

Methane, which can be obtained from biogas, can be used for heat and electricity production or as biofuel (Rasi et al. 2007). By using biogas as a fuel in vehicles, the emissions of CO_2, NO_x, hydrocarbons and CO can be drastically decreased compared to conventional gasoline and diesel engines.

Another example of biotechnical processes is the manufacturing of ethanol by fermentation, which applications include the use as a bio-fuel. By using biomass-based fuels in combination with Carbon Capture, Utilization and Storage (CCUS), it will result in a net decrease of CO_2 in the atmosphere (Feron & Hendriks 2005). Biogas and biotechnical processes have several advantages compared to traditional sources of energy. The biotechnical processes are using renewable energy sources, which can be used as substitutes for fossil fuels. In addition, use of biogas reduces the release of methane to the atmosphere. A side product from the production of biogas is a high quality digestate, which can be used as a fertilizer. (Petersson & Wellinger 2009)

Sulphur compounds, usually in the form of hydrogen sulphide (H_2S), are always present to some extent in biogases. Other compounds containing sulphur are organic sulphides, such as dimethyl sulphide (DMS) or dimethyl disulphide (DMDS), and methane thiol (methyl mercaptan, MeSH). In landfill, municipal waste and sewage digestion gases

halogenated hydrocarbons and siloxanes are usually present to some extent (Oasmaa et al. 2010). The requirements for the gas purity depend on the end use. Nevertheless, some components in the gas stream need to be removed in order to prevent corrosion (caused by water) and damage of the carbon capturing equipment (caused by e.g. sulphides). Carbon dioxide can be separated from biogas and landfill gas by several different technologies. The most widely used technologies for CO_2 separation from biogas are pressure swing adsorption and absorption technologies, such as water scrubbing, organic physical scrubbing (by Selexol™ or Genosorb®) and chemical scrubbing (by MEA or DMEA). (Petersson & Wellinger 2009)

Another biotechnical process, fermentation, is broadly used for production of fine chemicals, including amino acids, enzymes and antibiotics. These fermentation products are manufactured from starch and sugar, using feedstocks such as wheat, corn and sugarcane (de Jong et al. 2012). In addition, bio-based fuels are manufactured by fermentation. For instance ethanol, both fuel ethanol and ethanol for alcohol based beverages, is produced by fermenting six-carbon sugars (e.g. glucose) by yeast, thus producing ethanol and carbon dioxide. The concentration of CO_2 is exceptionally high (approximately 99%), which suggests that the sequestration of carbon is rather effortless and cost-effective. Hence, the only purification process needed is dehydration, followed by compression of the gas. However, some end uses require other purification steps, e.g. DMS needs to be removed from CO_2 used in food processes due to its odour. CO_2 originating from ethanol production has the largest market share of the CO_2 merchant market in the U.S. (33%), due to its effortless separation from ethanol. Common impurities in the CO_2 stream are organic compounds, including ethanol, methanol and sulphur compounds, such as H_2S and DMS. (Xu et al. 2010)

3.5 Impurities originating from the CO_2 separation techniques

Separation of carbon dioxide can be accomplished using the technologies discussed in chapter 2. However, degradation of the separation materials cause economic losses, loss in performance and potential environmental effects (Chi & Rochelle 2002). In addition, degradation products can end up in the separated CO_2 stream. Degradation of solvents has been the topic of several studies, but there are still a lot of uncertainties about the phenomena.

3.5.1 Absorption

Absorption technologies use solvents, such as MEA, to separate CO_2 from flue gas. Most solvents are easily degraded by compounds like fly ash, SO_x, NO_x and particulates (Aaron & Tsouris 2005). MEA, commonly used in absorption technologies, can degrade by three different types of degradation. The first is oxidative degradation, which requires oxygen and is catalysed by dissolved metals, including Fe, Cu and V (Chi & Rochelle 2002; Goff & Rochelle 2006). Oxidation of MEA proceeds via a series of free radical reactions which finally form ammonia (NH_3), aldehydes and carboxylic acid degradation products. Figure 4 presents the mechanism for MEA oxidation along with degradation products (Chi & Rochelle 2002). Sexton & Rochelle (2011) studied further degradation products of MEA, and determined that in the presence of an iron catalyst, the major degradation products of MEA oxidation is formate ($HCOO^-$), hydroxyethyl-formamide (HEF), hydroxyethyl imidazole (HEI) and NH_3. The minor degradation products include carboxylic acids, such as acetate and glycolate, nitrate/nitrite (NO_2^-/NO_3^-), NO_x/N_2O, CO, C_2H_4, acetaldehyde and formaldehyde. Secondly, MEA can degrade via polymerization of carbamate (formed when MEA reacts with CO_2) at high temperatures. Finally, thermal degradation takes place when MEA degrades at high temperatures (above 205 ^oC, the ideal temperature for MEA is 45 ^oC), which result in degradation of the solvents and lower the solubility of CO_2 (Aaron & Tsouris 2005; Chi & Rochelle 2002). This type of degradation is however unlikely, since the process temperature usually is lower. (Chapel et al. 1999; Aaron & Tsouris 2005)

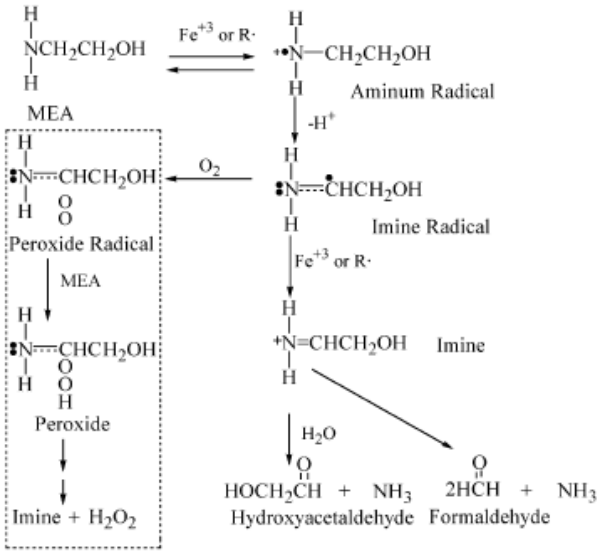

Figure 4. Degradation of MEA by single electron oxidation (Chi & Rochelle 2002).

Another concern for MEA degradation is acidic gases, such as SO_x, which react irreversibly with MEA to produce corrosive salts. Therefore, it is necessary to remove SO_x before the separation of CO_2. Preferably, the SO_2 levels should be kept under 19 ppmv (Chapel et al. 1999) to avoid the formation of stable salts with amines. In addition, sulphur trioxide (SO_3) results in both heat stable salts as well as corrosive H_2SO_4 aerosol in wet scrubbers. Other impurities that can cause degradation of MEA are fly ash, soot and NO_x compounds, which create the similar problem as SO_x compounds. Fly ash result in direct degradation of the solvent, but can also cause difficulties with the SO_2 scrubber, which indirectly has an effect on the degradation of MEA. Soot derived from heavy fuel oil stabilizes an amine mist above the CO_2 absorption zone. Therefore, a special mist eliminator should be installed to capture micro-sized MEA mist particles. (Chapel et al. 1999; Aaron & Tsouris 2005).

Literature studying impurities originating from materials in physical absorption is scarce. Aaron & Tsouris (2005) concluded that absorption technologies relying on physical absorption with solid sorbents, such as calcium and lithium hydroxides, may degrade by the formation of $CaCO_3$ on the surface of the packed beds.

3.5.2 Adsorption

Research of degradation of materials used in adsorption separation technologies is limited. Impurities including water, oxygen and trace components, such as SO_x and NO_x can lead to degradation of adsorbents. E.g. SO_2 has been reported to react with basic surface sites on several amine adsorbents (Sjostrom & Krutka 2010). Materials such as metal-organic frameworks (MOFs) and covalent organic frameworks (COFs) have many favourable features (high surface area and gas sorption capacities), but some are unstable in the presence of moisture. Bollini et al. (2011) studied the oxidative degradation of aminosilica materials under accelerating oxidation conditions for a wide range of temperatures. The author concluded that stability of the amines in the aminosilica structure is dependent on temperature. In addition, primary and tertiary amines at the end of a propyl linker were more stable than secondary amines at the end of propyl linkers. (Drage et al. 2012)

3.5.3 Membrane separation

The impurities found in the separated CO_2 stream by membrane separation are highly dependent on the membrane used. It has been noted that absorbent in gas absorption membranes degrade by the same principles as absorption based technologies. Furthermore, gas absorption membranes are also less structurally stable than metal or ceramic membranes (Meisen & Shuai 1997; Aaron & Tsouris 2005). The presence of water vapour decreases the permeability of N_2 and CO_2, by clogging the micropores in the membrane. Other components, such as fly ash, SO_x, NO_x, HCl and HF may react with the membrane and cause potential complications, which likely are similar to those caused by SO_2 on absorbents in absorption methods (section 3.5.1) (Chapel et al. 1999).

Scholes et al. (2009) studied the effect of minor components on polymeric membranes. Scholes concluded that the presence of SO_2, H_2S, NH_3 and water in polymeric membranes can lead to plasticization of the membrane. Plasticization forms a more rubbery material, which tend to result in a considerable loss in selectivity (Sanders 1988). In addition, plasticization of the polymeric membrane increases the diffusivity of penetrants (Scholes et al. 2009) and can lead to either a decrease or increase in permeability of the polymer (Wessling et al. 1991). However, plasticization is strongly dependent on high partial pressures, which indicates that compounds with low partial pressure only will have a negligible impact on plasticization. Acidic degradation of the membrane is likely when compounds such as SO_2, NO_x and halogens, react with water and form acids. The acids (sulfuric acid, nitric acid and halogen acids) then cause an acidic degradation of the membrane by attacking the polymer matrix and increasing the size of the free volume in the polymers, resulting in an increase of permeability. Scholes et al. (2009) reported a 30-fold increase of SO_2 permeability in a polysaccharide-based polymer when water was present. Furthermore, SO_2, NOx, H_2S, NH_3 and water have similar chemical properties as CO_2, which indicate that these components likely permeate through the membrane and end up in the separated CO_2 stream. CO, Ar and hydrocarbons were noted for a lower permeability compared to CO_2. Thus, it can be expected that these components will retain in the retentate stream.

4 Impurity impact on heterogeneous catalysts

This chapter will first give a brief overview of heterogeneous catalysis and hydrogenation reactions of CO_2. Next, the main impurities' effect on heterogeneous catalysts will be described. Due to excessive amount of literature on the subject, the following sections will focus on impurity effects relevant for CO_2 utilization by hydrogenation reactions. Special emphasis will be on the impurity effect on iron (Fe), copper (Cu) and cobalt (Co) based catalysts, since they are widely used in hydrogenation reactions (Twigg & Spencer 2001).

Bartholomew (2001) classified sulphur- and arsenic-containing species to be the most typical poisons for metals in hydrogenation, dehydrogenation and steam reforming reactions. In addition, nitrogen-containing compounds are common impurities in separated CO_2 streams. Thus, the focus will be on studying sulphur-, nitrogen- and arsenic-containing impurities. In addition, the effects of some minor contaminants will be discussed.

4.1 Heterogeneous catalysis

Catalysts are widely used in chemical processes, with approximately 85-90% of all chemical products being produced in catalytic processes. In several industries, such as the production of transportation fuels and production of bulk and fine chemicals, catalysts are indispensable. They are used in chemical processes due to their ability to increase the reaction rate without affecting the equilibrium, essentially changing themselves or being used up in the process. By using catalysts it is possible to operate in safer conditions, due to lower temperatures and decreased reactor volumes, and increase the process capacity. Thus, catalysts are necessary in both cost-effective and environmental points of view. (Chorkendorff & Niemantsverdriet 2003)

In heterogeneous catalysis the reactants and the catalyst exist in different phases. Most heterogeneous catalysts consist of an active component, a support and possible promoters. The supports are usually porous, providing a large surface area where the active component can be dispersed. The active component is commonly a pure metal or

metal alloy. Promoters, i.e. small amounts of active ingredients, can be added to the catalyst in order to increase the catalytic activity or modify the selectivity to desired products. (Fogler 1999)

The catalytic activity of a catalyst is not maintained with time, which means that the catalyst deactivates. The deactivation of the catalyst can occur by three different mechanisms; i) sintering (aging), ii) poisoning and iii) fouling or coking. Sintering is a gradual change in active surface area due to crystal agglomeration or by narrowing or closing of the pores inside the catalyst pellet. Poisoning occurs when a poisoning molecule becomes irreversibly chemisorbed to the active site of the catalyst. Thus, the reaction rate decreases with the decreasing numbers of active sites. Finally, fouling or coking occurs when carbonaceous materials are being deposited on the surface of the catalyst. Coking is a common reason for deactivation of reactions involving hydrocarbons. (Fogler 1999)

4.2 Hydrogenation of CO_2

The hydrogenation reactions included in this work is reverse water-gas shift (RWGS), Fischer-Tropsch, methanol synthesis and methanation. All reactions are further presented below.

RWGS (1) converts CO_2 to CO. Typically copper- or iron-based (Dorner et al. 2010) catalyst have been used for catalysing the RWGS reaction. (Wang et al. 2011)

$$CO_2 + H_2 \leftrightarrow CO + H_2O \qquad \Delta H_{298\,K} = 41.15 \frac{kJ}{mol} \qquad (1)$$

Carbon monoxide can then be further processed with the Fischer-Tropsch synthesis (FTS) (2), which produces a range of hydrocarbons used as sources of fuel. Typical metals used for catalysing the reaction are iron and cobalt. If iron is used as the FT-catalyst; RWGS (1) takes place with the FTS. (Dorner et al. 2010)

$$CO + 2H_2 \leftrightarrow -(CH_2)- + H_2O \qquad \Delta H_{298\,K} = -166 \frac{kJ}{mol} \qquad (2)$$

Methanation of CO_2 (3) produces methane and water. Methane can be further used for e.g. the production of syngas. Nickel-based catalysts have been the most widely studied catalyst for methanation. (Wang et al. 2011)

$$CO_2 + 4H_2 \leftrightarrow CH_4 + 2H_2O \qquad \Delta H_{298\,K} = -252.9 \frac{kJ}{mol} \qquad (3)$$

In addition, methanol can be produced by methanol synthesis (4) of CO_2. (Yoshihara & Campbell 1996)

$$CO_2 + 3H_2 \leftrightarrow CH_3OH + H_2O \qquad \Delta H_{298\,K} = -49.5 \frac{kJ}{mol} \qquad (4)$$

Copper catalysts are most suitable for methanol manufacturing and hydrogenation of specialty organic compounds. They are however not appropriate for Fischer-Tropsch reactions as they tend to have a low activity for breaking C-O bonds or forming C-C bonds. In contrast, iron catalysts promote the dissociation of CO and CO_2. Thus, iron-based catalysts are more suitable for methanation and Fischer-Tropsch synthesis. (Twigg & Spencer 2001)

4.3 Sulphur-containing impurities

4.3.1 Effect on Cu catalysts

Sulphur-containing impurities are known to have a great effect on Cu catalyst poisoning. Cu-based catalysts are extremely sensitive to even low levels of H_2S and other sulphur compounds. The sulphur levels should be kept below 1 ppm in order to retain activity of the Cu catalyst (Twigg & Spencer 2001). Copper catalysts are more vulnerable to thermal sintering of active metal than many other metallic catalysts. As a result, Cu catalysts require to be operated at lower temperatures, which thermodynamically favour adsorption of sulphur-containing poisons according to equation (5).

$$2Cu + H_2S \rightarrow Cu_2S + H_2 \qquad \Delta H_{298\,K} = -58.87 \frac{kJ}{mol} \qquad (5)$$

This results in site blocking of active sites on the catalyst. Commonly $Cu/ZnO/Al_2O_3$ catalysts are used for methanol synthesis (Twigg & Spencer 2003). By adding ZnO to the catalyst, the poisoning by sulphur can be limited, since a more thermodynamically stable zinc sulphide (ZnS) is formed (Twigg & Spencer 2001).

$$ZnO_{(s)} + H_2S_{(g)} \rightarrow ZnS_{(s)} + H_2O_{(g)} \qquad \Delta H_{298\,K} = -78.93 \frac{kJ}{mol} \qquad (6)$$

Quinn et al. (2004a) studied contaminants in syngas and their effect on a $Cu/ZnO/Al_2O_3$ catalyst in methanol synthesis. All studied sulphur-containing compounds, i.e. thiophene (C_4H_4S), methyl thiocyanate (CH_3SCN), carbon disulphide (CS_2) and carbonyl sulphide (COS), had a harmful effect on the rate of methanol synthesis. The study concluded that the sulphur-containing compounds reacted with the catalyst, and thus decreased the catalytic activity of the catalyst by site blocking, i.e. poisoning of the catalyst.

4.3.2 Effect on Fe and Co catalysts

Iron catalysts are also sensitive to sulphur-containing impurities. The effect of sulphur on iron (Fe) and cobalt (Co) catalyst has been extensively researched. However, many studies are slightly contradictory. The effect of sulphur on iron catalyst has been shown to both increase and decrease catalytic activity, as well as decrease and change the selectivity of iron catalyst (Ma et al. 2016). Hence, a consensus of the mechanism of sulphur poisoning of iron catalysts for Fischer-Tropsch synthesis and the ability of sulphur to poison iron have not, to date, been found to the knowledge of the author. The reason for inconsistency of results could be associated to different sulphur concentrations and/or process conditions used (Ma et al. 2016). Despite the contradiction, some results from the effect of sulphur on iron catalysts are presented below.

Sulphur-compounds, typically H_2S and SO_2, are usually present to some level in syngas, as was presented in Chapter 3. Several studies have suggested that sulphur only have a negative effect on the catalyst activity. Barthomolomew & Bowman (1985) studied the effect of 0.5-8 ppm H_2S on a cobalt/silica catalyst and four iron catalyst (unsupported,

silica-supported, K-promoted and B-promoted) in a micro fixed-bed reactor. They concluded that addition of low levels of H_2S in syngas (less than 2 ppm) resulted in a faster deactivation than higher levels of H_2S (5-6 ppm). The authors suggested that the reason for this was that lower levels resulted in physical blocking of catalysts by adsorption of sulfuric, while higher levels resulted in a surface sulphide having a different structure or a multiple sulphide layer. Moreover, no change in selectivity was observed. Anderson et al. (1965) studied the effect of H_2S in syngas in FTS in a fixed-bed reactor using reduced, carbided and nitrided fused iron oxide catalysts on MgO-support. The study was conducted for long time intervals (e.g. 56-100 days) at constant temperature (260 ^{o}C) or at constant hydrocarbon yield (by increasing the temperature from 260 ^{o}C to 390 ^{o}C). It was concluded that the catalyst deactivated linearly with the increasing concentration of sulphur until 75% of the activity was lost. However, sulphur was not found to alter the selectivity of the catalyst (Anderson et al. 1965; Ma et al. 2016).

Other studies have demonstrated the opposite effect of sulphur-containing compounds. Stenger & Satterfleld (1985) reported that addition of H_2S to syngas increased the catalyst activity by 60% at sulphur loadings of 1.3 mg S/g Fe for a reduced fused Fe_3O_4 catalyst suspended in both n-octacosane and phenanthrene, and promoted by K_2O. The authors believed this was due to reducing the effective concentration of potassium on the catalyst to an optimum value for maximum catalytic activity. For higher concentration of H_2S the catalyst started to deactivate. In addition, several studies (Karn et al. 1963) agreed on that by adding small quantities of sulphur compounds, such as H_2S on a reduced fused $Fe_3O_4/MgO/K_2O$ catalyst (Karn et al. 1963) and Na_2S on a precipitated iron Fischer-Tropsch catalyst (Bromfield & Coville 1999), during the precipitation procedure can extend the iron catalyst lifetime, enhance its activity and modify its selectivity (Bromfield et al. 1997). Depending on the sulphur loading, different reactions can be enhanced. Bromfield et al. (1999) suggested that a catalyst chemically modified with low sulphur concentrations results in a generation of metal centres which enhance the activity of the catalyst. In addition, the authors concluded that S^{2-} loadings exceeding 2000 ppm resulted in an increase in methane yield. By increasing the S^{2-} loading even further (to 20 000 ppm), an enhanced activity for water gas shift reaction was observed. Bromfield et al. (1997) had earlier concluded by an X-ray photoelectron spectroscopy (XPS) study that at low sulphur concentrations, the species found on the

sulphide precipitated-iron catalyst after calcination and reduction was mainly SO_4^{2+}, while higher loadings of sulphur resulted in S^{2-} as the dominant species. Hence, Bromfield et al. suggested that surface sulphates (SO_4^{2+}) result in enhancement of catalytic activity, while sulphides induce poisoning (Bromfield et al. 1997).

One of the latest studies conducted within the field was published in 2016 by Ma et al. The effect of H_2S in syngas on the FTS performance over a 100Fe/5.1Si/2.0Cu/3.0K catalyst was studied in a CSTR reactor. The study was conducted at three different temperatures, i.e. 230, 260 and 270 ^oC, and for several hundred hours. All catalysts were characterized by X-ray diffraction (XRD), Mössbauer spectroscopy and X-ray absorption near edge structure (XANES). The authors concluded that by adding sulphur to the syngas, the selectivities of alkenes and WGS were improved, yet with declining rates, while the methane selectivity declined. By progressively increasing the H_2S level from 100 ppb to 1 ppm, the upper limit for H_2S in syngas feed could be determined. Figure 5 illustrates the relationship between the H_2S level added to the syngas and the percentage of loss in CO conversion per day. The R^2 value for linear regression is very close to unity, which indicates a highly linear relationship between the two factors. Thus, the limit of H_2S level in syngas for zero deactivation is determined by extrapolating the plot, resulting in a limit of 50 ppb H_2S.

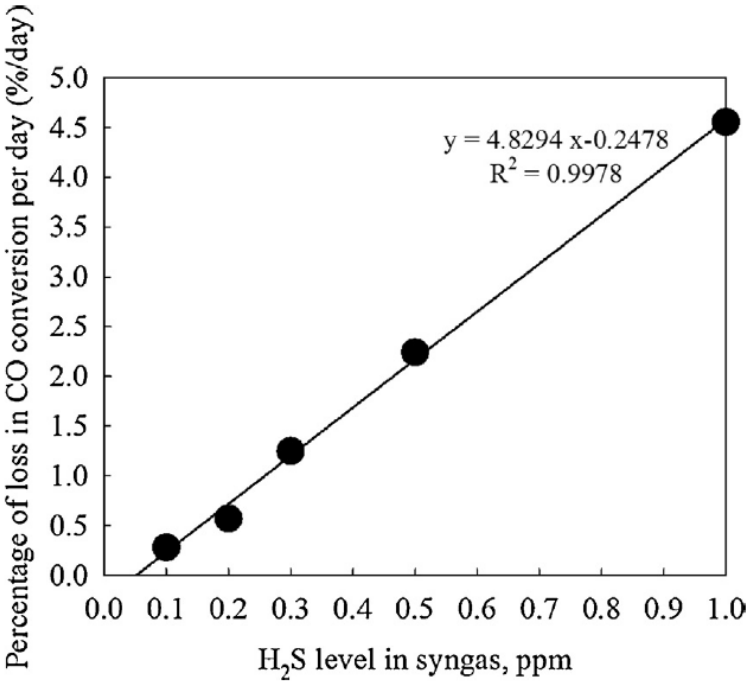

Figure 5. Relationship between added H_2S and CO conversion decrease percentage on 100Fe/5.1Si/3K/2Cu catalyst at 270 ^{o}C. (Ma et al. 2016)

In addition, the relationship between sulphur atoms added and active Fe atoms (Fe/S) lost was determined. The study concluded that Fe/S ratios increased with decreasing temperatures (i.e. 13.5 at 230 ^{o}C, 7.2 at 260 ^{o}C and 5.9 at 270 ^{o}C). This suggests that the strength of poisoning by sulphur was weakened at higher temperatures, which in turn suggests that site blocking is the reason for the deactivation. This was further supported by XRD, Mössbauer and XANES studies, which proposed that bulk Fe-S compounds were not formed to a significant extent and that the decrease in methane selectivity was caused by competitive adsorption between sulphur and hydrogen on the Fe catalyst surface. (Ma et al. 2016)

The reactor type also plays a central role in poisoning of the Fe catalyst. Jager & Espinoza (1995) compared the effect of sulphur impurities on fixed bed and slurry bed reactors using a precipitated iron catalyst, and concluded that for the same conditions the loss in conversion due to poisoning by sulphur was 1.5 to 2 times higher for a slurry bed reactor than for the fixed bed reactor (Jager & Espinoza 1995). Different sulphur-containing compounds have been shown to behave differently in reactors. According to Dry (1990), H_2S adsorbs more rapidly at the reactor inlet, while other sulphur

compounds, such as COS and CH_3SH, are less strongly adsorbed and so they could penetrate deeper into the catalyst bed.

Iron and cobalt catalysts have also been used in methanation reactions (Agarwal et al. 1980). 13-100 ppb H_2S was reported to reduce methanation rates of Co/Al_2O_3 and Fe/Al_2O_3 catalysts. For each sulphur atom added to the surface, two surface Co or Fe atoms were eliminated. The reason was considered site blocking of the catalyst surface by sulphur. (Agarwal et al. 1980; Ma et al. 2016)

Ma et al. (2016) compared the effect of sulphur on cobalt (0.5%Pt-25%Co/Al_2O_3) and iron catalysts (100Fe/5.1Si/3.0K/2.0Cu) at 230 ^{o}C. The poisoning effect of sulphur appeared to be slightly higher with cobalt. However, the study speculated that this may be due to that the cobalt catalyst had been partially deactivated by oxidation before the measuring of the sulphur impact.

4.4 Nitrogen-containing impurities

The effect of nitrogen-containing compounds on metal catalysts is less severe than the effect of sulphur-containing compounds, and the poisoning can be reversed by mild hydrogen treatment (Saib et al. 2010). Nitrogen-containing compounds have little effect on catalysts in the Fischer-Tropsch synthesis. No information concerning the effects of MEA on catalysts has been found.

Borg et al. (2011) studied the effect of 4.1 ppmv NH_3 on cobalt catalysts ($Co/Re/Al_2O_3$, $Co/Re/NiAl_2O_4$, $Co/Re/SiO_2$ and $Co/Re/TiO_2$) in the Fischer-Tropsch synthesis. Neither the activity nor the selectivity of the catalyst was affected. In contrast, Pendyala et al. (2013) found that the addition of ammonia lead to significant changes in both catalyst activity (Co/Pt/Al2O3-catalyst) and product composition. The rate of deactivation appeared to correlate with the concentration of ammonia added and the selectivity of higher olefins increased slightly with increasing ammonia concentration.

Ma et al. (2015a) studied the effect of ammonia in syngas on the Fischer-Tropsch synthesis performance of a 100Fe/5.1Si/2.0Cu/3.0K catalyst. The ammonia added to the syngas originated from ammonia gas (NH_3), ammonium hydroxide solution (NH_4OH) or ammonium nitrate solution (NH_4NO_3). Ammonium nitrate was expected to form NH_3

and NO_x. The study concluded that up to 200 ppm NH_3 did not appear to have a significant effect on the catalyst deactivation or selectivity. Nevertheless, 400 ppm NH_4NO_3 lead to a rapid deactivation of the Fe catalyst. In addition, the selectivity of light hydrocarbon products was increased. The deactivation was proposed to be a result of dissociated HNO_3 that oxidizes the catalytically active iron carbides (formed by CO reduction and reaction with Fe) to magnetite (Fe_3O_4). The proposed reactions (unbalanced) for the formation of magnetite are presented below. Iron carbides react with NO_x dissociated from HNO_3 or ammonium nitrate to form magnetite:

$$Fe_5C_2 + NO_x \rightarrow Fe_3O_4 + N_2 + CO_2 \quad (7)$$

HNO_3 reacts directly with iron carbide, forming iron nitrate ($Fe(NO_3)_3$). Next, iron nitrate is reduced to magnetite:

$$Fe_5C_2 + HNO_3 \rightarrow Fe(NO_3)_3 + NO_x + CO_2 + H_2O \quad (8)$$

$$Fe(NO_3)_3 + H_2 \rightarrow Fe_3O_4 + NO_x + H_2O \quad (9)$$

Thus, Ma et al. (2015a) suggested that the deactivation was caused by oxidation of iron carbides, not by adsorption or site blocking. The study also compared the effects of ammonia between Fe and Co catalysts. They concluded that Fe catalysts appear to be more resistant to ammonia than Co catalysts under typical FTS conditions.

Quinn et al. (2004a) studied the effect of contaminants in syngas in methanol synthesis over a $CuO/ZnO/Al_2O_3$ catalyst. It was concluded that the nitrogen-containing compounds, i.e. cyanide (HCN), acetonitrile (CH_3CN) and methylamine (C_3NH_2), had no effect on catalyst activity.

4.5 Arsenic-containing impurities

Bartholomew (2001) classified arsenic-containing compounds as severe poisons in hydrogenation and Fischer-Tropsch synthesis. Arsenic-containing impurities in syngas can originate from the feedstock. E.g. arsenic oxides in coal form volatile compounds,

principally arsine (AsH_3), during gasification (Quinn et al. 2004b). Arsine is a powerful methanol synthesis poison, and levels as low as 150 ppbv resulted in a fast deactivation of the $CuO/ZnO/Al_2O_3$ catalyst. The reason of deactivation was proposed to be dissociative adsorption of arsine on the Cu surface to form gaseous H_2 and Cu_3As. The calculated arsine level on Cu catalysts was only 10 ppbv. (Quinn et al. 2004b)

4.6 Other impurities

4.6.1 Hydrohalides (HF, HCl and HBr) and methyl halides (CH_3Cl and CH_3F)

Hydrohalides (HX, X= F, Cl, Br) are strong acids and also present in syngas to some extent. Ma et al. (2015b) studied the effect of hydrohalids in FTS on a Fe/Si/Cu/K catalyst. Co-feeding less than 2 ppm of HCl or HBr in syngas did not significantly affect the Fe catalyst. By increasing the level to 3-5 ppm, a slow deactivation of the catalyst was observed. HF showed a weaker poisoning effect than HCl and HBr. When the HX levels increased 20 ppm, a decrease in C_{5+} and CO_2 selectivities were observed. This is likely the result of halide ions adsorbing onto the iron catalyst surface and thus, hindering CO adsorption. In contrast, the methane selectivity was increased when the HX level increased 20 ppm. The different halides had different effects on the iron catalyst. It was concluded that at 270 ^{o}C, the Fe/X- ratio (i.e. the relationship between X-added and Fe atoms lost) for the halides were; Fe/F^-=0.33, Fe/Cl^-=0.78 and Fe/Br^-=0.85. Thus, HBr showed the strongest poisoning effect of the halides (Ma et al. 2015b). Quinn et al. (2004a) studied the effect of methyl chloride (CH_3Cl) and methyl fluoride (CH_3F) on a $Cu/ZnO/Al_2O_3$ catalyst in methanol synthesis. Both compounds, especially CH_3Cl, had a severe effect on the rate of methanol formation. Adding 2.01 ppm CH_3Cl in syngas resulted in a high deactivation rate of 0.657%/h. CH_3Cl even resulted in decreasing catalyst activity after the removal from the syngas feed, which was proposed to be due to CH_3Cl reacting quantitatively with the catalyst, while 80% of added CH_3F simply passed through the reactor without reacting. The main effect of poisoning by chlorine has earlier been ascribed to increased sintering, which is due to the formation of low-melting CuCl (Twigg & Spencer 2001). In addition, ZnO, which often is present in Cu catalysts, can form Zn halides by reacting with e.g. HCl, which further increases sintering.

4.6.2 Alkali, bicarbonate and chloride

The effect of alkali, bicarbonate and chloride addition to syngas on the FT synthesis has also been investigated. KCl, NaCl, $KHCO_3$ and $NaHCO_3$ were co-fed with syngas and their impact on an iron catalyst (100Fe/5.12Si/2.0Cu/3.0K) was studied. All compounds had an insignificant effect on the Fe catalyst deactivation. The catalyst activity and selectivities for methane, C_{5+} and olefins where nearly unaffected after 40 ppm (for $NaHCO_2$ and $KHCO_3$) or 100 ppm (or NaCl and KCl) had been added to syngas at 270 ^{o}C. However, the CO_2 selectivity increased slightly after feeding the impurities, due to enhanced WGS. (Ma et al. 2013)

4.6.3 Phosphine (PH_3)

Phosphine (PH_3) was found to poison a $Cu/Zn/Al_2O_3$ catalyst in a methanol synthesis study conducted by Quinn et al. (2004a). By adding 1.91 ppmv PH_3 into syngas feed, the rate constant decreased immediately. The reason for deactivation was believed to be dissociative adsorption of PH_3, which forms Cu_3P on the catalyst surface.

4.6.4 Oxidation

Oxidation of active iron carbide to inactive iron magnetite (Fe_3O_4) in the Fischer-Tropsch synthesis results in a decrease in active surface area of the catalyst (Dry 1990). In addition, oxidation can also alter the selectivity of the catalyst (Jager & Espinoza 1995), since the formation of magnetite enhances the WGS reaction on the expense of FTS. Thus, as the partial pressure of H_2O, which is the main single product of FTS, increases, it can be expected that oxidation of the catalyst takes place.

EXPERIMENTAL PART

6 Aim and content of the experimental part

The aim of the experimental part was to study how impurities affect hydrogenation of CO_2 and the catalysts used. Monoethanolamine (MEA) was chosen as one of the impurities since there were no earlier studies, in the knowledge of the author, on the effect of MEA on CO_2 hydrogenation catalysts. Hydrogen sulphide (H_2S) was chosen as the other impurity since it is a commonly found impurity in separated CO_2 streams and a typical catalyst poison. In addition, earlier researches studying the effect of H_2S on CO_2 hydrogenation were quite contradictory.

The experimental part consists of 1) Temperature Programmed Desorption (TPD) experiments and 2) Reaction experiments in a plug flow reactor (PFR). The TPD experiments were conducted in order to study how MEA and sulphur affect the formation of methane, as well as adsorption of the reactant gases on the catalyst, while the plug flow reactor experiments studied more in detail how the conversion and formation of products change during different poisoning scenarios by H_2S.

7 Material and methods

This chapter presents the experimental setup, the analysis methods, catalysts, execution of experiments and calculation methods for both sets of experiments.

7.1 Experimental setup

7.1.1 Temperature programmed desorption

The TPD experiments were conducted in order to observe 1) adsorption properties of the catalyst, 2) the effect of MEA on methane formation and 3) the effect of H_2S on methane formation. Four different catalysts were tested. The setup of the experiments conducted in the TPD apparatus is presented in Figure 6.

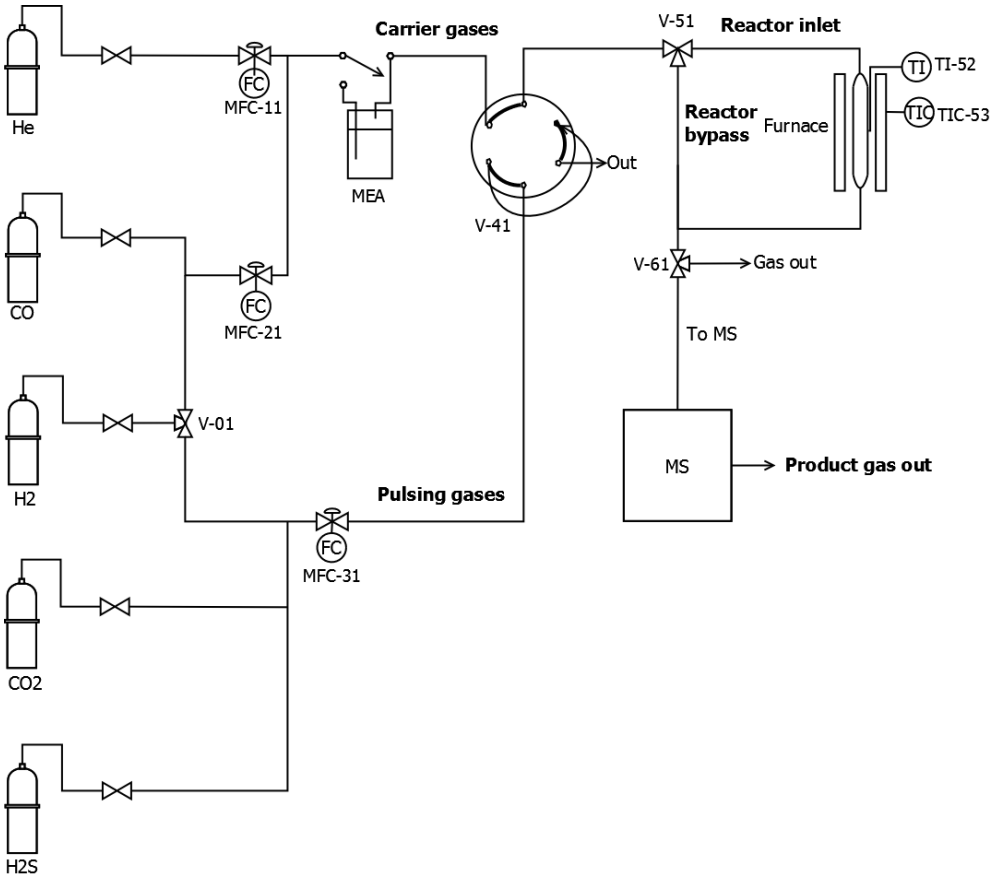

Figure 6. PI-diagram of the setup of TPD experiments.

Three-way valve V-01 was manually operated to set whether H_2 would be pulsed or used as a carrier gas. The mass flows were adjusted by three mass flow controllers (MFC-11, MFC-21 and MFC-31). Their specs are shown in Table 8. All mass flow controllers were calibrated before starting the experiment. Helium flow was adjusted by mass flow controller MFC-11, while the other carrier gas flows, i.e. H_2 and CO, were adjusted by mass flow controller MFC-21. The gases that were pulsed, i.e. H_2, CO_2 and H_2S, were regulated by mass flow controller MFC-31.

Table 8. Mass flow meters in TPD experiments.

Name	Gas	Max flow (nl/min)	Model	Producer	Number
MFC-01	N_2	0.5	F-201CV-1K0-AAD-11-V	Bronkhorst	M10211485C
MFC-11	N_2	0.5	F-201CV-1K0-AAD-11-V	Bronkhorst	M10211485A
MFC-21	CO	0.5	F-201C-FB-33-V	Bronkhorst	920253A

MEA was added by bubbling the carrier gas through an impinger filled with MEA at room temperature. Valve V-41 was operated manually and was used for pulsing 1 ml of gas. This served also a function of calibration. The carrier gases flowed through the valve at all times, either directly, as presented in Figure 6, or through the loop carrying the pulsing gas. The manual three-way valve V-51 controlled whether the gas flowed to the reactor or reactor bypass. When MEA connection was made, it was switched to bypass to prevent air from entering the reactor.

The reaction took place in a glass tube with a catalyst bed. A temperature indicator (TI-52) showed the temperature inside the reactor. The temperature was adjusted by the furnace (TIC-53). The manual three-way valve V-61 regulated whether the gas was led out without analysis or to the mass spectrometer for analysis.

In the experiments, five different gases were used. The purity of the gases is presented in Table 9. In addition, an H_2S-containing gas, consisting of 99.2 ppm H_2S in nitrogen (see Table 12) was used for the poisoning experiments.

Table 9. Gases used in TPD experiments.

Gas	Purity (%)	Producer
He	99.996	AGA AB
H_2	99.999	AGA AB
CO_2	99.99	AGA AB
CO	99.97	AGA AB

For analysing the TPD product gas, a mass spectrometer (Balzers GAM400) was used. The monitored mass numbers and their corresponding key fragments are summarized in Table 10. The mass number of MEA is 61. Yet, mass numbers 30 and 42 were also monitored for recognizing MEA, based on the mass spectrum of MEA (Anonymous, 2016).

Table 10. Monitored mass numbers in TPD experiments.

Mass number	Key fragments
2	H_2
4	He
15	CH_3+
16	CH_4
18	H_2O
28	N_2, CO, C_2H_6
30	MEA
31	CH_2OH+
32	O_2, CH_3OH
34	H_2S
42	MEA
44	CO_2
61	MEA

7.1.2 Reaction experiments in plug flow reactor

The reaction experiments were carried out in a plug flow reactor. The tests were conducted in order to study the effect of H_2S on selectivity and conversion of iron catalysed FT synthesis and Cu catalysed methanol synthesis. The experimental setup is presented in Figure 7.

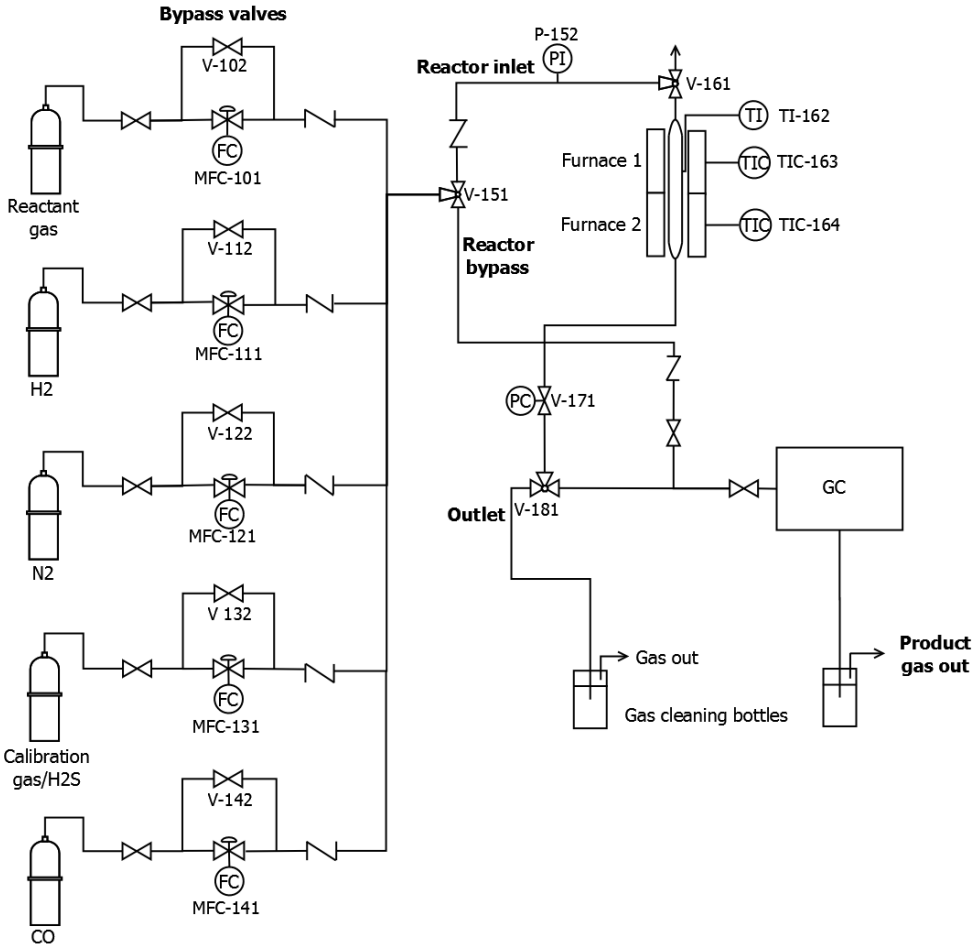

Figure 7. PI-diagram of experimental setup of plug flow reactor experiments.

The flow rates of gases to the reactor were adjusted by thermal mass flow controllers (MFC-101, MFC-111, MFC-121, MFC-131 and MFC-141). All mass flow controllers are specified in detail in Table 11. The mass flow controllers were calibrated before starting the experiments.

Table 11. Mass flow meters in reaction tests.

Name	Gas	Max flow (nl/min)	Model	Producer	Number
MFC-101	CO_2	2	F-201CV-5K0-ABD-11-V	Bronkhorst	M15205143A
MFC-111	H_2	0.15	F-201C-RAA-11-V	Bronkhorst	M0206450E
MFC-121	CO	0.05	F-201CV-RAA-11-V	Bronkhorst	M0206450D
MFC-131	Calib (N_2)	2.5	F-201C-RAA-33-V	Bronkhorst	M6202701A
MFC-141	CO	0.2	F-201C-RAA-11-V	Bronkhorst	M2202691D

By using the bypass valves (V-102, V-112, V-122, V-132 and V-142) the reactor could be flushed or pressurized. The manual three-way valve V-151 controlled the flow to either reactor or bypass. The reactor was bypassed to be able to analyse the composition of the feed gases. The three-way valve in the reactor inlet (V-161) controlled the flow to either reactor or outlet. The pressure could be manually controlled by valve V-171, a Tescom 26-1716 backpressure valve. The pressure was measured by a pressure gauge (P-152). The manual three-way valve in the reactor outlet (V-181) directed the reactor outlet gas to either outlet or to the gas chromatograph (GC) for analysis. The reactor was heated by furnace blocks TIC-163 and TIC-164. The temperature was measured from both heating blocks and from inside the reactor. The gas lines from the outlet line of the reactor to the GC were heated to 150 ^{o}C and insulated to prevent condensation of products. The dimensions of the reactor tube were 420 mm x 12 mm (i.d.). The material of the reactor was AISI-316. A picture of the reactor is presented in Appendix 1.

The product gas from the reaction experiments was analysed by an on-line Agilent 6890N gas chromatograph (GC). The GC was equipped with two different detectors, 1) a thermal conductivity detector (TCD), which analysed the non-condensable gases (i.e. H_2, N_2, CO and CO_2) and C_1-C_2 hydrocarbons, and 2) a flame ionization detector (FID), which analysed hydrocarbons (C_1-C_{14}) and oxygenated organic compounds. A sketch of the GC is presented in Figure 8. The TCD was connected to columns PorapakQ and Carboxen 1000. PorapakQ was a precolumn, which prevented higher hydrocarbon products from entering the Carboxen-column. The PorapakQ column was backflushed by the AUX gas. The FID was connected to INNOWAX, a polar column, and DB1, a non-polar column.

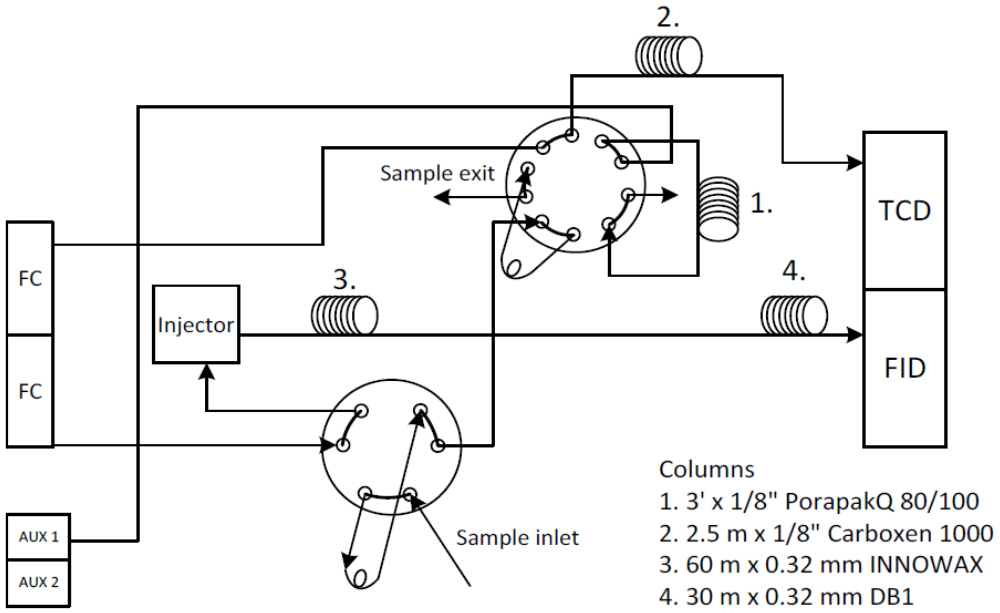

Figure 8. Gas chromatograph internals sketch.

Argon (16.1 ml/min) functioned as the carrier gas for the TCD and helium (2.3 ml/min) for the FID. The temperature program of the GC oven was the following; 1) 40 ^{o}C for 3 minutes, 2) temperature increase 10 ^{o}C/min to 210 ^{o}C, 3) stable at 210 ^{o}C for the rest of the experiment. One experiment lasted for 30 minutes. The different compounds were recognized by their retention times.

The reactant gas was a pre-mixed gas consisting of H_2, CO_2 and N_2. Nitrogen was used as the internal standard in GC calculations. In addition, a calibration gas consisting of CH_4, CO, H_2, CO_2 and N_2 was analysed for determining the response factors of methane. Two different gases, consisting of 4.8 ppm and 99.2 ppm H_2S respectively, were used for the poisoning experiments. Table 12 summarizes the composition of gases used in the experiments, provided by AGA AB.

Table 12. Gases used for plug flow reactor experiments. All bottles were analysed and certified by AGA AB.

Compound	Calibration gas vol-%	Reactant gas 1 vol-%	Reactant gas 2 vol-%	Poisoning gas 1 vol-%	Poisoning gas 2 vol-%
H_2	15	71.3	71.3	0	0
N_2	52.0	5.0	5.0	100	100
CO_2	15	23.7	23.7	0	0
CH_4	3.0	0	0	0	0
CO	15	0	0	0	0
H_2S	0	0	0	4.8 ppm	99.2 ppm

The gases used for catalyst reduction, i.e. N_2, H_2 and CO, had purities of 99.999% (N_2 and H_2) and 99.97% (CO). All three gases were analysed and certified by AGA AB.

For verifying that H_2S passed all the way through the reactor, a Dräger Tube-pump was used to measure the H_2S level in the outgoing gas. The Dräger glass tubes showed the H_2S level on a scale from 0 to 200 ppm. The measurement was conducted on the outgoing gas of the gas cleaning bottles.

7.2 Catalysts

The focus was to test catalysts suitable for producing FT-products and methanol. Two Fe- and a Cu-based catalyst were used for the experiments. In addition, a Ni-based catalyst was tested in the TPD experiments. The Cu- and Ni-based catalysts were commercial catalysts by BASF. A summary of all catalysts is presented in Table 13.

Table 13. Catalysts studied.

Name	Catalyst composition	Pellet size (mm)	Density (g/cm3)	BET surface area (m2/g)	Producer	Experiments
FeMn	5Fe/5Mn/Al_2O_3[a]	~7x1.2	0.42	200	in-house	TPD & PFR
low α -Fe	100Fe/4.6Si/2Cu/1.4K[b]	precipitated	Unknown	Unknown	in-house	TPD & PFR
Cu	Unknown[c]	1.5x1.5	1.8	64.8	BASF	TPD & PFR
Ni	Unknown[d]	0.2-0.3	Unknown	Unknown	BASF	TPD

TPD= Temperature programmed desorption experiments, PFR= Reaction tests in plug flow reactor
[a]Numbers refer to weight-% of catalyst. [b]Numbers refer to atomic ratio.
[c]CuO: 50<wt%<75, ZnO 15<wt%<20. [d]NiO: 15 wt%.

The precipitated low α-Fe catalyst had been prepared in-house for an earlier master's thesis (Laukka 2013). The catalyst was prepared by precipitating $Fe((NO)_3)_3 \cdot 9H_2O$ and

$SiC_8H_{20}O_4$ from an aqueous solution by an ammonium hydroxide solution. The promoter solution, prepared by $Cu(NO_3)_2 \cdot 3H_2O$ and K_2CO_3, was then impregnated on the dried catalyst. Next, the catalyst was dried in a rotary vacuum evaporator. Finally, the calcination was conducted in air at 350 ^oC for three hours. The preparation method was adapted from Gnanamani et al. (2012).

The other in-house catalyst, the impregnated FeMn-based catalyst supported by Al_2O_3 (Harshaw, 0.42 cm^3/g) was prepared by impregnating the dried support by a $Fe(NO_3)_3 \cdot 9H_2O$ solution and $Mn(NO_3) \cdot 4H_2O$ solution. The flask was tapped and left to absorb overnight. The catalyst was then dried in a rotary vacuum evaporator and calcinated in air at 400 ^oC. The catalyst recipe is presented in Appendix 2 (Reinikainen 2016).

7.3 Execution of experiments

7.3.1 TPD and pulse reaction experiments

0.7-1.4 g of catalyst, i.e. enough catalyst to cover the thermocouple pocket inside the glass tube to ensure correct follow-up of temperature, was weighed. Next, the glass tube was placed in the equipment and helium flow was set on. A leak test was performed by verifying that no other compound than helium was found by the mass spectrometer.

Figure 9 illustrates the work flow of the TPD experiments.

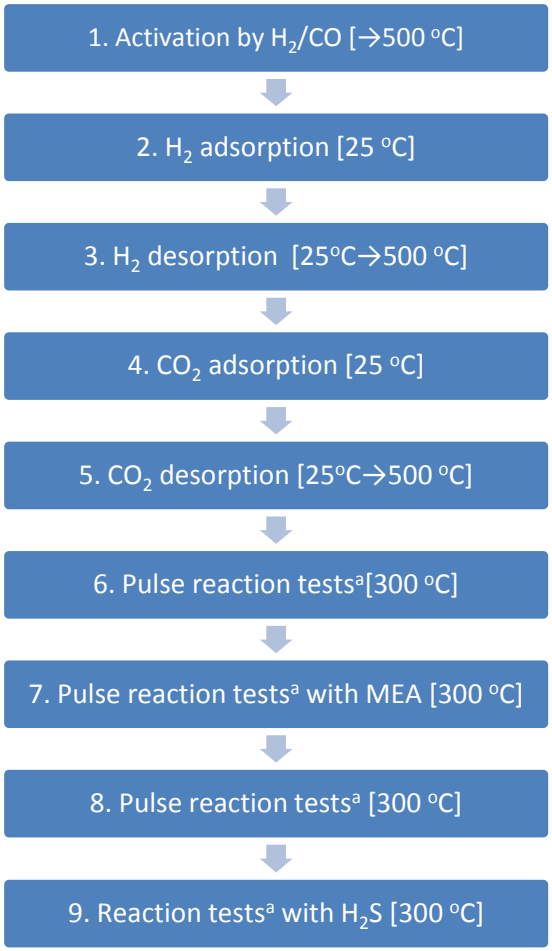

Figure 9. Illustration of work flow for experiments conducted in the TPD apparatus. [a]CO_2 pulsed to hydrogen flow.

The catalysts were reduced in an H_2 flow while following the consumption of hydrogen and production of water. The activation of the Ni and Cu catalysts was performed in 90 vol-% He and 10 vol-% H_2 flow. For Fe catalysts CO was used instead of H_2 (i.e. 90 vol-% He and 10 vol-% CO). The total flow in all experiments was 150 ml/min. All TPD tests were conducted in atmospheric pressure. The temperature was increased by 5 °C per minute to 500 °C, where it remained for 60 minutes. The Ni catalyst's activation remained at 500 °C overnight, to ensure complete reduction of the catalyst.

First, a catalyst characterization was conducted by studying the chemisorption volume of H_2 and CO_2. For the adsorption tests, where either H_2 or CO_2 was adsorbed on the catalyst at 25 °C by pulsing 1 ml of gas in a constant He flow until the catalyst was saturated, the first peaks were smaller in size than the following if the compound was

adsorbed. An example of this is presented in Figure 10. It can be noticed that the first peak is barely visible and the second and third peak slightly smaller than the following, since H_2 is adsorbed to the unsaturated catalyst. For each experiment the compound in question was pulsed 8-9 times, to ensure that the peak size would remain constant. Thus, it was possible to calculate how much of the compound had been adsorbed on the catalyst. The average of the constant peaks also worked as a correlation between area and volume of the pulsing gas.

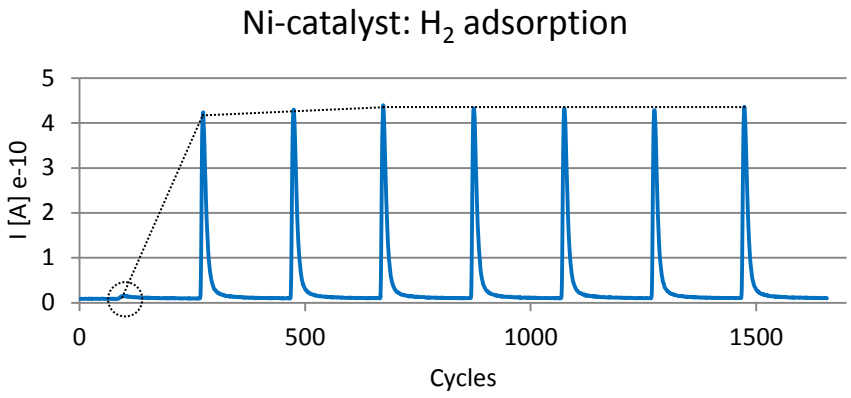

Figure 10. H_2 adsorption fo Ni-catalyst. The first injection of H_2 is clearly adsorbed to the catalyst.

After this, a temperature programmed desorption (TPD) of H_2 or CO_2 was conducted to ensure that the same amount that was adsorbed by the catalyst also desorbed. The temperature was programmed to increase 5 ^{o}C per minute to 500 ^{o}C, where it remained constant for 60 minutes. The TPD experiment was conducted in a constant He flow of 150 ml/min. A desorption peak is presented below (Figure 11), where H_2 is desorbed from the Ni catalyst. If the mass spectrum showed a completely flat line, it was assumed that nothing was desorbed from the catalyst.

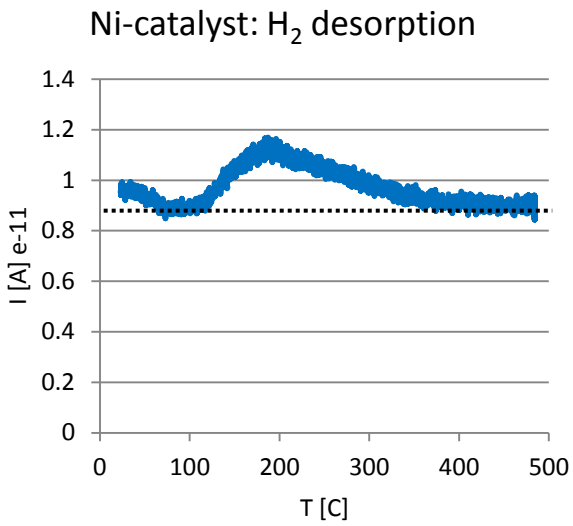

Figure 11. H_2 desorption from Ni catalyst.

The pulse reaction tests were performed at 300 °C in 150 ml/min H_2 flow. CO_2 was pulsed and the amount and type of products formed were studied. However, it was early concluded that only CH_4 was easily detected of the products. The peak size reference of CH_4 was tested using the calibration gas in Table 12. For studying the effect of MEA, three different stages were studied: 1) Initial reaction without MEA, 2) Reaction tests with MEA connected to the system and 3) Recovery, to study whether the catalyst recovered from being exposed to MEA. For each test a least 8 pulses were given, from which the average peak size was calculated. The MEA concentration in the carrier gas was calculated to be 573 ppm at T=25 °C, which was based upon the approximate vapour pressure of MEA at T=25 °C (Belabbaci et al. 2009).

Finally, the effect of H_2S on the catalyst was analysed. The reaction conditions were the same as for the above described reaction tests. First it was studied how the catalyst behaved before poisoning by H_2S. Next, 1 ml of 99.2 ppm H_2S was pulsed to the system and its effect was observed by continuing the reaction by pulsing CO_2. This procedure was repeated until totally 25 ml of the poisoning gas (or 14 ml in the case of Cu catalyst) had been pulsed. The amount of poisoning pulses at once was gradually increased, since the experiment was rather time-consuming.

7.3.2 Reaction experiments in PFR

The plug flow reactor was packed by placing quartz wool in the middle of the reactor on a metal rod and placing 2.5 g of catalyst on it. The tube was carefully closed and set to place. A leak test was performed by pressurizing the reactor to 20 bar with nitrogen and keeping it there for 5 minutes. The reactor was then pressurized with nitrogen three times to ensure that air would be removed. An illustration of the work flow is presented in Figure 12.

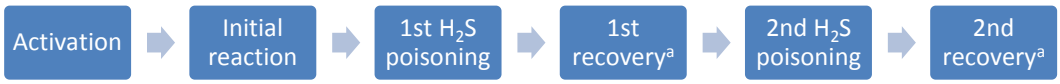

Figure 12. Work flow of the reaction tests in PFR. [a]Same reactant gas flow as initial reaction.

The activation of the Fe-based catalyst was performed by 100 ml/min CO flow at 250 ^{o}C in atmospheric pressure for 2 hours. For the Cu-based catalyst, activation occurred in 50 ml/min H_2 and 50 ml/min N_2 at 250 ^{o}C, where it remained for 2 hours.

Following activation of catalyst, the reactor was pressurized with reactant gas to the desired pressure. The temperature, pressure and reactant gas flow was individually adjusted for each set of experiments to reach a conversion between 5% and 25%. Due to the highly exothermic reactions, the temperature inside the reactor was slightly higher than the set temperature. The reaction conditions for each experiment can be found in Table 14.

Table 14. Reaction conditions and mass flows. All poisonings, except for the first poisoning of low α-Fe, were conducted by Poisoning gas 2.

Catalyst	T	P	Initial and recovery flow		First poisoning			Second poisoning		
	^{o}C	bar	Reactant gas (l/h)	Poisoning gas (l/h)	Reactant gas (l/h)	Poisoning gas (l/h)	H_2S level	Reactant gas (l/h)	Poisoning gas (l/h)	H_2S level
FeMn	300	25	10	0	6.7	3.4	33.2	6.0	9.1	59.8
low α-Fe	190	20	15	0	11.6	3.4	1.1[a]	7.3	12.8	63.2
Cu	230	30	10	0	6.7	3.4	33.2	4.7	7.1	60

[a]Conducted with Poisoning gas 1

After each poisoning, it was checked whether the catalyst recovered from it (see Figure 12). Thus, five different stages were studied for each catalyst (except for FeMn, for which the recovery stage following the first poisoning was skipped). For each stage, several GC analyses were done to make sure that the reaction had reached a pseudo-stationary condition. Furthermore, for each poisoning stage the H_2S concentration in the out-going gas was controlled by the Dräger pump to verify that H_2S passed all way through the reactor. Only then, the next stage was initiated. The calibration and reactant gases were analysed as such, to provide references for the calculations of the measurements.

The reason for the rather high H_2S-levels during poisoning was that the initially used poisoning gas, consisting of 4.8 ppm H_2S finished quickly after the first test. The following poisonings were performed with a higher concentrated gas consisting of 99.2 ppm H_2S. In addition, the mass flow controller did not work properly for very low mass flows, and hence the minimum constant mass flow obtained for the poisoning gas was 3.4 l/h, which corresponds to a weight hourly space velocity (WHSV) for H_2S of $1.8 \cdot 10^{-7}$ $g_{H2S}/h \cdot g_{cat}$. All WHSVs are presented in sections 8.2.1-8.2.3.

7.4 Calculation methods

7.4.1 TPD and pulse reaction experiments

The results obtained from the mass spectrometer were in the form of ion current [A]. In addition, temperature of the catalyst bed and time were recorded together with the mass spectrum.

Each pulse given produced a steep peak to the mass spectrum. For the desorbed compounds, a broader peak was illustrated by the MS. The areas of peaks were obtained by numerical integration.

For the reaction tests with MEA and H_2S, where the amount of produced methane was studied, a reference peak was needed. A peak reference for CH_4 was calibrated by pulsing 1 ml of calibration gas with known composition (see Table 12).

The areas were used to calculate the volume of the adsorbed/desorbed/formed compound. First, the volume of the gas was calculated by Equation (10). Secondly, the

molar volume of compound i was calculated by Equation (11). Thirdly, the amount of moles was calculated by Equation (12).

$$V_i = \frac{A}{A_{ref}} \cdot V_{pulse} \quad (10)$$

Where V_{pulse}=1 ml, A= area of adsorbed H_2/CO_2, desorbed H_2/CO_2 or formed CH_4 and A_{ref}=the area of 1 ml pulsed compound. Subscript i refer to compound i.

$$V_{m,i} = \frac{M_i}{\rho_i} \quad (11)$$

Where $V_{m,i}$=molar volume, M_i=molar mass and $\rho_{m,i}$=density.

$$n_i = \frac{V_i}{V_{m,\,i}} \quad (12)$$

Where n_i=amount of moles.

7.4.2 Reaction experiments

An Excel template used for the calculations of FT products is presented in Appendix 3. The amount of formed products was calculated by the GC peak areas. Nitrogen was used as the internal standard.

Detector responses were corrected by response factors (RFs), which were obtained by analysing reactant and calibration gases (H_2, CO_2, CO and CH_4) or from literature (Dietz 1967).

$$RF = \frac{\frac{A_i}{V\%_i}}{\frac{A_{N_2}}{V\%_{N_2}}} \quad (13)$$

Where A=peak area and V%=volume percentage of a compound. Subscript i refer to compound i. The initial flow rates were calculated by Equation (14).

$$\dot{n}_{i,0} = \frac{V\%_i \cdot \dot{V}_{tot}}{V_m} \quad (14)$$

Where V_m= molar volume, 0.022414 l/mmol at STP. STP was defined as 273.15 K and 1.01325 bar. The nitrogen flow was assumed to remain constant, see Equation (15). The molar flows of TCD components H_2, CO, CO_2 and C_2-hydrocarbons in the outlet were calculated by Equation (16).

$$\dot{n}_{N_2,0} = \dot{n}_{N_2} \quad (15)$$

$$\dot{n}_i = \frac{\left(\frac{A_i}{RF_{H_2}}\right)}{A_{N_2}} \cdot \dot{n}_{N_2} \quad (16)$$

A correlation between the TCD and FID values was determined by analysing methane in the calibration gas. The column connected to the FID did not separate methane and C_2-products. According to earlier in-house experience a fair assumption was that 2/3 of the C_1+C_2 products would be methane. Hence, the molar flow of methane could be calculated.

$$\dot{n}_{CH_4} = \frac{0.667 \cdot A_{C1+C2,FID}}{RF_{CH_4,TCD} \cdot \frac{A_{CH_4,FID}}{A_{CH_4,\,TCD}}} \cdot \frac{\dot{n}_{N_2}}{A_{N_2}} \quad (17)$$

The molar flows of the compounds recognized by FID were calculated using the methane flow.

$$\dot{n}_{i,FID} = \frac{1}{M_i} \cdot \frac{\frac{A_i}{RF_i}}{\frac{A_{CH_4,TCD} \cdot \frac{A_{CH_4,FID}}{A_{CH_4,\,TCD}}}{RF_{CH4,FID}}} \cdot \dot{n}_{CH_4,TCD} \cdot M_{CH_4} \quad (18)$$

The total carbon flow out of the reactor was thus calculated by adding the molar carbon flows of all carbon products.

The conversion was calculated based on Equation (19).

$$X_{CO_2} = \frac{\dot{n}_{CO_2,0} - \dot{n}_{CO_2}}{\dot{n}_{CO_2,0}} \cdot 100\% \quad (19)$$

However, the CO_2 GC peaks fluctuated more than expected between samples. This resulted in that the calculated conversions did not correlate with the amount of formed products. Therefore, Equation (20), assuming the carbon mass balance being 100%, was used for conversion calculations for samples where the problem became apparent.

$$X_{CO_2} = \frac{\dot{n}_{C,OUT}}{\dot{n}_{CO_2,0}} \cdot 100\% \quad (20)$$

Where $\dot{n}_{C,OUT}$ is the sum of carbon molar flows of carbon products. For the Cu catalyst, where mostly carbon monoxide and methanol were formed, another approach for conversion calculations was used.

$$X_{CO_2} = Y_{MeOH}^{CO_2} + Y_{CO}^{CO_2} \quad (21)$$

The yield for the Fe-based catalyst samples was calculated by Equation (22).

$$Y_i^{CO_2} = \frac{N_{C,i} \cdot \dot{n}_{i,\,out}}{\dot{n}_{CO_2,0}} \cdot 100\% \quad (22)$$

Where N refers to the amount of carbon atoms in component i. For the Cu-catalyst, another approach was used for calculating the yield. The methanol flow was first calculated by Equation (23).

$$\dot{n}_{MeOH} = \frac{\frac{A_{MeOH}}{RF_{\frac{MeOH}{CH_4}}}}{\frac{A_{CH_4,\,FID}}{A_{CH_4,\,TCD}} \cdot A_{N_2}} \cdot \dot{n}_{N_2} \quad (23)$$

Where RF_{MeOH}=1.857, which had been determined in an earlier thesis (Frilund 2016). The yields of CO and methanol for the Cu catalyst were then defined by Equation (22).

The selectivity of each product was calculated with the same method for all catalysts.

$$S_i^{CO_2} = \frac{Y_i^{CO_2}}{X_{CO_2}} \cdot 100\% \quad (24)$$

The weight hourly space velocity (WHSV) was defined as Equation (25).

$$WHSV = \frac{\dot{m}_{i.0}}{m_{cat}} \quad (25)$$

Where $\dot{m}_{i,0}$ refers to the initial mass flow of component i and m_{cat} to the catalyst weight.

8 Results and discussion

8.1 TPD and pulse reaction experiments

Characterization of the catalyst was conducted by adsorbing H_2 or CO_2 in 25 °C, followed by temperature programmed desorption by increasing the temperature by 5 °C/min to 500 °C. The amount of adsorbed and desorbed H_2 and CO_2 for each of the studied catalyst in TPD experiments is presented Table 15.

Table 15. Amount of adsorbed and desorbed H_2 and CO_2 from studied catalysts. The adsorption tests were conducted in 25 °C at atmospheric pressure.

	H_2		CO_2	
Catalyst	Adsorbed [µmol/g]	Desorbed [µmol/g]	Adsorbed [µmol/g]	Desorbed [µmol/g]
Cu	0	5.2	43.8	45.8
Ni	56.4	57.0	0	0
FeMn	0	0	89.2	96.7
low α-Fe	0	0	0.2	0

For the pulse reaction tests the temperature was set to 300 °C. The measured reaction temperatures and catalyst weights are presented in Table 16.

Table 16. Measured reaction temperatures and catalyst masses in TPD experiments.

Catalyst	T_{meas} [°C]	m_{cat} [g]
Cu	296.7 ± 0.3°C	1.335
Ni	292.8 ± 0.3°C	0.748
FeMn	306.5 ± 0.3°C	0.731
low α-Fe	301.6 ± 0.3°C	0.979

CO_2 was then pulsed in a constant H_2 flow. It was noted that only methane and carbon monoxide was detected and consequently formed of the products. Hence, the main reactions of the pulse reaction tests were assumed to be the methanation reaction (26), the RWGS (27) and the FT synthesis to methane (28).

$$CO_2 + 4H_2 \leftrightarrow CH_4 + 2H_2O \quad (26)$$

$$CO_2 + H_2 \leftrightarrow CO + H_2O \quad (27)$$

$$CO + 3H_2 \leftrightarrow CH_4 + H_2O \quad (28)$$

As discussed in section 3.5.1, MEA can decompose by oxidative degradation, polymerization of carbamate or thermal degradation. Since the temperature of the reaction tests (300 ^{o}C) is significantly higher than the reported temperature for MEA degradation (205 ^{o}C) it is expected that MEA, to some extent, degrades to ammonia, aldehydes and carboxylic acid (Chi & Rochelle 2002) during the reaction tests. Some minor degradation products include nitrates and nitrites, NO_x/N_2O, CO, C_2H_4, acetaldehyde and formaldehyde (Sexton & Rochelle 2011). The effect of MEA on methane formation for each catalyst is presented in Table 17. In addition, the amount of moles of pulsed CO_2 per catalyst weight is presented.

Table 17. Effect of MEA on CH_4 formation for catalysts in pulse reaction tests. The values of formed methane refer to amount of CH_4 formed from one pulse CO_2. Reaction conditions were T=300 ^{o}C at atmospheric pressure.

Catalyst	Pulsed CO_2 [$\mu mol_{CO2}/g_{cat}$]	Formation of CH_4 [$\mu mol_{CH4}/g_{cat}$]		
		Initial reaction	Reaction with MEA	Recovery
Cu	33.4	1.3	1.5	1.1
Ni	59.6	24.5	23.0	18.6
FeMn	61.0	7.3	2.8	3.0
low α-Fe	45.6	7.5	9.7	7.5

The effect of H_2S on formation of CH_4 on catalysts in pulse reaction tests is presented in Table 18. The total amount of moles of pulsed H_2S per catalyst weight is presented in Table 19.

Table 18. Effect of H_2S on CH_4 formation of catalysts in pulse reaction tests. Reaction conditions were T=300 ^{o}C at atmospheric pressure. [a]Not tested. [b]Poisoning gas.

	Formation of CH_4 [$\mu mol_{CH4}/g_{cat}$]								
V [ml] of PG[b] pulsed	0	1	2	4	6	9	14	20	25
Cu	0.8	0.8	0.7	0.6	0.6	0.6	0.6	[a]	[a]
Ni	18.9	17.8	17.5	16.9	16.5	16.4	15.2	14.8	14.4
FeMn	2.2	2.2	2.1	2.0	1.9	2.0	2.0	2.0	1.8
low a-Fe	6.7	6.6	6.4	6.0	6.7	6.2	6.1	5.8	6.0

Table 19. Total amount of moles H_2S per catalyst weight. [a]Not tested. [b]Poisoning gas.

	Total H_2S poisoning [$\mu mol_{H2S}/g_{cat}$]							
V [ml] of PG[b] pulsed	1	2	4	6	9	14	20	25
Cu	0.003	0.007	0.01	0.02	0.03	0.05	[a]	[a]
Ni	0.006	0.01	0.02	0.04	0.05	0.08	0.12	0.15
FeMn	0.006	0.01	0.02	0.4	0.05	0.09	0.12	0.15
low a-Fe	0.005	0.009	0.02	0.03	0.04	0.06	0.09	0.11

8.1.1 Cu catalyst

The Cu catalyst adsorbed CO_2 (Table 15), whereas no H_2 was adsorbed. Figure 13 illustrates the effect of MEA on methane formation for the Cu catalyst.

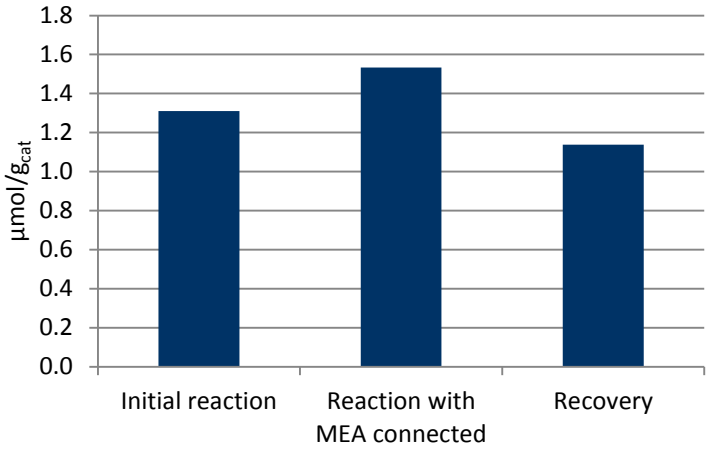

Figure 13. Effect of MEA on CH_4 formation for Cu catalyst. The tests were conducted in a constant H_2 flow by pulsing CO_2 at T=300 °C in atmospheric pressure.

Each column refers to the amount of formed methane from 1 ml pulsed CO_2 (corresponding to 33.4 $\mu mol/g_{cat}$). Interestingly, the formation of methane is increased when MEA was fed to the carrier gas. The reason for this is not known, but since the total amount of formed methane was fairly low, one possibility is simply inaccuracy in experimental setup or calculations. However, when comparing the mass spectra before and during MEA poisoning (see Appendix 4, Figure 1 and Figure 2) it can be noticed that the formation of water was increased during CO_2 pulsing when MEA was fed to the reactor (Appendix 4, Figure 2). This would indicate that more products, to which water was a by-product, were formed. The methane peaks are also broader in size during MEA poisoning than before and after. This eliminates the possibility of a calculation mistake.

The methanation reaction (3), produces more water (2:1) than the methanol synthesis in correlation to carbon dioxide. Thus, one explanation is that MEA and its degradation products affect the selectivity of the catalyst towards forming more methane. However, the recovery stage shows that when MEA feed was stopped the formation of methane dropped slightly below the formation of the initial reaction. This, on the other hand, is supporting a study conducted by Quinn et al. (2004), who concluded that nitrogen-containing compounds, such as ammonia, appeared to have no effect on an $CuO/ZnO/Al_2O_3$ catalyst. The effect of H_2S on methane formation is presented in Figure 14.

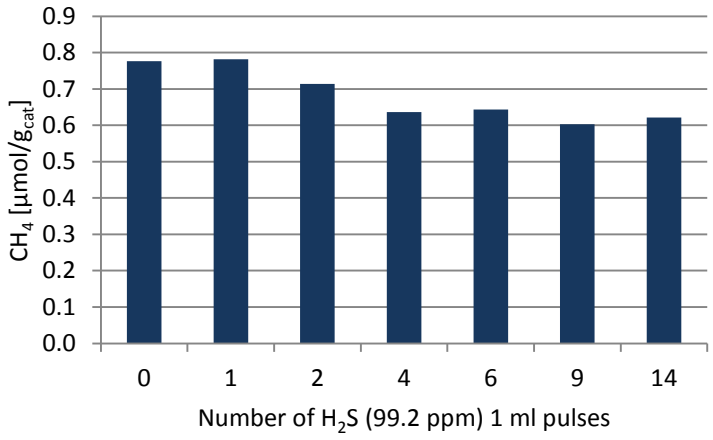

Figure 14. Effect of H_2S on CH_4 formation for Cu catalyst. The tests were conducted in a constant H_2 flow by pulsing CO_2 at T=300 ^{o}C in atmospheric pressure.

As expected, the formation of methane was decreased when H_2S was pulsed at the catalyst. After four pulses of H_2S (0.01 $\mu mol_{H2S}/g_{cat}$) the CH_4 formation had decreased by 18%. After 14 pulses (0.05 $\mu mol_{H2S}/g_{cat}$) the catalyst produced 20% less methane than initially. However, it should be noted that the amount of formed methane is remarkably low compared to e.g. the CH_4 formation for the Ni catalyst, since a Cu catalyst is unsuitable for methane formation. Nevertheless, no methanol, which is the favoured product of Cu catalysts, was detected by the MS, probably because the methanol synthesis requires higher pressures.

8.1.2 Ni catalyst

The Ni catalyst adsorbed and desorbed H_2 (see Table 15), whereas no CO_2 was adsorbed or desorbed by the catalyst. Figure 15 illustrates the effect of MEA on the Ni catalyst.

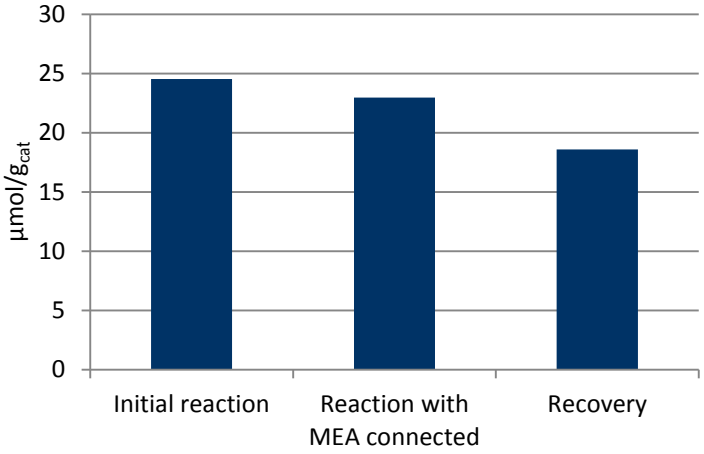

Figure 15. Effect of MEA on CH_4 formation for Ni catalyst. The tests were conducted in a constant H_2 flow by pulsing CO_2 at T=300 °C in atmospheric pressure.

The Ni catalyst is a well-known methanation catalyst and produces a great amount of methane compared to the other catalysts (Wang et al. 2011). One pulse CO_2 (59.6 µmol/g_{cat}) formed 24.5 µmol/g_{cat} CH_4 in the initial reaction. The formation of CH_4 was decreased when the catalyst was exposed to MEA. In addition, the recovery phase shows a small drop in methane formation compared to the formation when MEA was fed. Figure 4-Figure 6 in Appendix 4 present the mass spectra of reaction tests with MEA. Figure 16 presents the effect of H_2S on methane formation for the Ni-based catalyst.

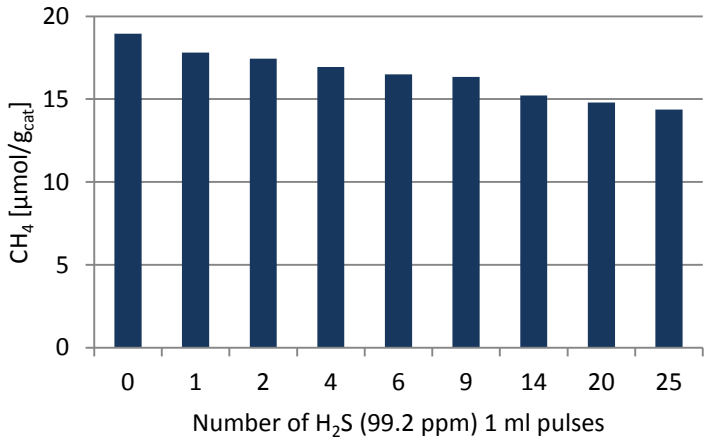

Figure 16. Effect of H_2S on CH_4 formation for Ni catalyst. The tests were conducted in a constant H_2 flow by pulsing CO_2 at T=300 °C in atmospheric pressure.

The Ni catalyst was sensitive to H_2S and lost its activity gradually when exposed to H_2S. A quite linear decrease in methane formation can be seen in both Figure 15 and Figure 16. The behaviour of H_2S is expected; however, the continued decrease in methane formation after MEA feed was stopped was unexpected. Thus, one reason to the continuous decrease in catalyst activity could be coking of the catalyst.

8.1.3 Fe-based catalyst

The FeMn catalyst adsorbed and desorbed CO_2, while no adsorption of CO_2 or H_2 was observed for the low α-Fe catalyst (Table 15). Figure 17 and Figure 18 present the effect of MEA on the Fe-based catalysts.

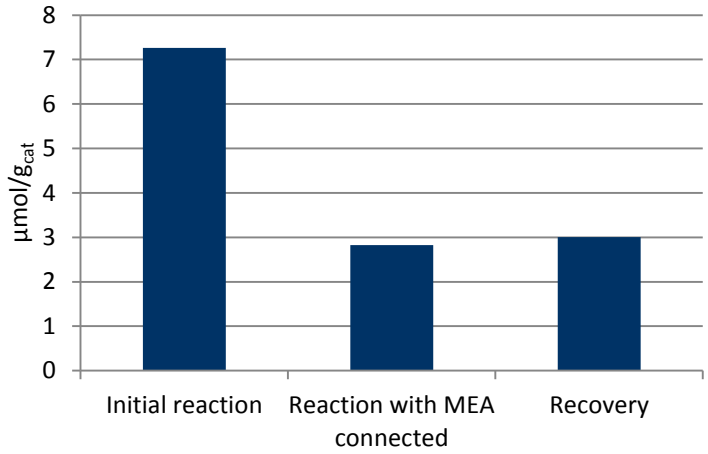

Figure 17. Effect of MEA on CH_4 formation for FeMn catalyst. The tests were conducted in a constant H_2 flow by pulsing CO_2 at T=300 °C in atmospheric pressure.

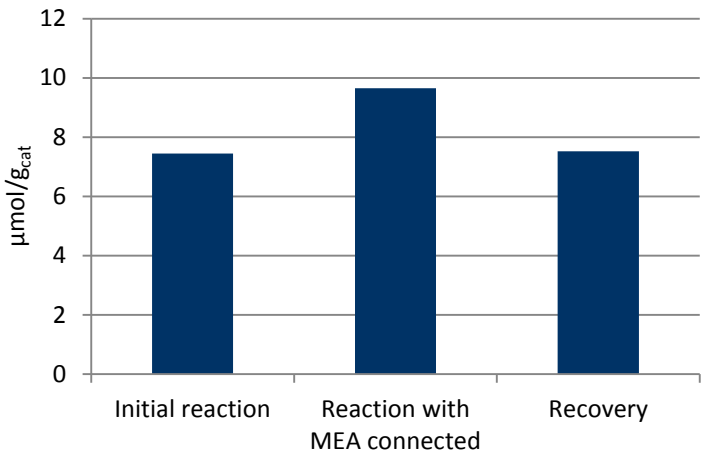

Figure 18. Effect of MEA on CH_4 formation for low α-Fe catalyst. The tests were conducted in a constant H_2 flow by pulsing CO_2 at T=300 ^{o}C in atmospheric pressure.

The effect of MEA differs drastically between the two Fe-based catalysts. One reason to this is the difference in metal content of the catalysts (5% for FeMn compared to >90% for low α-Fe). The FeMn catalyst was an impregnated catalyst with active sites scattered on the support, while the low a-Fe catalyst was precipitated, thus consisting only of active metals. The FeMn catalyst appeared to be quite sensitive to the exposure of MEA, and the formation rate of methane dropped drastically for the reaction tests with MEA. In addition, the catalyst did not recover from the MEA exposure. An explanation for this behaviour could be that e.g. NO_x compounds, that can be a minor degradation product from MEA (Sexton & Rochelle 2011), react with the active iron carbides to form magnetite (Ma et al. 2015a). Thus, active sites of the catalyst are lost.

Interestingly, the low α-Fe catalyst performed better when MEA was fed to the system. However, the catalyst returned to the initial formation rate of methane when MEA feed was stopped. Ma et al. (2015a) studied the effect of ammonia on iron catalysts and observed that during 400 ppm NH_3 poisonings on a Fe catalyst, the selectivity of light hydrocarbons increased. Since the TPD tests only focus on methane formation, there is a possibility that the methane selectivity and amount has increased with the loss of other products that were not monitored, such as higher hydrocarbons. The low α-Fe catalyst produced several different hydrocarbons (presented later in Figure 25), so there is a possibility that the selectivity has simply increased for only methane formation.

Appendix 4 presents the mass spectra for the tests with Fe-based catalysts. Figure 19 and Figure 20 illustrate the effect of H_2S on Fe-based catalysts.

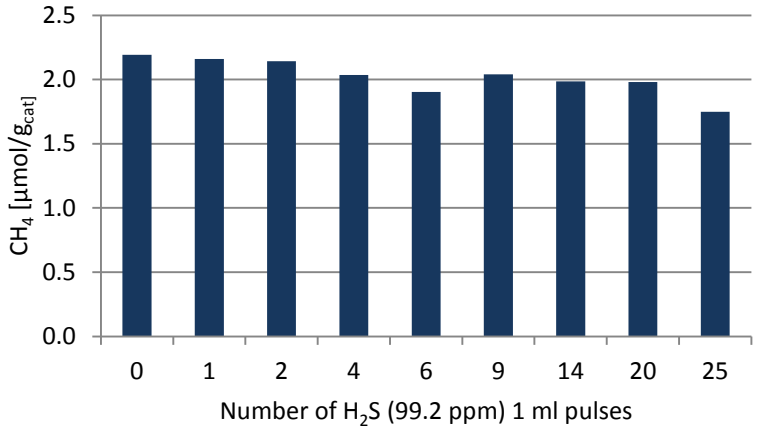

Figure 19. Effect of H_2S on CH_4 formation for FeMn catalyst. The tests were conducted in a constant H_2 flow by pulsing CO_2 at T=300 °C in atmospheric pressure.

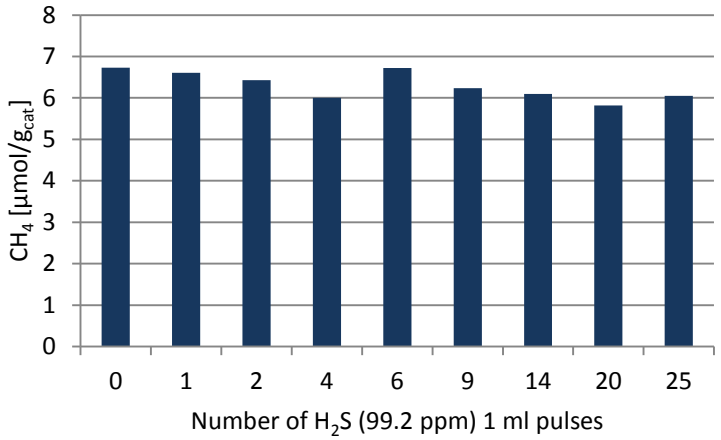

Figure 20. Effect of H_2S on CH_4 formation for low α-Fe catalyst. The tests were conducted in a constant H_2 flow by pulsing CO_2 at T=300 °C in atmospheric pressure.

Both catalysts showed a slight decrease in activity during H_2S poisoning. However, the effect was not as significant as for Cu and Ni catalysts. It should be noted when evaluating the results that the FeMn catalyst already had been partly deactivated by MEA prior to the H_2S poisoning (see Figure 9).

Interestingly, the low α-Fe catalyst showed an increase in activity after 6 ml of the H_2S containing poisoning gas (corresponding to 0.03 $\mu mol_{H2S}/g_{cat}$) had been pulsed. This may be either an erroneous point or a positive effect of H_2S that has been discussed in several studies (Stenger & Satterfleld 1985; Karn et al. 1963; Bromfield & Coville 1999). As mentioned in section 4.3.2, the effect of H_2S on Fe catalysts is slightly contradictory, as sulphur has been shown to both increase and decrease catalytic activity.

8.1.4 Conclusion

Figure 21 summarizes the effect of MEA on catalysts. It can be assumed that MEA degrades to some extent to ammonia, aldehydes and carboxylic acids.

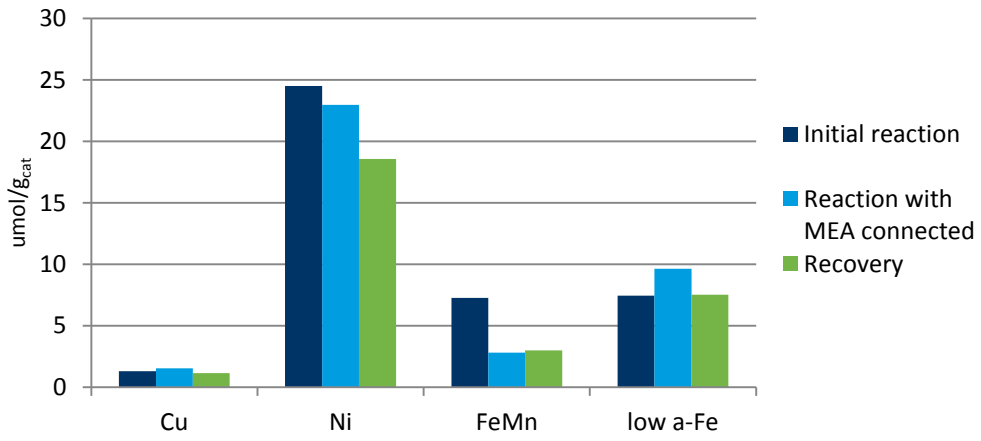

Figure 21. Catalyst comparison of the effect of MEA on CH_4 formation.

The formation of methane was increased during MEA poisoning for the Cu and low α-Fe catalysts, but returned to the initial state when MEA feed was stopped. The reason of this is unknown, but a change in selectivity is a possible explanation to the behaviour. Since MEA is carried into the system by the carrier gas, it can be excluded that e.g. a degradation product of MEA with the same atomic mass as methane would be the reason for the increased amount of formed product.

In contrast, the formation of methane was decreased during MEA feed for the FeMn catalyst. The catalyst did not recover from the MEA poisoning, which would support the theory that iron carbide is oxidized to magnetite by e.g. NO_x compounds originating

from MEA. The Ni catalyst shows a linear decrease even after MEA feed was stopped. The reason for the continuous decrease in activity is believed to be coking of the catalyst.

A catalyst comparison of the effects of H_2S is presented in Figure 22. When studying the graph, it should be taken into account that the Cu catalyst was exposed to only 14 H_2S pulses, when all other catalysts were exposed to 25 pulses. In addition, the catalyst masses differ, and thus a catalyst comparison where number of H_2S pulses is the only parameter is not entirely precise. However, Table 19 presents the total amount of H_2S that have been pulsed per catalyst weight for each catalyst. The numbers above the columns in Figure 22 refer to the percent of formed methane compared to initially formed methane of the catalyst. Initial CH_4 formation [µmol/g_{cat}] for each catalyst is found in the upper right corner.

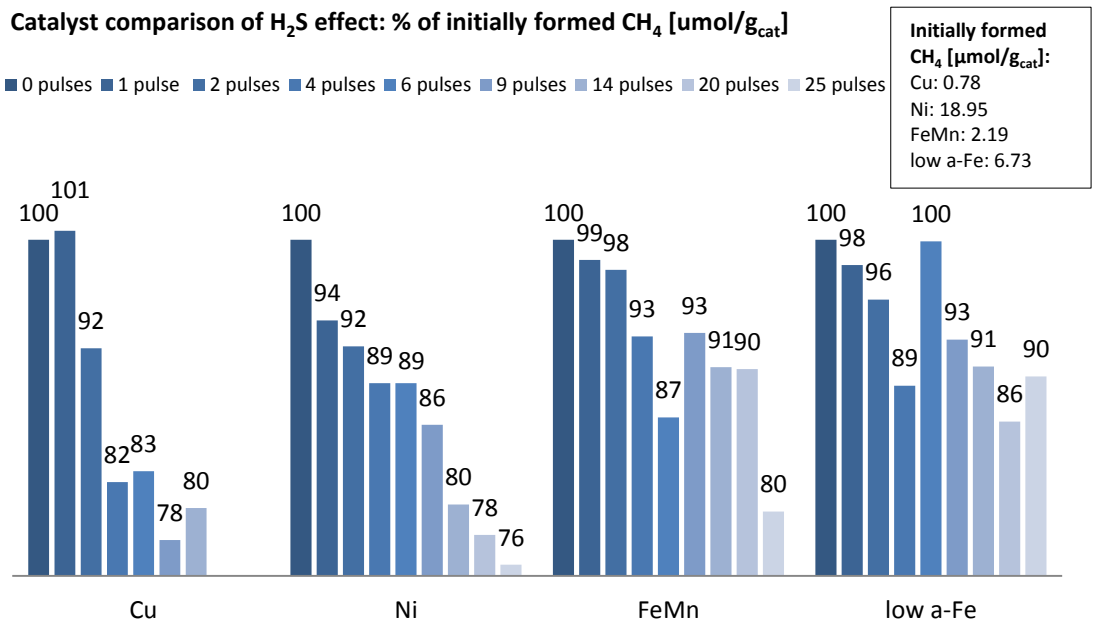

Figure 22. Catalyst comparison of H_2S effect. The numbers above columns refer to the percent of formed CH_4 compared to initially formed CH_4 by the catalyst.

It appears as if the Fe-based catalysts were less sensitive to H_2S than Ni and Cu catalysts during the prevailing conditions. As seen in Figure 22, the decrease in CH_4 formation is steeper for Ni and Cu catalyst. The Cu and Ni catalysts have lost around 20% of their

activity after 14 ml of the poisoning gas have been pulsed to the system, while the Fe-based catalysts only have lost 9% of their activity after 14 pulses.

8.2 Reaction tests

In the following section, the results of the reaction tests are discussed for each catalyst separately. The results of the calibration tests with calculated response factors are presented in Table 20.

Table 20. Calibration tests for reaction tests in plug flow reactor.

Test		Composition					RF			
	Gas[a]	N_2	H_2	CO_2	CO	CH_4	H_2	CO_2	CO	CH_4
124	RG	5	71.3	23.7	0	0	11.11	1.01	-	-
125	RG	5	71.3	23.7	0	0	11.26	1.03	-	-
126	RG	5	71.3	23.7	0	0	11.25	1.02	-	-
127	Calib	52	15	15	15	3	11.67	1.04	0.95	3.19
128	Calib	52	15	15	15	3	11.52	1.05	0.95	3.21
129	Calib	52	15	15	15	3	11.50	1.06	0.95	3.20
[a]RG= Reaction gas, Calib=Calibration gas							11.38	1.03	0.95	3.20

8.2.1 Cu catalyst

CO_2 hydrogenation to methanol was used as the test reaction with the Cu catalyst. The reaction tests for the Cu catalyst were conducted at set point 230 ^{o}C and 30 bar pressure. All Cu reaction tests are presented in Table 21.

Table 21. Cu catalyst reaction tests conducted in plug flow reactor.

Stage	T.o.S.	Test	T_{meas}	$\dot{V}_{RG}$	$\dot{V}_{PG}$	c_{H2S}	WHSV		
	[h]	number	°C	[nl/h]	[l/h]	[ppm]	CO_2 [g/h·g_{cat}]	H_2 [g/h·g_{cat}]	H_2S [g/h·g_{cat}]
Initial	8	244	234.2	10.0	0.0	0.0	1.9	0.3	0
		245	234.1	10.0	0.0	0.0	1.9	0.3	0
		246	234.1	10.0	0.0	0.0	1.9	0.3	0
		247	234.1	10.0	0.0	0.0	1.9	0.3	0
		248	234	10.0	0.0	0.0	1.9	0.3	0
		249	234.1	10.0	0.0	0.0	1.9	0.3	0
		250	234	10.0	0.0	0.0	1.9	0.3	0
		251	234	10.0	0.0	0.0	1.9	0.3	0
1st poisoning	72	254	233.6	6.7	3.4	33.2	1.2	0.2	$1.8\cdot10^{-7}$
		255	233.5	6.7	3.4	33.2	1.2	0.2	$1.8\cdot10^{-7}$
		256	233.5	6.7	3.4	33.2	1.2	0.2	$1.8\cdot10^{-7}$
		257	233.5	6.7	3.4	33.2	1.2	0.2	$1.8\cdot10^{-7}$
		258	233.5	6.7	3.4	33.2	1.2	0.2	$1.8\cdot10^{-7}$
		259	233.5	6.7	3.4	33.2	1.2	0.2	$1.8\cdot10^{-7}$
		260	233.5	6.7	3.4	33.2	1.2	0.2	$1.8\cdot10^{-7}$
		261	233.5	6.7	3.4	33.2	1.2	0.2	$1.8\cdot10^{-7}$
		262	233.5	6.7	3.4	33.2	1.2	0.2	$1.8\cdot10^{-7}$
		263	233.4	6.7	3.4	33.2	1.2	0.2	$1.8\cdot10^{-7}$
1st recovery	16	265	234.1	10.0	0.0	0.0	1.9	0.3	0
		266	234	10.0	0.0	0.0	1.9	0.3	0
		267	234	10.0	0.0	0.0	1.9	0.3	0
		268	234.1	10.0	0.0	0.0	1.9	0.3	0
		269	234	10.0	0.0	0.0	1.9	0.3	0
2nd poisoning	8	290	232.6	4.7	7.1	60.0	0.9	0.1	$3.7\cdot10^{-7}$
		291	232.6	4.7	7.1	60.0	0.9	0.1	$3.7\cdot10^{-7}$
		292	232.4	4.7	7.1	60.0	0.9	0.1	$3.7\cdot10^{-7}$
		293	232.4	4.7	7.1	60.0	0.9	0.1	$3.7\cdot10^{-7}$
		294	232.2	4.7	7.1	60.0	0.9	0.1	$3.7\cdot10^{-7}$
2nd recovery	8	304	233.7	10.0	0.0	0.0	1.9	0.3	0
		305	233.8	10.0	0.0	0.0	1.9	0.3	0
		306	233.8	10.0	0.0	0.0	1.9	0.3	0
		307	233.8	10.0	0.0	0.0	1.9	0.3	0
		308	233.6	10.0	0.0	0.0	1.9	0.3	0
		309	233.7	10.0	0.0	0.0	1.9	0.3	0
		310	233.6	10.0	0.0	0.0	1.9	0.3	0
		311	233.5	10.0	0.0	0.0	1.9	0.3	0

Poisoning gas 2, consisting of 99.2 ppm H_2S, was used during the poisoning stages. Thus, the poisoning concentrations were 33.2 ppm H_2S ($WHSV_{H2S}=1.8\cdot10^{-7}$ $g_{H2S}/h\cdot g_{cat}$) for the 1st poisoning and 60 ppm H_2S ($WHSV_{H2S}=3.7\cdot10^{-7}$ $g_{H2S}/h\cdot g_{cat}$) for the 2nd poisoning. The results from the reaction tests in the plug flow reactor are shown in Table 22.

Table 22. Results for all poisoning stages for Cu catalyst at conditions T=230 °C and p=30 bar.

	Conversion [%]	Yield [%]		Selectivity [%]		
	$X(CO_2)$	Y(CO)	Y(MeOH)	S(CO)	S(MeOH)	S(others)
Reactant gas	17.5	9.6	7.9	54.7	45.3	0.004
1st poisoning	13.9	9.2	4.7	66.2	33.7	0.191
Recovery	12.7	7.3	5.4	57.5	42.3	0.212
2nd poisoning	14.2	10.5	3.7	73.8	26.1	0.105
Recovery	15.6	9.1	6.5	57.8	41.7	0.554

The change in conversion and selectivities of products between stages is illustrated in Figure 23, where the right side axis denotes the conversion and the left side axis the selectivity.

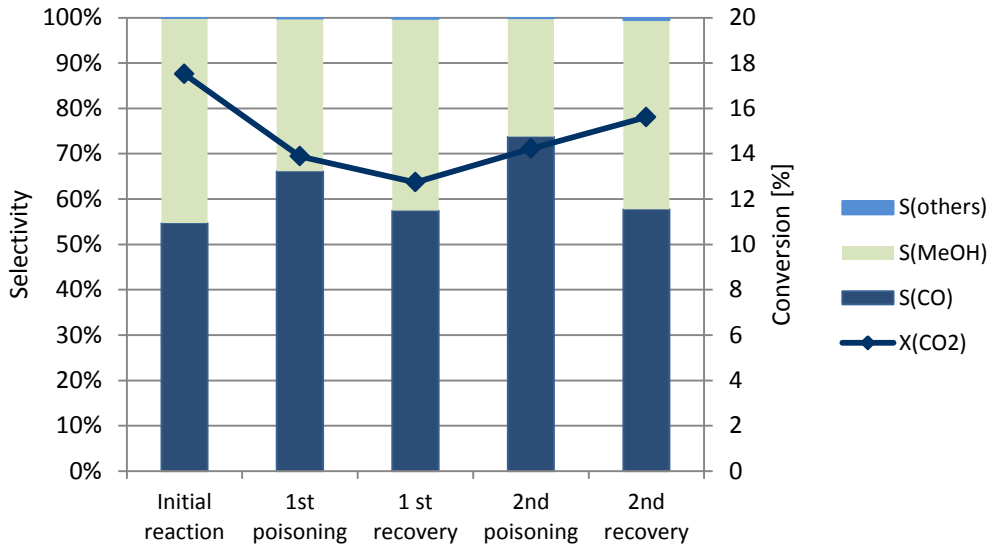

Figure 23. Change in conversion and selectivity during poisoning of Cu catalyst by H_2S. The H_2S concentration during 1st poisoning was 33.2 ppm and during 2nd poisoning 60 ppm. The reaction conditions were T=230 °C at p=30 bar.

The main product of the reaction is methanol and CO, which combined selectivities are above 99.45% in all five stages. The main part of other products formed is methane and ethane, of which selectivities reach a maximum of 0.17% and 0.01%, respectively, during the 2nd recovery stage. During the poisoning stages, the selectivity of CO increases on the expense of methanol with more than 10% compared to the initially and recovery stages. The yields of methanol and CO (Table 22) suggest that the formation of CO remains rather constant during H_2S poisoning, while the formation of methanol is

decreased. The RWGS reaction (1), which decomposes CO_2 to CO, competes with the CO_2 hydrogenation reaction (4). At high temperatures, such as 230 ^{o}C, the RWGS has a lower Gibbs free energy than the CO_2 hydrogenation reaction (Arena et al. 2014), resulting in being more spontaneous than the CO_2 hydrogenation reaction. Hence, the CO_2 hydrogenation is more dependent on the activity of the catalyst than the RWGS. Therefore, the decrease in methanol formation could be described by that some active sites are deactivated by H_2S by site blocking.

Another explanation for the increase in selectivity for CO during poisoning is that the weight hourly space velocities (WHSV) and partial pressures of CO_2 and H_2 are significantly lower during the poisoning experiments. The WHSV of CO_2 is 1.9 $g_{CO2}/h \cdot g_{cat}$ during the initial and recovery stages, but only 1.2 $g_{CO2}/h \cdot g_{cat}$ and 0.9 $g_{CO2}/h \cdot g_{cat}$ during the first and second poisoning, respectively. A longer contact time with a highly active catalyst could trigger secondary reactions, such as decomposition of methanol to CO or increase the extent of RWGS reaction (Yoshihara & Campbell 1996).

A drop in conversion from 17.5% to 13.9% is observed during the first poisoning stage (i.e. poisoning by 33.2 ppm). This would suggest that H_2S blocks the active sites of the catalyst. During the next stages, the conversion remains rather stable until the 2nd recovery. The second recovery demonstrates a conversion of 15.6%, which implies a conversion drop of only 1.9% compared to the initial reaction. Thus, it would suggest that the poisoning to some extent is reversible. Hence, the activity of the Cu catalyst appears to remain rather stable. According to earlier studies, e.g. a study conducted by Twigg & Spencer (2001), Cu catalyst are extremely sensitive to H_2S, and the H_2S level should be below 1 ppm in order for the catalyst activity to remain constant. However, the activity of the BASF Cu catalyst that was studied in this experiment remained surprisingly well. The catalyst consists of 15-20 weight% ZnO, which is known to limit the poisoning by forming thermodynamically stable zinc sulphide (ZnS) according to Reaction (6) (Twigg & Spencer 2001). However, this cannot be the only reason for the well-maintained activity, since the out-going concentration of sulphur was controlled with a Dräger pump.

8.2.2 FeMn catalyst

Table 23 summarizes the reactions measurements with the FeMn catalyst.

Table 23. FeMn catalyst reaction tests conducted in plug flow reactor.

Stage	T.o.S.	Test	T_{meas}	$\dot{V}_{RG}$	$\dot{V}_{PG}$	c_{H2S}	WHSV		
	[h]	number	°C	[nl/h]	[nl/h]	[ppm]	CO_2 [g/h·g_{cat}]	H_2 [g/h·g_{cat}]	H_2S [g/h·g_{cat}]
Initial	8	174	304	10.0	0.0	0.0	1.9	0.3	0
		175	303.9	10.0	0.0	0.0	1.9	0.3	0
		176	303.9	10.0	0.0	0.0	1.9	0.3	0
1st poisoning	24	200	303.6	6.7	3.4	33.2	1.2	0.2	$1.8\cdot10^{-7}$
		201	303.6	6.7	3.4	33.2	1.2	0.2	$1.8\cdot10^{-7}$
		202	303.6	6.7	3.4	33.2	1.2	0.2	$1.8\cdot10^{-7}$
		203	303.6	6.7	3.4	33.2	1.2	0.2	$1.8\cdot10^{-7}$
		204	303.8	6.7	3.4	33.2	1.2	0.2	$1.8\cdot10^{-7}$
		205	303.7	6.7	3.4	33.2	1.2	0.2	$1.8\cdot10^{-7}$
		206	303.8	6.7	3.4	33.2	1.2	0.2	$1.8\cdot10^{-7}$
		207	303.8	6.7	3.4	33.2	1.2	0.2	$1.8\cdot10^{-7}$
		208	303.7	6.7	3.4	33.2	1.2	0.2	$1.8\cdot10^{-7}$
		209	303.7	6.7	3.4	33.2	1.2	0.2	$1.8\cdot10^{-7}$
		210	303.7	6.7	3.4	33.2	1.2	0.2	$1.8\cdot10^{-7}$
		211	303.8	6.7	3.4	33.2	1.2	0.2	$1.8\cdot10^{-7}$
		212	303.7	6.7	3.4	33.2	1.2	0.2	$1.8\cdot10^{-7}$
		213	303.7	6.7	3.4	33.2	1.2	0.2	$1.8\cdot10^{-7}$
		214	303.7	6.7	3.4	33.2	1.2	0.2	$1.8\cdot10^{-7}$
2nd poisoning	24	217	303.7	6.0	9.1	59.8	1.1	0.2	$4.7\cdot10^{-7}$
		218	303.7	6.0	9.1	59.8	1.1	0.2	$4.7\cdot10^{-7}$
		219	303.5	6.0	9.1	59.8	1.1	0.2	$4.7\cdot10^{-7}$
		220	303.5	6.0	9.1	59.8	1.1	0.2	$4.7\cdot10^{-7}$
		221	303.4	6.0	9.1	59.8	1.1	0.2	$4.7\cdot10^{-7}$
		222	303.3	6.0	9.1	59.8	1.1	0.2	$4.7\cdot10^{-7}$
2nd recovery	24	226	303.7	10.0	0.0	0.0	1.9	0.3	0
		227	303.7	10.0	0.0	0.0	1.9	0.3	0
		228	303.6	10.0	0.0	0.0	1.9	0.3	0
		229	303.5	10.0	0.0	0.0	1.9	0.3	0
		230	303.5	10.0	0.0	0.0	1.9	0.3	0
		231	303.6	10.0	0.0	0.0	1.9	0.3	0
		233	303.9	10.0	0.0	0.0	1.9	0.3	0
		234	303.8	10.0	0.0	0.0	1.9	0.3	0

The reaction tests with the in-house impregnated FeMn catalyst were conducted at 300 °C and 25 bar pressure. Poisoning gas 2 was used in both poisoning stages, resulting in poisoning concentration of 33.2 ppm ($WHSV_{H2S}=1.8\cdot10^{-7}$ $g_{H2S}/h\cdot g_{cat}$) and 59.8 ppm ($WHSV_{H2S}=4.7\cdot10^{-7}$ $g_{H2S}/h\cdot g_{cat}$) for the 1st and 2nd poisoning, respectively. Conversion,

reaction yield and selectivities are presented for some products in Table 24 and Table 25.

Table 24. Calculated conversion and yields for experiments with FeMn catalyst at T=300 °C and p=25 bar.

	Conversion [%]	Yield [%]						
	CO_2	CO	C1+C2	C3+C4	C5-C12	MeOH	EtOH	PrOH
Reactant gas	18.82	3.7	10.978	2.131	0.398	2.2	0.087	0.012
1st poisoning	0.03	0	0.006	0.002	0	0	0	0
2nd poisoning	0.01	0	0.004	0.001	0	0	0	0
Recovery	0.11	0	0.059	0.011	0	0	0.002	0.001

Table 25. Calculated selectivities for experiments with FeMn catalyst at T=300 °C and p=25 bar.

Selectivity [%]	CO	C1+C2	C3+C4	C5-C12	MeOH	EtOH	PrOH	Others
Reactant gas	19.7	58.3	11.3	2.2	11.8	0.5	0.06	0
1st poisoning	0	18.1	5.8	0	75.4	0.4	0	0.25
2nd poisoning	0	35.5	8.3	0	56.0	0	0	0.25
Recovery	0	55.6	10.2	0	28.6	2.0	0.62	2.98

The change in conversion and selectivities between stages is showed in Figure 24. The right side axis denotes the conversion and the left side axis the selectivity.

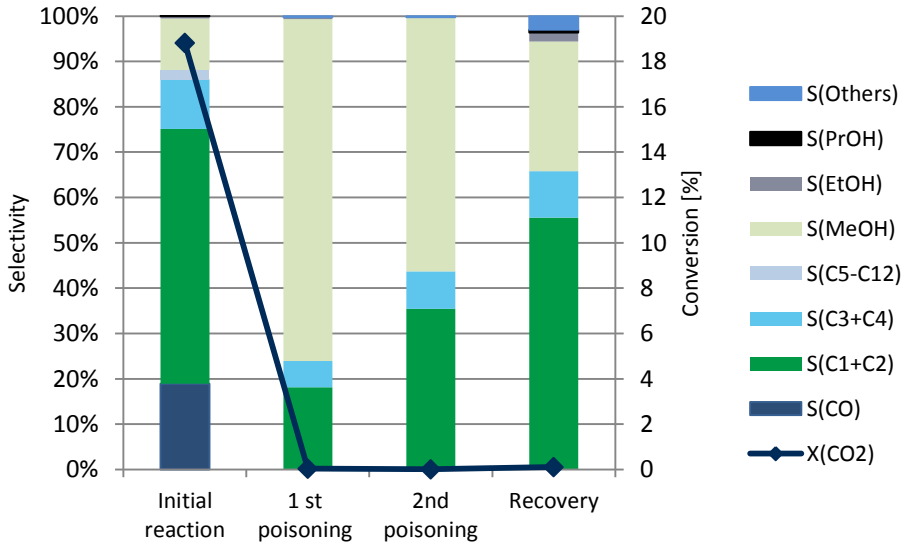

Figure 24. Change in conversion and selectivities of products during H_2S poisoning of FeMn-catalyst. The H_2S poisoning levels were 33.2 ppm and 59.8 ppm. Reaction conditions were T=300 °C and p=25 bar. "Others" refers to C13+ and all oxygenates except for methanol, ethanol and propanol.

As presented in Figure 24, the FeMn catalyst was very sensitive to H_2S, and the conversion dropped drastically already at the 1st poisoning stage and did not recover. The initial reaction's main products were lower hydrocarbons, carbon monoxide and methanol. For the poisoning and recovery stages the methanol selectivity increased compared to the initial reaction. In addition, the selectivity of methane and CO decreased during the first poisoning, which would support a study conducted by Ma et al. (2015b), which concluded that adding H_2S to syngas improves the selectivities of alkenes and WGS, while decreasing the methane selectivity. However, since the catalyst is practically deactivated at this point, little focus and reliability should be put to the presented selectivities. Other products formed include hydrocarbons with more than 13 carbon atoms and other oxygenated products than methanol, ethanol and propanol.

8.2.3 Low α –Fe-catalyst

All reaction tests conducted with the low α-Fe catalyst are presented in Table 26.

Table 26. Low α-Fe catalyst reaction tests conducted in plug flow reactor.

Stage	T.o.S.	Test	T_{meas}	$\dot{V}_{RG}$	$\dot{V}_{PG}$	c_{H2S}	WHSV		
	[h]	number	°C	[nl/h]	[nl/h]	[ppm]	CO_2 [g/h·g_{cat}]	H_2 [g/h·g_{cat}]	H_2S [g/h·g_{cat}]
Initial	4	31	192.1	15.0	0.0	0.0	2.8	0.4	0
		32	192.1	15.0	0.0	0.0	2.8	0.4	0
		37	192.1	15.0	0.0	0.0	2.8	0.4	0
1st poisoning	8	39	191.8	11.6	3.4	1.1	2.2	0.3	$8.5 \cdot 10^{-9}$
		40	192	11.6	3.4	1.1	2.2	0.3	$8.5 \cdot 10^{-9}$
		41	192	11.6	3.4	1.1	2.2	0.3	$8.5 \cdot 10^{-9}$
		42	192	11.6	3.4	1.1	2.2	0.3	$8.5 \cdot 10^{-9}$
1st recovery	64	44	192.1	15.0	0.0	0.0	2.8	0.4	0
		45	192.1	15.0	0.0	0.0	2.8	0.4	0
		46	192.1	15.0	0.0	0.0	2.8	0.4	0
		47	192.2	15.0	0.0	0.0	2.8	0.4	0
2nd poisoning	64	59	191.2	7.3	12.8	63.2	1.4	0.2	$6.6 \cdot 10^{-7}$
		60	191.1	7.3	12.8	63.2	1.4	0.2	$6.6 \cdot 10^{-7}$
		61	191	7.3	12.8	63.2	1.4	0.2	$6.6 \cdot 10^{-7}$
		62	191	7.3	12.8	63.2	1.4	0.2	$6.6 \cdot 10^{-7}$
		63	191	7.3	12.8	63.2	1.4	0.2	$6.6 \cdot 10^{-7}$
		64	191.1	7.3	12.8	63.2	1.4	0.2	$6.6 \cdot 10^{-7}$
		65	191.1	7.3	12.8	63.2	1.4	0.2	$6.6 \cdot 10^{-7}$
		66	191.1	7.3	12.8	63.2	1.4	0.2	$6.6 \cdot 10^{-7}$
		67	191.2	7.3	12.8	63.2	1.4	0.2	$6.6 \cdot 10^{-7}$
2nd recovery	24	69	191	15.0	0.0	0.0	2.8	0.4	0
		70	191.6	15.0	0.0	0.0	2.8	0.4	0
		71	191.9	15.0	0.0	0.0	2.8	0.4	0
		72	192	15.0	0.0	0.0	2.8	0.4	0
		73	192	15.0	0.0	0.0	2.8	0.4	0
		74	192	15.0	0.0	0.0	2.8	0.4	0
		76	192	15.0	0.0	0.0	2.8	0.4	0
		77	192.1	15.0	0.0	0.0	2.8	0.4	0
		78	192.2	15.0	0.0	0.0	2.8	0.4	0
		79	192	15.0	0.0	0.0	2.8	0.4	0
		80	192	15.0	0.0	0.0	2.8	0.4	0

The reaction conditions for the reaction tests of the low α-Fe-catalyst were set point 190 °C and p=20 bar. The first poisoning was performed by poisoning gas 1, consisting of 4.8 ppm H_2S. Poisoning gas 2 (99.2 ppm H_2S) was used for the second poisoning stage. Thus, the H_2S level of the first poisoning was 1.1 ppm ($WHSV_{H2S}=8.5 \cdot 10^{-9}$ $g_{H2S}/h \cdot g_{cat}$), and 63.2 ppm H_2S ($WHSV_{H2S}=6.6 \cdot 10^{-7}$ $g_{H2S}/h \cdot g_{cat}$) for the second poisoning.

Table 27 presents the conversion and yields of products for low α-Fe catalyst. Selectivites of products are shown in Table 28.

Table 27. Conversion and yields of reaction tests with low α-Fe-catalyst at T=190 °C and p=20 bar.

	Conversion [%]	Yield [%]						
	CO_2	CO	C1+C2	C3+C4	C5-C12	MeOH	EtOH	PrOH
Reactant gas	1.70	0	0.623	0.387	0.396	0.027	0.083	0.015
1st poisoning	1.41	0	0.507	0.327	0.328	0.020	0.072	0.012
1st recovery	1.71	0	0.628	0.392	0.408	0.027	0.084	0.015
2nd poisoning	0.06	0	0.006	0.004	0.006	0	0.002	0
2nd recovery	0.03	0	0.013	0.006	0.007	0.001	0.001	0

Table 28. Selectivities of formed products in reaction tests with low α-Fe-catalyst at T=190 °C and p=20 bar.

Selectivity [%]	CO	C1+C2	C3+C4	C5-C12	MeOH	EtOH	PrOH	Others
Reactant gas	0	36.6	22.7	23.3	2.3	4.9	0.9	9.1
1st poisoning	0	35.9	23.2	23.2	2.5	5.1	0.9	9.5
1st recovery	0	36.7	22.9	23.8	2.2	4.9	0.9	8.4
2nd poisoning	0	9.4	5.9	9.9	3.4	2.9	0.3	68.0
2nd recovery	0	40.4	19.1	21.5	3.1	3.8	0.6	12.6

Figure 25 illustrates the change in conversion and selectivities of products for low α-Fe catalyst.

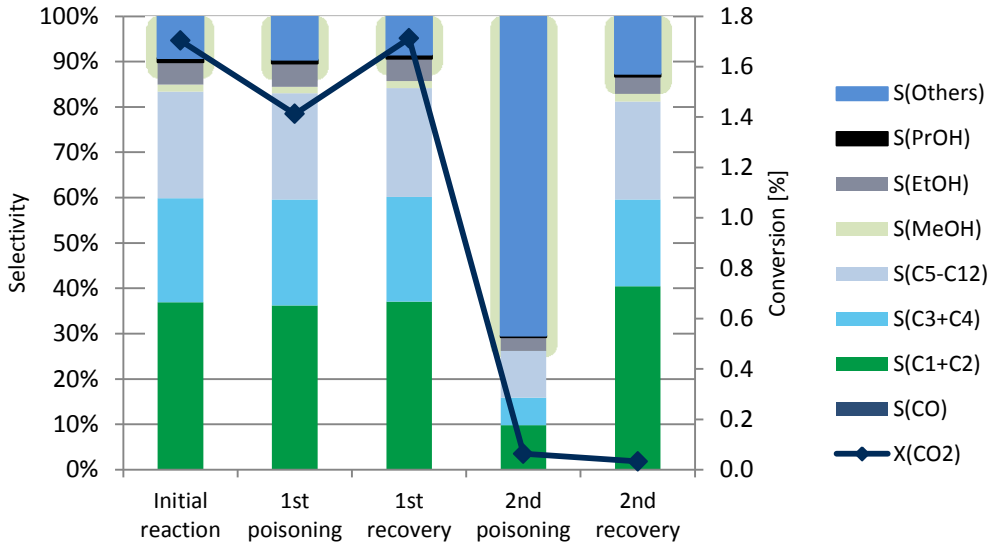

Figure 25. Change in conversion and selectivities of products during H_2S poisoning of low α-Fe-catalyst. The H_2S poisoning levels were 1.07 ppm and 63.2 ppm. "Others" refers to C13+ and all oxygenates except for methanol, ethanol and propanol. Reaction conditions were T=190 °C at 20 bar.

When exposed to 1.1 ppm H_2S (i.e. 1st poisoning), the conversion for low α-Fe catalyst dropped slightly. However, the catalyst made a full recovery from the poisoning. During the second poisoning the conversion dropped to only 0.06% and the catalyst did not recover from the second poisoning. As demonstrated by Figure 25, the selectivities of products remain constant for all stages except for 2nd poisoning by 63.2 ppm H_2S, which is due to the low amount of products formed. Unfortunately, the difference in poisoning levels (i.e. 1 ppm and 60 ppm) is very large, which is why it is difficult to draw conclusions about the catalyst's resistance of H_2S. Furthermore, the conversion of the low α-Fe catalyst is significantly lower than for other catalysts studied. Hence, it would have been better to increase either temperature or pressure in the beginning of the experiments, to obtain a higher initial conversion.

The catalyst produced mainly hydrocarbons, methane being the main product with selectivity around 24% for all stages except for 2nd poisoning. Since the selectivity remained quite constant, it can be assumed that the poison deactivated some sites completely while other sites remained unaffected. This supports several studies (Barthomolomew & Bowman 1985; Anderson et al. 1965), which suggest that H_2S have no impact on the selectivity of products.

Ma et al. (2016) studied the effect of H_2S on a similar catalyst (100Fe/5.1Si/2.0Cu/3.0K) as the one discussed above. The safe limit of H_2S in syngas was then concluded to be 50 ppb for zero deactivation. The low α-Fe catalyst tested made a full recovery from 1.1 ppm, i.e. over double the safe limit proposed by Ma et al. (2016). However, that experiment of Ma et al. was conducted for a longer time, which may have led to the lower H_2S limit than shown in this experiment. Thus, it would have been interesting to test how the catalyst would behave if exposed to 1.1 ppm more than once.

8.2.4 Conclusion of reaction experiments

The Fe-based catalysts appeared to be more sensitive to H_2S than the Cu catalyst tested. The conversions of the reaction tests with both Fe-based catalysts dropped completely at the higher poisoning by 60 ppm H_2S and the catalysts did not recover from the poisoning, while the Cu catalyst showed great resistance to H_2S and recovered almost completely. One reason for the great resistance of the Cu catalyst is believed to be the promoter ZnO. However, the low α-Fe catalyst recovered completely from 1 ppm H_2S, but deactivated at the next level tested; 60 ppm. The low α-Fe catalyst was promoted by potassium (K), which some studies (Bartholomew & Bowman 1985) suggest to improve the resistance to H_2S poisoning, possibly as an adsorbent. No poisoning experiment of 30 ppm H_2S of the low α-Fe catalyst was conducted, which unfortunately resulted in a rather large difference between the H_2S levels tested. Therefore, it is difficult to conclude when the catalyst actually deactivated. The other Fe-based catalyst, FeMn, was not promoted and deactivated directly at 30 ppm. Since the recovery test was skipped, it was not possible to control whether the catalyst would have recovered.

When evaluating the results and comparing catalysts, it should be taken into account that other factors, such as reaction temperature, pressure and physical form of catalyst (e.g. pellets or powder) also may have an effect on the poisoning resistance (Ma et al. 2016).

The selectivity of the Cu catalyst remained constant in the initial and recovery stages. During the poisoning stages the CO selectivity increased slightly on the expense of the methanol selectivity. For the Fe-based catalysts the selectivity was highest for lower hydrocarbons. The selectivity of products remained constant for all tests with low α-Fe-catalyst, with the second poisoning being the only exception. The selectivity of products

for the FeMn catalyst changed rather much between the stages, which is believed to be due to the low amount of formed products.

8.3 Error estimation

This section discusses some possible error sources of the experimental work of TPD tests and reaction tests in PFR.

8.3.1 TPD and pulse reactor experiments

One likely error source of the TPD experiments was the heating of the reactor, since the heating system was not insulated. The diameter of the glass tube was 17 mm while the diameter of the aperture in the oven was 24 mm. Thus, a gap of circa 4 mm existed between the reactor and the heating element. This resulted in heat losses. In addition, the glass tube was placed in the oven by adjusting the height, attempting to place the catalyst in the middle of the oven, where the temperature was expected to be highest. This was operated manually, and it is likely that even a small difference in reactor placement led to significant deviations in temperature. The accuracy of the measured temperature was ±0.3 ^{o}C. Moreover, the heating element broke during the experimental work and had to be replaced. The new element appeared to be more efficient, which resulted in higher reaction temperatures for the later executed experiments (i.e. low a-Fe and FeMn catalysts). A table of measured reaction temperatures is presented in Table 16.

Another error source was that the filament of the mass spectrometer burned in the middle of the measurements and had to be replaced. Thus, the low α-Fe catalyst tests were restarted with a new filament, which may contribute to some differences in the functioning of the mass spectrometer. By comparing the mass spectra of other catalysts with the mass spectra of low α-Fe (Appendix 4) a clear difference can be seen.

An error that should be taken into account when evaluating results is the difference in catalyst masses. The catalyst masses varied from 0.73 g to 1.34 g. Thus, analysing the effect of sulphur by comparing the number of sulphur pulses given was not completely accurate.

8.3.2 Reaction tests

The main error source of the reaction tests was believed to be the mass flow controllers, especially the mass flow controllers of the poisoning (MFC-131) and reactant gases (MFC-101). Since the maximum flows of these controllers were rather high, the accuracy of smaller mass flows appeared to be unreliable. Smaller poisoning concentrations than 30 ppm was not possible with Poisoning gas 2, since the minimum constant mass flow reachable with the controller was 3.4 l/h. When attempting to set the flow below 3.4 l/h, the flow stopped completely. In addition, some rather large deviations in N_2 area, which was used as the internal standard and inert, were observed during the tests. This implies inaccuracy with either mass flow controller of the reactant gas (MFC-101 in Figure 7), mass flow controller of N_2 gas (MFC-121 in Figure 7) or the GC.

The heating element is another possible source of error. The temperature indicator inside the reactor was unlikely completely representative to catalyst temperature. In addition, the pressure was set manually and indicated on a rough scale, which likely resulted in small variations in pressure. Yet, temperature and pressure are assumed to be only minor error sources.

Another possible error source is condensation of products in the GC. In the presented calculations it is assumed that no condensation takes place, since the lines to the GC were heated and insulated. However, it should be taken into account when evaluation the results that no condensation is assumed.

9 Conclusion and proposals for future studies

In this thesis, the effect of impurities, i.e. MEA and H_2S, on CO_2 hydrogenation and its catalysts has been studied. The effect of MEA has been scarcely researched and further studies in the field are recommended. In this study the effect of MEA on methane formation was evaluated. Interestingly, the formation of methane increased for an in-house Fe-based catalyst, 100Fe/4.6Si/2Cu/1.4K (composition in atomic ratio), and a commercial Cu-based catalyst (BASF catalyst; 50-75 wt-% CuO and 15-20 wt-% ZnO) during poisoning by MEA. The suggested reason for this is a modification of selectivity of the catalyst. Therefore, further studies analysing the product selectivity would be required to confirm the theory. Both catalysts' methane formation rates returned to the initial level during the recovery phase. The methane formation of the impregnated in-house Fe-based catalyst, 5Fe/5Mn/Al_2O_3 (composition in weight ratio), showed opposing results. During MEA exposure the amount of methane formed from 1 ml CO_2 pulse (corresponding to 61.0 µmol/g_{cat}) declined from 7.3 µmol/g_{cat} to 2.8 µmol/g_{cat}, from which the catalyst did not recover. It is suggested that the reason for the decline in activity is related to loss of active sites. NO_x, which is a minor degradation product of MEA, is proposed to oxidize the active iron carbide sites on the catalyst to inactive magnetite, which has a clear impact since the catalyst only consist of 5 weight-% iron.

The effect of H_2S on CO_2 hydrogenation was also studied by TPD experiments. However, the results were only considered as indicative. The reaction tests in PFR presented more detailed results for the H_2S poisoning, where the selectivity of products could be studied. The Cu-based catalyst maintained its activity surprisingly well during the experiment. The conversion decreased by less than 4% during the 30 ppm and 60 ppm poisonings, and recovered almost completely. The selectivity was slightly modified during the poisoning phases. When H_2S was present, the selectivity of CO was promoted on expense of the selectivity of methanol. It is suggested that this phenomena occurs as the RWGS has a lower Gibbs free energy and thus occur more spontaneous than the methanol synthesis, which is more dependent on the activity of the catalyst. Another explanation would be the significantly lower weight hourly space velocity of CO_2 and H_2 during poisonings, which may trigger secondary reactions such as decomposition of methanol or RWGS. The Fe-based catalysts showed a poorer resistance to sulphur than

the Cu catalyst. The FeMn-based catalyst deactivated at the first poisoning by 30 ppm, and did not recover. The precipitated iron catalyst (low α-Fe catalyst) showed a 0.3% decrease in conversion during the first poisoning by 1.1 ppm H_2S, but recovered completely. The catalyst was deactivated during the second poisoning conducted by 60 ppm and did not recover. The selectivity of the low α-Fe catalyst remained constant during the experiments, which suggest that some active sites on the catalyst deactivated completely, while other remained unaffected. The results considering H_2S poisoning obtained from TPD experiments and PFR reaction experiments were contradictory. Since the TPD experiments were only indicative, more reliability was placed on the PFR reaction experiments. Due to poorly functioning mass flow controllers and lack of suitable poisoning gas, the H_2S poisoning levels were rather high in the PFR reaction experiments. In addition, the poisoning gas consisted of N_2, which altered the weight hourly space velocities and thus the conversion. In future poisoning experiments, it would be recommended to either inject H_2S without affecting the WHSVs or use more precise mass flow controllers that manage to control fairly small mass flows.

10 References

Aaron, D. & Tsouris, C., 2005. Separation of CO2 from Flue Gas: A Review. *Separation Science and Technology*, 40(1), pp.321–348.

Agarwal, P.K., Fitzharris, W.D., Katzer, J.R., Delmon, B. & Froment, G.F., 1980. *Catalyst deactivation*, Elsevier.

Anderson, R.B., Karn, F.S., Kelly, R.E. & Shultz, J.F., 1965. United States Bureau of Mines Reports: Sulfur Poisoning of fixed beds of iron catalysts in the Fischer-Topsch synthesis. In Washington D.C.: United States. Government Printing Office, p. 11.

Anonymous, Monoethanolamine. *National Institute of Standars and Technology*. Available at: http://webbook.nist.gov/cgi/cbook.cgi?ID=C141435&Mask=200 [Accessed September 26, 2016].

Arena, F., Mezzatesta, G., Spadaro, L. & Trunfio, G., 2014. Latest advances in the catalytic hydrogenation of carbon dioxide to methanol/dimethylether. In B. M. Bhanage & M. Arai, eds. *Transformation and Utilization of Carbon Dioxide*. Berlin: Springer-Verlag Berlin Heidelberg, pp. 103–130.

Bartholomew, C.H., 2001. Mechanisms of catalyst deactivation. *Applied Catalysis A: General*, 212(1-2), pp.17–60.

Bartholomew, C.H. & Bowman, R.M., 1985. Sulfur poisoning of cobalt and iron fischer-tropsch catalysts. *Applied Catalysis*, 15(1), pp.59–67.

Barthomolomew, C.. & Bowman, R.M., 1985. Sulfur poisoning of cobalt and iron fischer-tropsch catalysts. *Applied Catalysis*, 15(1), pp.59–67.

Belabbaci, A., Razzouk, A., Mokbel, I., Jose, J. & Negadi, L., 2009. Isothermal vapor-liquid equilibria of (monoethanolamine + water) and (4-methylmorpholine + water) binary systems at several temperatures. *Journal of Chemical and Engineering Data*, 54(8), pp.2312–2316.

Borg, O., Hammer, N., Enger, B.C., Myrstad, R., Lindvg, O.A., Eri, S., Skagseth, T.H. & Rytter, E., 2011. Effect of biomass-derived synthesis gas impurity elements on

cobalt Fischer-Tropsch catalyst performance including in situ sulphur and nitrogen addition. *Journal of Catalysis*, 279(1), pp.163–173.

Bromfield, Coville, Bromfield, T.C. & Coville, N.J., 1997. Surface characterization of sulfided precipitated-iron Fischer-Tropsch catalysts by X-ray photoelectron spectroscopy. *Applied Surface Science*, 119(1-2), pp.19–24.

Bromfield, T.C. & Coville, N.J., 1999. The effect of sulfide ions on a precipitated iron Fischer–Tropsch catalyst. *Applied Catalysis A: General*, 186(1-2), pp.297–307.

Chapel, D.G., Mariz, C.L. & Ernest, J., 1999. Recovery of CO2 from Flue Gases : Commercial Trends. *Canadian Society of Chemical Engineers Annual Meeting*, p.17.

Chi, S. & Rochelle, G., 2002. Oxidative degradation of monoethanolamine. *Industrial & engineering chemistry research*, 41(17), pp.4178–4186.

Chorkendorff, I. & Niemantsverdriet, J.W., 2003. *Concepts of Modern Catalysis and Kinetics*, Weinheim: WILEY-VCH Verlag GmbH & Co. KGaA.

Cormos, C.-C., 2011. Evaluation of power generation schemes based on hydrogen-fueled combined cycle with carbon capture and storage (CCS). *International Journal of Hydrogen Energy*, 36(5), pp.3726–3738.

Cormos, C.-C., 2012. Integrated assessment of IGCC power generation technology with carbon capture and storage (CCS). *Energy*, 42(1), pp.434–445.

Dietz, W.A., 1967. Response Factors for Gas Chromatographic Analyses. *Journal Of Gas Chromatography*, 5(2), pp.68–71.

Dorner, R.W., Hardy, D.R., Williams, F.W. & Willauer, H.D., 2010. Heterogeneous catalytic CO2 conversion to value-added hydrocarbons. *Energy & Environmental Science*, 3(7), pp.884–890.

Drage, T.C., Snape, C.E., Stevens, L. a., Wood, J., Wang, J., Cooper, A.I., Dawson, R., Guo, X., Satterley, C. & Irons, R., 2012. Materials challenges for the development of solid sorbents for post-combustion carbon capture. *Journal of Materials Chemistry*, 22(7), p.2815.

Dry, M.E., 1990. Fischer-Tropsch synthesis over iron catalyst. *Catalysis Letters*, 7,

pp.241–252.

Fennerty, K., Friedmann, S.J., Fowler, M., Hattan, A., Herzog, H., Meldon, J., Newmark, R., Redman, E. & Thompson, J., 2009. Coal Without Carbon - An Investment Plan for Federal Action. *A Clean Air Task Force Report*. Available at: http://www.catf.us/resources/publications/files/Coal_Without_Carbon.pdf [Accessed March 11, 2016].

Feron, P.H.M. & Hendriks, C.A., 2005. CO2 capture process principles and costs. *Oil and Gas Science and Technology*, 60(3), pp.451–459.

Fogler, S., 1999. Catalysis and Catalytic Reactors. In *Elements in Chemical Reaction Engineering*. Upper Saddle River, New Jersey: Prentice Hall PTR, pp. 581–686.

Frilund, C., 2016. *CO2 hydrogenation to methanol, Master's thesis*. Aalto University.

Gasification & Syngas Technologies Council, 2016a. Environmental Benefits of Gasification. Available at: http://www.gasification-syngas.org/applications/environmental-benefits-of-gasification/ [Accessed March 17, 2016].

Gasification & Syngas Technologies Council, 2016b. The Gasification Inustry. Available at: http://www.gasification-syngas.org/resources/the-gasification-industry/ [Accessed March 17, 2016].

Gnanamani, M.K., Hamdeh, H.H., Shafer, W.D., Ma, W., Pendyala, V.R.R., Sparks, D.E. & Davis, B.H., 2012. Fischer-Tropsch Synthesis: Effect of pretreatment conditions on activity and selectivity of Fe catalysts. In *SynFuel 2012, International Symposium on Alternative Clean Synhtetic Fuels, 29th-30th June 2012*. Munich, Germany.

Goff, G.S. & Rochelle, G.T., 2006. Oxidation inhibitors for copper and iron catalyzed degradation of monoethanolamine in CO 2 capture processes. *Industrial and Engineering Chemistry Research*, 45(8), pp.2513–2521.

Gupta, M., Coyle, I., Thambimuthu, K. & Canada, N.R., 2003. CO 2 Capture Technologies and Opportunities in Canada. *"Strawman Document for CO2 capture and Storage (CC&S) Technology Roadmap", 1st Canadian CC&S Technology Roadmap Workshop, 18th-19th September 2003*. Available at: http://www.graz-

cycle.tugraz.at/pdfs/co2_capture_strawman_feb2004.pdf [Accessed March 10, 2016].

Higman, C., 2014. State of the Gasification Industry: Worldwide Gasification Database 2014 Update. *Gasification Technologies Conference, 29th of October 2014*. Available at: http://www.gasification-syngas.org/uploads/downloads/GTC_Database_2014.pdf [Accessed March 29, 2016].

Imran, M., Kumar, D., Kumar, N., Qayyum, A., Saeed, A. & Bhatti, M.S., 2014. Environmental concerns of underground coal gasification. *Renewable and Sustainable Energy Reviews*, 31, pp.600–610.

Jager, B. & Espinoza, R., 1995. Advances in Low-Temperature Fischer-Tropsch Synthesis. *Catalysis Today*, 23(1), pp.17–28.

de Jong, E., Higson, A., Walsh, P. & Wellisch, M., 2012. Bio-based Chemicals: Value added products from Biorefineries. *Report for IAE Bioenergy - Task42*. Available at: http://www.ieabioenergy.com/wp-content/uploads/2013/10/Task-42-Biobased-Chemicals-value-added-products-from-biorefineries.pdf [Accessed March 4, 2016].

Kargari, A. & Takht Ravanchi, M., 2012. Carbon Dioxide: Capturing and Utilization. *Greenhouse Gases - Capturing, Utilization and Reduction*, 1, pp.3–30.

Karn, F.S., Schultz, J.., Kelly, R.E. & R.B., A., 1963. Poisoning of Iron Catalysts by H2S in Synthesis Gas. *ACS Publications*, 2(1), pp.43–47.

Last, G. V & Schmick, M., 2011. Identification and Selection of Major Carbon Dioxide Stream Compositions. *Report prepared for the U.S. Department of Energy*.

Laukka, M., 2013. *Rautakatalyytin perustuva biomassan nesteytysprosessi, Master's thesis*. Aalto University.

Li, B., Duan, Y., Luebke, D. & Morreale, B., 2013. Advances in CO 2 capture technology : A patent review. *Applied Energy*, 102, pp.1439–1447.

Lin, H., Wei, X., Merkel, T.C., Lin, H., Wei, X. & Baker, R., 2010. Power plant post-combustion carbon dioxide capture : an opportunity for membranes. *Journal of*

Membrane Science, 359(2016), pp.126–139.

Liu, H. & Shao, Y., 2010. Predictions of the impurities in the CO2 stream of an oxy-coal combustion plant. *Applied Energy*, 87(10), pp.3162–3170.

Ma, W., Jacobs, G., Kang, J., Sparks, D.E., Gnanamani, M.K., Pendyala, V.R.R., Shafer, W.D., Keogh, R.A., Graham, U.M., Thomas, G.A. & Davis, B.H., 2013. Fischer-Tropsch synthesis. Effect of alkali, bicarbonate and chloride addition on activity and selectivity. *Catalysis Today*, 215, pp.73–79.

Ma, W., Jacobs, G., Sparks, D.E., Shafer, W.D., Hamdeh, H.H., Hopps, S.D., Pendyala, V.R.R., Hu, Y., Xiao, Q. & Davis, B.H., 2015. Effect of ammonia in Syngas on the Fischer-Tropsch Synthesis Performance of a Precipitated Iron Catalyst. *Applied Catalysis A: General*, 326, pp.149–160.

Ma, W., Jacobs, G., Sparks, D.E., Thomas, G.A., Shafer, W.D., Sparks, D.E., Pendyala, V.R.R., Hopps, S.G., Maclennan, A., Hamdeh, H.H., Hu, Y. & Davis, B.H., 2016. Effect of H2S in syngas on the Fischer-Tropsch synthesis performance of a precipitated iron catalyst. *Journal of Catalysis*, 513, pp.127–137.

Ma, W., Jacobs, G., Thomas, G.A., Shafer, W.D., Sparks, D.E., Hamdeh, H.H. & Davis, B.H., 2015. Fischer-Tropsch Synthesis: Effects of Hydrohalic Acids in Syngas on a Precipitated Iron Catalyst. *ACS Catalysis*, 5, pp.3124–3136.

Meisen, A. & Shuai, X., 1997. Research and development issues in CO2 capture. *Energy Conversion and Management*, 38(96), pp.S37–S42.

Oasmaa, A., Monteverde, M. & Di Felice, R., 2010. Report on biofuels for SOFC applications. Available at: http://www.vtt.fi/files/projects/largesofc/large_sofc_biofuels_wp6_public.pdf [Accessed March 4, 2016].

Olivier, Jos, G.J., Janssens-Maenhout, G., Muntean, M. & Peters, J. a. H.W., 2013. Trends in Global CO2 Emissions: 2013 Report. *PBL Netherlands Environmental Assessment Agency*. Available at: http://edgar.jrc.ec.europa.eu/news_docs/pbl-2013-trends-in-global-co2-emissions-2013-report-1148.pdf [Accessed March 4, 2016].

Pendyala, V.R.R., Gnanamani, M.K., Jacobs, G., Ma, W., Shafer, W.D. & Davis, B.H., 2013.

Fischer-Tropsch synthesis: Effect of ammonia impurities in syngas feed over a cobalt/alumina catalyst. *Applied Catalysis A: General*, 468, pp.38–43.

Petersson, A. & Wellinger, A., 2009. Biogas upgrading technologies–developments and innovations. *Report prepared for IEA Bioenergy*. Available at: http://www.iea-biogas.net/files/daten-redaktion/download/publi-task37/upgrading_rz_low_final.pdf [Accessed March 4, 2016].

Porter, R.T.J., Fairweather, M., Pourkashanian, M. & Woolley, R.M., 2015. The range and level of impurities in CO2 streams from different carbon capture sources. *International Journal of Greenhouse Gas Control*, 36, pp.161–174.

Quinn, R., Dahl, T.A. & Toseland, B.A., 2004. An evaluation of synthesis gas contaminants as methanol synthesis catalyst poisons. *Applied Catalysis A: General*, 272(1-2), pp.61–68.

Quinn, R., Mebrahtu, T., Dahl, T.A., Lucrezi, F.A. & Toseland, B.A., 2004. The role of arsine in the deactivation of methanol synthesis catalysts. *Applied Catalysis A: General*, 264(1), pp.103–109.

Rasi, S., Veijanen, A. & Rintala, J., 2007. Trace compounds of biogas from different biogas production plants. *Energy*, 32(8), pp.1375–1380.

Reinikainen, M., 2016. *Preparation of 5Fe-5Mn-Al2O3-catalyst. Working paper. Impregnated Fe-Mn-Al2O3-catalyst*, VTT Technical Research Center in Finland, Espoo.

Riet, M. van der, 2008. Underground coal gasification. *Proceedings of the SAIEE Generation Conference*. Available at: http://www.rmwg.co.za/Presentations/power_converence/09_Underground_Coal_Gasification_Mark_Van_Der_Riet.pdf [Accessed March 17, 2016].

Rochelle, G.T., 2009. Amine scrubbing for CO2 capture. *Science*, 325, pp.1652–1654.

Romano, M.C., Anantharaman, R., Arasto, A., Ozcan, D.C., Ahn, H., Dijkstra, J.W., Carbo, M. & Boavida, D., 2013. Application of advanced technologies for CO2 capture from industrial sources. *Energy Procedia*, 37, pp.7176–7185.

Saib, A.M., Moodley, D.J., Ciobîc, I.M., Hauman, M.M., Sigwebela, B.H., Weststrate, C.J., Niemantsverdriet, J.W. & Van De Loosdrecht, J., 2010. Fundamental understanding of deactivation and regeneration of cobalt Fischer-Tropsch synthesis catalysts. *Catalysis Today*, 154(3-4), pp.271–282.

Sanders, E.S., 1988. Penetrant-induced plasticization and gas permeation in glassy polymers. *Journal of Membrane Science*, 37(November 1986), pp.63–80.

Sass, B., Monzyk, B., Ricci, S., Gupta, A., Hindin, B. & Gupta, N., 2005. Impact of SOx and NOx in Flue Gas on CO2 separation, compression, and pipeline transmission. In *Carbon Dioxide Capture in for Storage in Deep Geologic Formations*. Oxford: Elsevier, Ltd, pp. 955–981.

Scholes, C. a., Kentish, S.E. & Stevens, G.W., 2009. Effects of Minor Components in Carbon Dioxide Capture Using Polymeric Gas Separation Membranes. *Separation & Purification Reviews*, 38(1), pp.1–44.

Sexton, A.J. & Rochelle, G.T., 2011. Reaction products from the oxidative degradation of monoethanolamine. *Industrial and Engineering Chemistry Research*, 50(2), pp.667–673.

Shultz, J.F., Hofer, L.J.E., Karn, F.S. & Anderson, R.B., 1962. Studies of the fischer-tropsch synthesis. prepoisonikg of iron catalysts by sulfur compounds. *The journal of Physical Chemistry*, 2717(2), pp.501–506.

Sircar, S., 2002. Pressure swing adsorption. *Industrial & engineering chemistry research*, 41, pp.1389–1392.

Sjostrom, S. & Krutka, H., 2010. Evaluation of solid sorbents as a retrofit technology for CO2 capture. *Fuel*, 89(6), pp.1298–1306.

Songolzadeh, M., Soleimani, M., Ravanchi, T.M. & Songolzadeh, R., 2014. Carbon Dioxide Separation from Flue Gases: A technologyical Review Emphasizing Reduction in Greenhouse Gas Emissions. *the Scientific World Journal*, 2014, p.34.

Stenger, H. & Satterfleld, C.N., 1985. Effects of Sulfur Poisoning of a Reduced Fused Magnetite Catalyst in the Fischer-Tropsch Synthesis. *Ind. Eng. Chem. Process Des. Dev.*, 24(1977), pp.415–420.

Thiruvenkatachari, R., Su, S., An, H. & Yu, X.X., 2009. Post combustion CO2 capture by carbon fibre monolithic adsorbents. *Progress in Energy and Combustion Science*, 35(5), pp.438–455.

Twigg, M. V & Spencer, M.S., 2003. Deactivation of copper metal catalysts for methanol decomposition, methanol steam reforming and methanol synthesis. *Topics in Catalysis*, 22(3-4), pp.191–203.

Twigg, M. V. & Spencer, M.S., 2001. Deactivation of supported copper metal catalysts for hydrogenation reactions. *Applied Catalysis A: General*, 212(1-2), pp.161–174.

U S Environmental Protection Agency, 2015. Inventory of U . S . Greenhouse Gas Emissions and Sinks: 1990-2013. , p.564. Available at: https://www3.epa.gov/climatechange/Downloads/ghgemissions/US-GHG-Inventory-2015-Main-Text.pdf [Accessed March 17, 2016].

Walspurger, S. & Dijk, H. a. J. Van, 2012. EDGAR CO2 purity: type and quantities of impurities related to CO2 point source and capture technology: a Literature study. , (August), p.48. Available at: http://www.ecn.nl/docs/library/report/2012/e12054.pdf [Accessed March 17, 2016].

Wang, W., Wang, S., Ma, X. & Gong, J., 2011. Recent advances in catalytic hydrogenation of carbon dioxide. *Chemical Society reviews*, 40(7), pp.3703–27.

Wessling, M., Schoeman, S., van der Boomgaard, T. & Smolders, C.A., 1991. Plasticization of gas separation membranes. *Gas Separation & Purification*, 5(4), pp.222–228.

White, C.M., Strazisar, B.R., Granite, E.J., Hoffman, J.S. & Pennline, H.W., 2003. Separation and Capture of CO2 from Large Stationary Sources and Sequestration in Geological Formations. *EM: Air and Waste Management Association's Magazine for Environmental Managers*, 2247(JUNE), pp.29–34.

Xu & Moulijn, J. a, 1996. Mitigation of CO2 by Chemical Conversion: Plausible Chemical Reactions and Promising Products. *Energy & Fuels*, 10(2), pp.305–325.

Xu, G., Liang, F., Yang, Y., Hu, Y., Zhang, K. & Liu, W., 2014. An improved CO2 separation

and purification system based on cryogenic separation and distillation theory. *Energies*, 7(5), pp.3484–3502.

Xu, Y., Isom, L. & Hanna, M.A., 2010. Adding value to carbon dioxide from ethanol fermentations. *Bioresource Technology*, 101(10), pp.3311–3319.

Yeh, J.T., Pennline, H.W. & Resnik, K.P., 2001. Study of CO 2 Absorption and Desorption in a Packed Column. *Energy & Fuels*, 15(2), pp.274–278.

Yoshihara, J. & Campbell, C.T., 1996. Methanol Synthesis and Reverse Water–Gas Shift Kinetics over Cu(110) Model Catalysts: Structural Sensitivity. *Journal of Catalysis*, 161(2), pp.776–782.

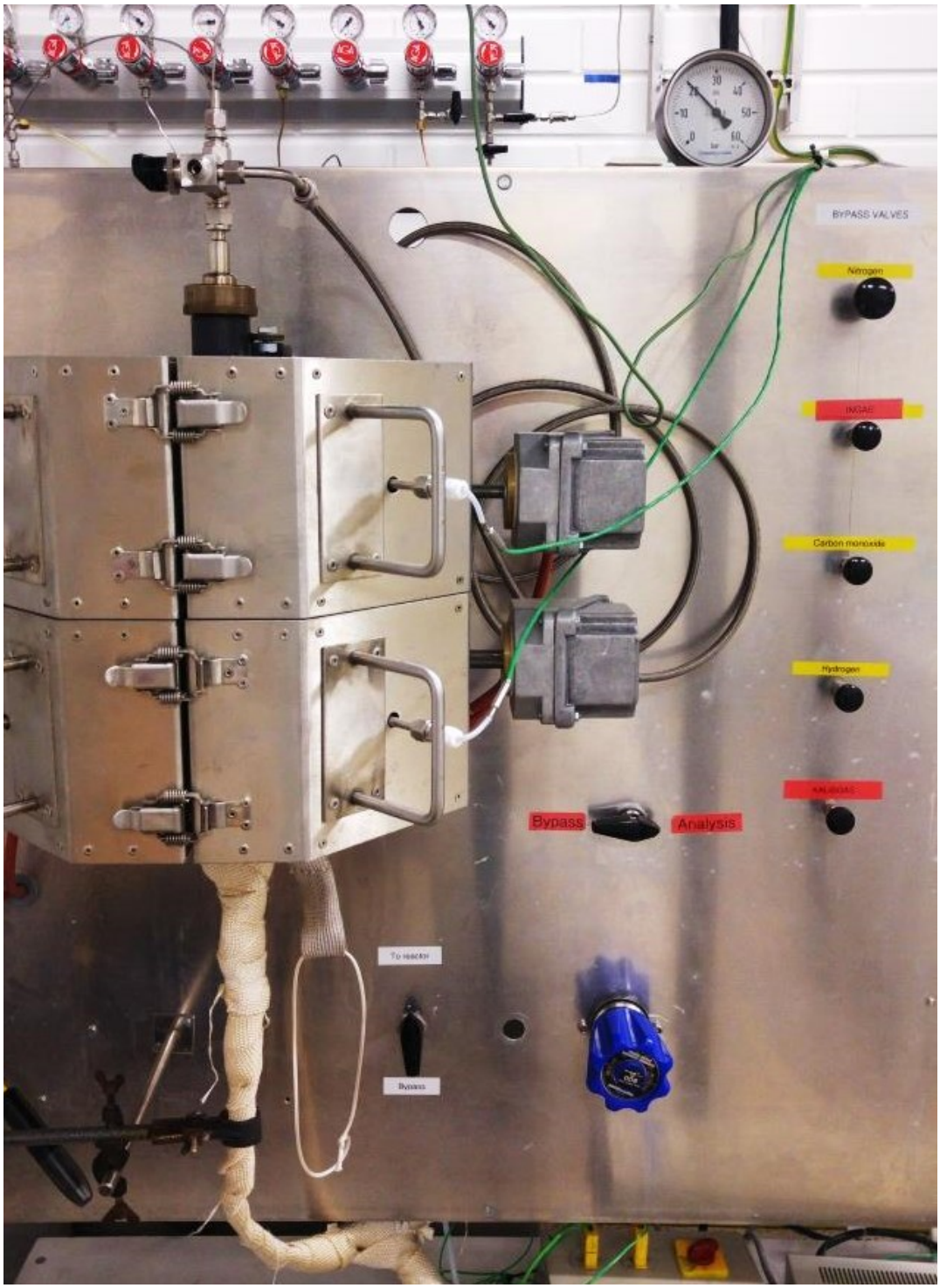

Figure 1. Picture of the experimental setup of the plug flow reactor.

Impregnated Fe-Mn-Al2O3-catalyst

26.4.2016

Preparation of 5Fe-5Mn-Al2O3-catalyst

What is needed:
2-neck flask 200-250 ml
Vacuum unit
Measure cylinders 10 ml
Magnetic stirrer
Stopcock to the bigger joint
Dropping funnel for the smaller joint
”Bird’s nest heater”
Rotary vacuum evaporator
Calcination oven and tube
Puralox SCFa 200-alumina
Mn(N) and Fe(N)-hydrates

The recipe below can me multiplied to suit the need.

1. Put 20 g Puralox SCFa-200 –support in the flask. Attach stopcock and dropping funnel. Heat in a bird’s nest at 150°C for 2 h under vacuum. Increase vacuum slowly in the beginning.
2. While the support is drying prepare impregnation mixtures:
   - Weigh 7,36 g $Fe(NO_3)_3 \cdot 9H_2O$ in a measure cylinder and add water until final volume is 5 ml. Insert a magnet and stir.
   - Weigh 4,56 g Mn(N)- $4H_2O$ in a measure cylinder and add water until final volume is 5 ml. Insert a magnet and stir.
3. Cool down leaving vacuum in the flask.
4. Mix the two solutions in the dropping funnel and impregnate the solution on the support with a fast opening of the stopcock.
   Tap the flask for 10 min. Leave for overnight.
5. Dry next day in a rotary vacuum evaporator equipped with a special joint (see figure below). Water bath at 80°C increase vacuum slowly. Continue until dry.
6. Calcine in flowing air at 400°C. Use rotary calcinator.

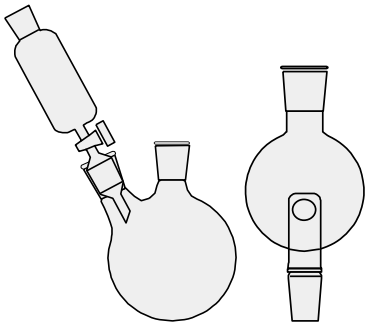

Sample information		**15 l/h INGAS, 190 C (192,2 C), 20 bar**									
CO Conversion, %		**#DIV/0!**		C:\Chem32\1\Data\FAH01\SIG1000047.D			Sampling time			6/13/2016 8:13	
CO2 Conversion, %		**25.76**		C:\HPCHEM\1\DATA\FT-02\SIG20034.D			TOS/h			1020824:13	
H2 Conversion, %		**25.48**									
			Response	Amount	**Mol%**	Mw	Weight	**Weight-%**	Carbon	Mol/h	**Product**
	0		factor	mol/h		g/mol	g/h		Atoms	Carbon	**Mol-% C**
H2	11223.83		11.158	3.55E-01		2.0158	7.16E-01				
N2	94.97985		1	3.35E-02		28.01	9.39E-01				
CO	0		0.94779	0.00E+00	**0.00**	28.0104	0.00E+00	**0.00**	1	0.00E+00	**0.00**
CH4	1		3.23208	2.60E-04	**38.51**	16.0426	4.17E-03	**11.66**	1	2.60E-04	**13.11**
CO2	338.463		1.05626	0.00E+00		44.0098	0.00E+00				
C2H2	0		1.681	0.00E+00	**0.00**	26.0378	0.00E+00	**0.00**	2	0.00E+00	**0.00**
C2H4	0		2.67	0.00E+00	**0.00**	28.0536	0.00E+00	**0.00**	2	0.00E+00	**0.00**
C2H6	0		2.315	0.00E+00	**0.00**	30.0694	0.00E+00	**0.00**	2	0.00E+00	**0.00**
C1+C2	155.0884		0.97	-	**-**	-	1.52E-02	**42.62**	1	-	
C2(b)	0		0.97	-	**-**	28.0536	0.00E+00	**0.00**	2	-	
C3	56.16381		0.98	1.24E-04	**18.36**	44.0962	5.46E-03	**15.28**	2	2.48E-04	**12.50**
n-C4+1-C4=	12.81051		1.07	2.03E-05	**3.01**	56.1072	1.14E-03	**3.19**	4	8.13E-05	**4.11**
C4=(b)	21.45707		0.98	3.72E-05	**5.51**	56.1072	2.09E-03	**5.84**	4	1.49E-04	**7.51**
C4=(d)	0.786025		1.02	1.31E-06	**0.19**	56.1072	7.34E-05	**0.21**	4	5.23E-06	**0.26**
n-C5	1.6848		1.04	2.14E-06	**0.32**	72.1498	1.54E-04	**0.43**	5	1.07E-05	**0.54**
C5=(a)	10.84671		0.99	1.49E-05	**2.21**	70.134	1.04E-03	**2.92**	5	7.44E-05	**3.76**
C5=(b)	0.396553		0.99	5.44E-07	**0.08**	70.134	3.82E-05	**0.11**	5	2.72E-06	**0.14**
AcH	0.387099		0.35	2.39E-06	**0.35**	44.053	1.05E-04	**0.29**	2	4.78E-06	**0.24**
2 Me-C5	0.389274		1.03	4.18E-07	**0.06**	86.1766	3.60E-05	**0.10**	6	2.51E-06	**0.13**
3 Me-C5	0.294502		1.03	3.16E-07	**0.05**	86.1766	2.72E-05	**0.08**	6	1.90E-06	**0.10**
n-C6	9.062357		1.03	9.73E-06	**1.44**	86.1766	8.38E-04	**2.35**	6	5.84E-05	**2.95**
C6=(a)	8.401179		0.99	9.61E-06	**1.42**	84.1608	8.09E-04	**2.26**	6	5.76E-05	**2.91**
C6=(b)	0.295954		0.99	3.38E-07	**0.05**	84.1608	2.85E-05	**0.08**	6	2.03E-06	**0.10**
C6=(c)	0.323743		0.99	3.70E-07	**0.05**	84.1608	3.12E-05	**0.09**	6	2.22E-06	**0.11**
2 Me-C6	0.192462		1	1.83E-07	**0.03**	100.2034	1.83E-05	**0.05**	7	1.28E-06	**0.06**
3 Me-C6	0.317703		1	3.02E-07	**0.04**	100.2034	3.03E-05	**0.08**	7	2.11E-06	**0.11**
n-C7	7.994		1	7.60E-06	**1.13**	100.2034	7.62E-04	**2.13**	7	5.32E-05	**2.69**
Acetone	0		0.49	0.00E+00	**0.00**	98.1876	0.00E+00	**0.00**	3	0.00E+00	**0.00**
C7=(a)	6.651766		1	6.45E-06	**0.96**	98.1876	6.34E-04	**1.77**	7	4.52E-05	**2.28**
Me-C7(a)	0.172808		1	1.44E-07	**0.02**	114.2302	1.65E-05	**0.05**	8	1.15E-06	**0.06**
Me-C7(b)	0.15202		1	1.27E-07	**0.02**	114.2302	1.45E-05	**0.04**	8	1.01E-06	**0.05**
MeOH	3.160394		0.23	4.09E-05	**6.06**	32.042	1.31E-03	**3.66**	1	4.09E-05	**2.06**
n-C8	7.252538		1.03	5.87E-06	**0.87**	114.2302	6.71E-04	**1.88**	8	4.70E-05	**2.37**
C8=(a)	4.92955		0.97	4.31E-06	**0.64**	112.2144	4.84E-04	**1.35**	8	3.45E-05	**1.74**
EtOH	14.73548		0.46	6.62E-05	**9.82**	46.0688	3.05E-03	**8.54**	2	1.32E-04	**6.69**
C8=(b)	0.531245		1.03	4.38E-07	**0.06**	112.2144	4.91E-05	**0.14**	8	3.50E-06	**0.18**
C8=(c)	0		1.03	0.00E+00	**0.00**	112.2144	0.00E+00	**0.00**	8	0.00E+00	**0.00**
n-C9	7.050712		0.98	5.34E-06	**0.79**	128.257	6.85E-04	**1.92**	9	4.81E-05	**2.43**
C9=(a)	3.771634		1.02	2.79E-06	**0.41**	126.2412	3.52E-04	**0.99**	9	2.51E-05	**1.27**
C9=(b)	0.423046		1.02	3.13E-07	**0.05**	126.2412	3.95E-05	**0.11**	9	2.82E-06	**0.14**
PrOH	2.998482		0.6	7.92E-06	**1.17**	60.0956	4.76E-04	**1.33**	3	2.38E-05	**1.20**
C9=(c)	0		1.02	0.00E+00	**0.00**	126.2412	0.00E+00	**0.00**	9	0.00E+00	**0.00**
n-C10	6.785128		0.99	4.59E-06	**0.68**	142.2838	6.53E-04	**1.83**	10	4.59E-05	**2.32**
C10=(a)	2.884566		1.01	1.94E-06	**0.29**	140.268	2.72E-04	**0.76**	10	1.94E-05	**0.98**
C10=(b)	0.590187		1.01	3.97E-07	**0.06**	140.268	5.57E-05	**0.16**	10	3.97E-06	**0.20**
BuOH	1.94525		0.66	3.79E-06	**0.56**	74.1224	2.81E-04	**0.79**	4	1.52E-05	**0.77**
C10=(c)	0		1.01	0.00E+00	**0.00**	140.268	0.00E+00	**0.00**	10	0.00E+00	**0.00**
C10=(d)	0		1.01	0.00E+00	**0.00**	140.268	0.00E+00	**0.00**	10	0.00E+00	**0.00**
n-C11	6.418766		0.99	3.95E-06	**0.59**	156.3106	6.18E-04	**1.73**	11	4.35E-05	**2.19**
C11=	2.093858		0.99	1.31E-06	**0.19**	154.2948	2.02E-04	**0.56**	11	1.44E-05	**0.73**
C5-OH	2.144549		0.71	3.26E-06	**0.48**	88.1492	2.88E-04	**0.81**	5	1.63E-05	**0.82**
n-C12	6.05127		1	3.38E-06	**0.50**	170.3374	5.77E-04	**1.61**	12	4.06E-05	**2.05**
C12=	1.350209		1	7.64E-07	**0.11**	168.3216	1.29E-04	**0.36**	12	9.17E-06	**0.46**
C6-OH	1.187706		0.74	1.28E-06	**0.19**	119.066	1.53E-04	**0.43**	6	7.71E-06	**0.39**
n-C13	5.615725		1	1.47E-06	**0.22**	364.13	5.35E-04	**1.50**	13	1.91E-05	**0.96**
HOAc	0		0.24	0.00E+00	**0.00**	182.3484	0.00E+00	**0.00**	2	0.00E+00	**0.00**
C13=	0.865415		1	4.52E-07	**0.07**	182.3484	8.25E-05	**0.23**	13	5.88E-06	**0.30**
n-C14	5.123693		1	2.46E-06	**0.36**	198.391	4.88E-04	**1.37**	14	3.44E-05	**1.74**
C-14=	0.559225		1	2.71E-07	**0.04**	196.3752	5.33E-05	**0.15**	14	3.80E-06	**0.19**
Other	34.78771		1				3.31E-03	**9.27**			
C15-C25(calc)				1.30E-05	**1.93**		3.41E-03	**9.53**		2.79E-04	**14.10**
Total	417.1251			6.74E-04	**100.00**		3.57E-02	**100.00**		1.98E-03	**100.00**
				Amount	**Mol%**		Weight	**Weight-%**		Mol	**Product**
				mol/h			g/h			Carbon	**Mol-% C**

Figure 1. The image presents the first sheet of the Excel template, which was used for calculations of FT products in reaction tests.

Sample information	0 15 l/h INGAS, 190 C (192,2 C), 20 bar	<=Tr <=Rt

File information	TCD	FID
File name	C:\Chem32\1\Data\FAH01\SIG1000047.D	C:\HPCHEM\1\DATA\FT-02\SIG20034.D

X (CO)	#DIV/0!	X(CO2)	25.76	X(H2)	25.48

Name	Area	Mol-%	Weight-%
H2	0.00		
N2	94.98		
CO	0.00	0.0	0.0
CH4	1.00	38.5	11.7
CO2			
C2H2	0.00	0.0	0.0
C2H4	0.00	0.0	0.0
C2H6	0.00	0.0	0.0
C1+C2	155.09	-	42.6
C2(b)	0.00	-	0.0
C3	56.16	18.36	15.3
n-C4+1-C4=	12.81	3.01	3.2
C4=	22.24	5.71	6.0
n-C5	1.68	0.32	0.4
C5=	11.24	2.29	3.0
i-C6	0.68	0.11	0.2
n-C6	9.06	1.44	2.3
C6=	9.02	1.53	2.4
i-C7	0.51	0.07	0.1
n-C7	7.99	1.13	2.1
C7=	6.65	0.96	1.8
i-C8	0.32	0.04	0.1
n-C8	7.25	0.87	1.9
C8=	5.46	0.70	1.5
n-C9	7.05	0.79	1.9
C9=	4.19	0.46	1.1
n-C10	6.79	0.68	1.8
C10=	3.47	0.35	0.9
n-C11	6.42	0.59	1.7
C11=	2.09	0.19	0.6
n-C12	6.05	0.50	1.6
C12=	1.35	0.11	0.4
n-C13	5.62	0.22	1.5
C13=	0.87	0.07	0.2
n-C14	5.12	0.36	1.4
C-14=	0.56	0.04	0.1
C15-25 (calc)		1.9	9.5
Other			9.3
HC-total		81.4	84.2
AcH	0.39	0.4	0.3
Acetone	0.00	0.0	0.0
MeOH	4.93	6.1	3.7
EtOH	14.74	9.8	8.5
PrOH	3.00	1.2	1.3
BuOH	1.95	0.6	0.8
C5-OH	2.14	0.5	0.8
C6-OH	1.19	0.2	0.4
HOAc	0.00	0.0	0.0
Oxy-total		18.6	15.8
Total		100	100

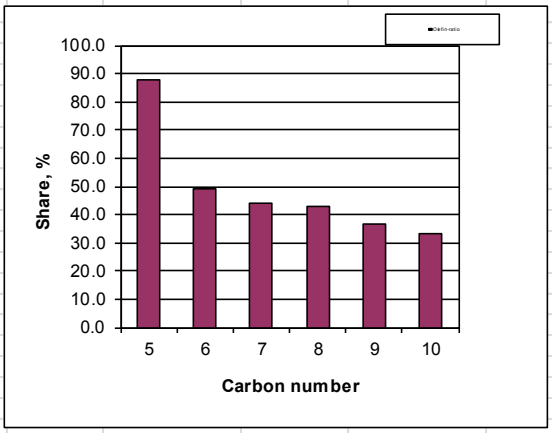

alpha (HC)	0.85
alpha (oxy)	0.39

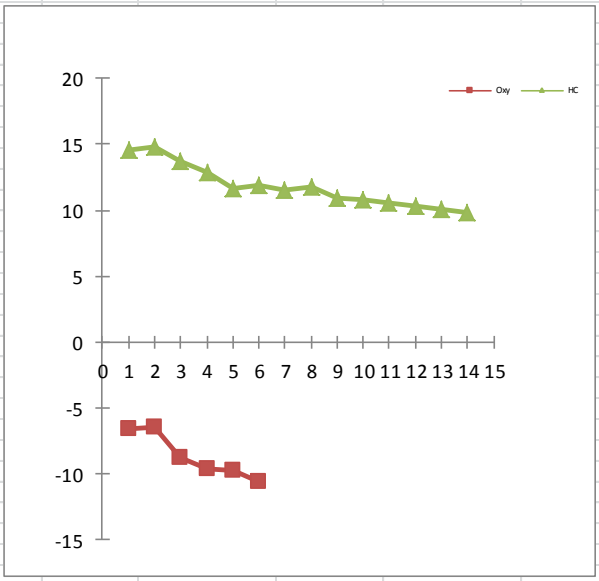

Figure 2. The image presents the second sheet of the Excel template which was used for calculations of FT products in reaction tests.

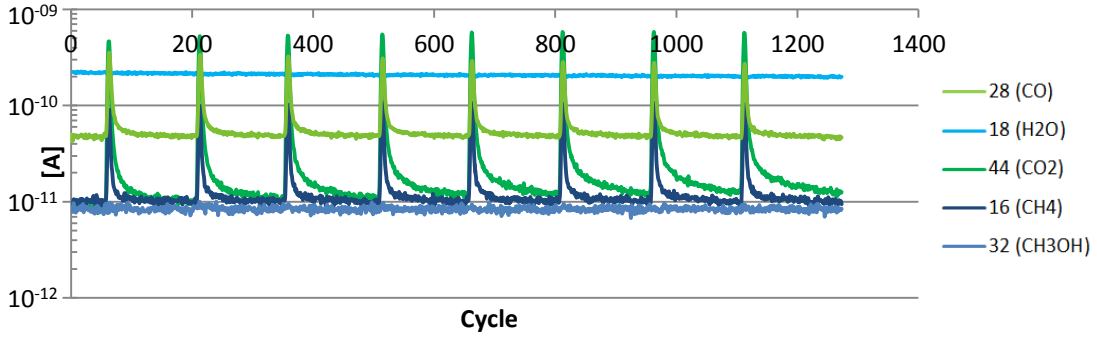

Figure 1. Mass spectrum of CH_4 formation for Cu catalyst before MEA poisoning. Reaction conditions were T=300 °C at atmospheric pressure.

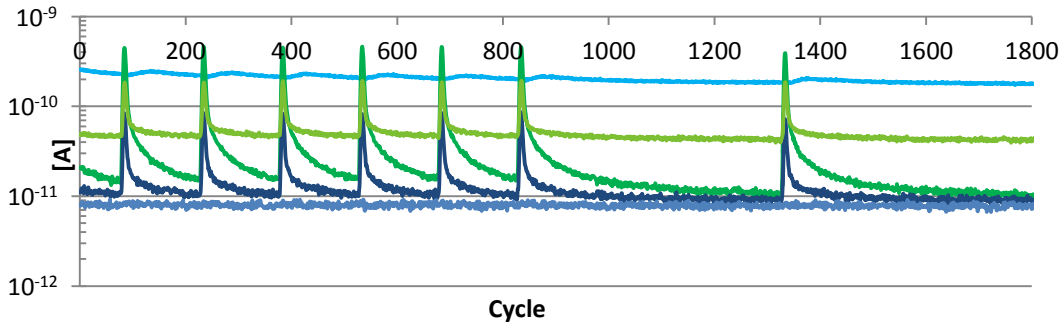

Figure 2. Mass spectrum of CH_4 formation for Cu catalyst during MEA poisoning. Reaction conditions were T=300 °C at atmospheric pressure.

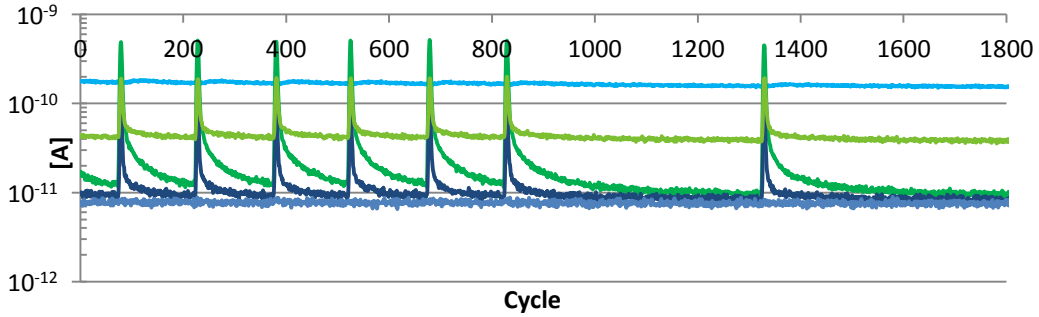

Figure 3. Mass spectrum of CH_4 formation for Cu catalyst after MEA poisoning. Reaction conditions were T=300 °C at atmospheric pressure.

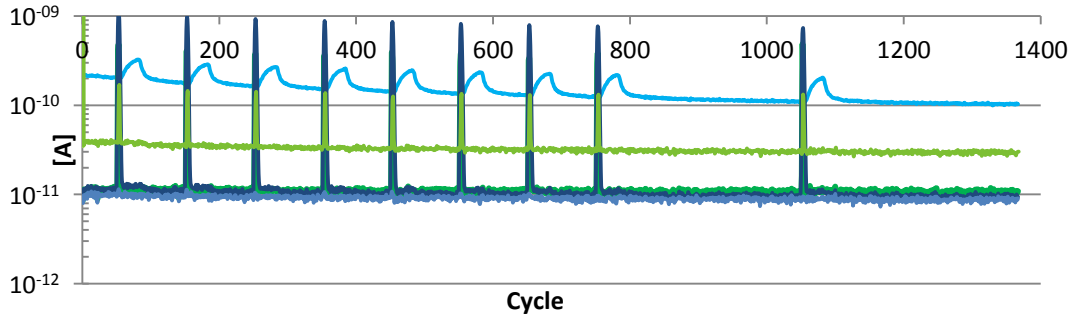

Figure 4. Mass spectrum of CH_4 formation for Ni catalyst before MEA poisoning. Reaction conditions were T=300 °C at atmospheric pressure.

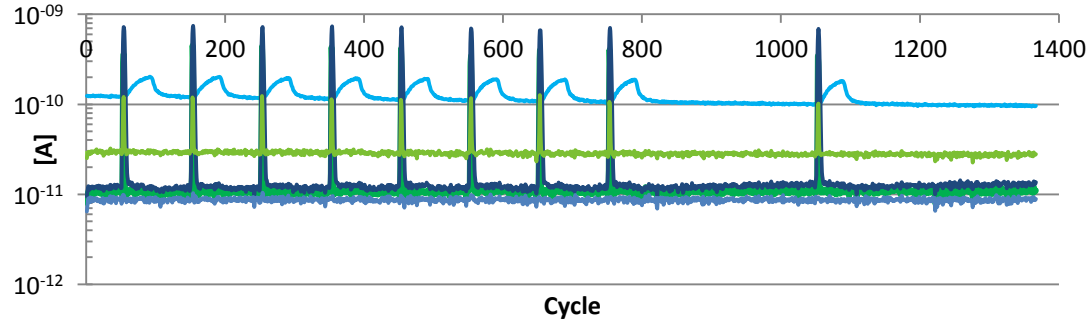

Figure 5. Mass spectrum of CH_4 formation for Ni catalyst during MEA poisoning. Reaction conditions were T=300 °C at atmospheric pressure.

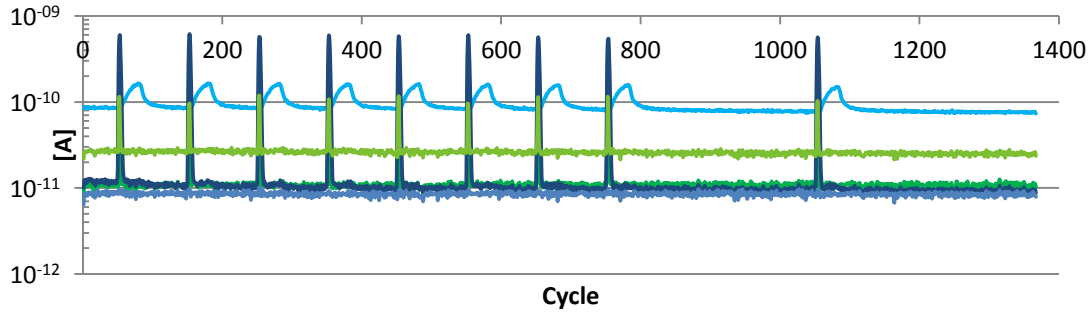

Figure 6. Mass spectrum of CH_4 formation for Ni catalyst after MEA poisoning. Reaction conditions were T=300 °C at atmospheric pressure.

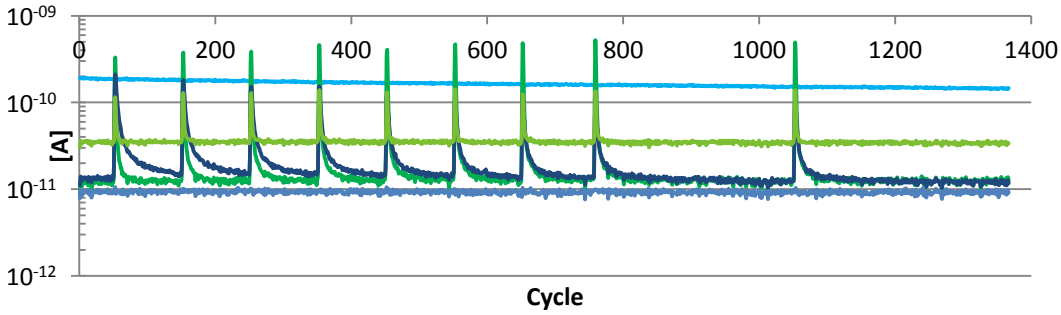

Figure 7. Mass spectrum of CH_4 formation for FeMn catalyst before MEA poisoning. Reaction conditions were T=300 °C at atmospheric pressure.

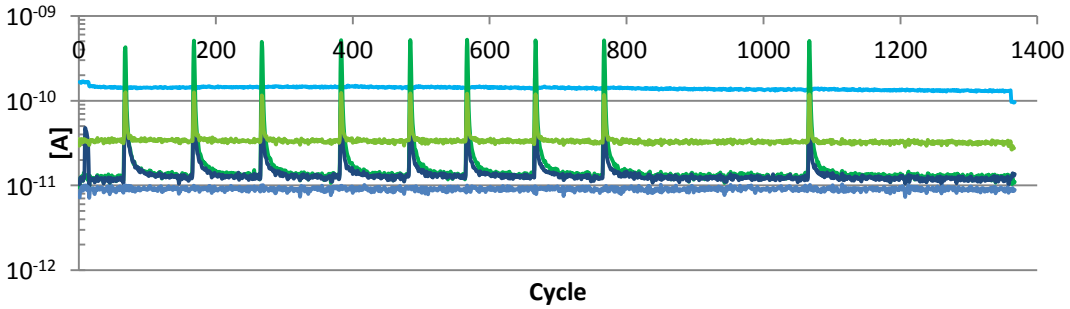

Figure 8. Mass spectrum of CH_4 formation for FeMn catalyst during MEA poisoning. Reaction conditions were T=300 °C at atmospheric pressure.

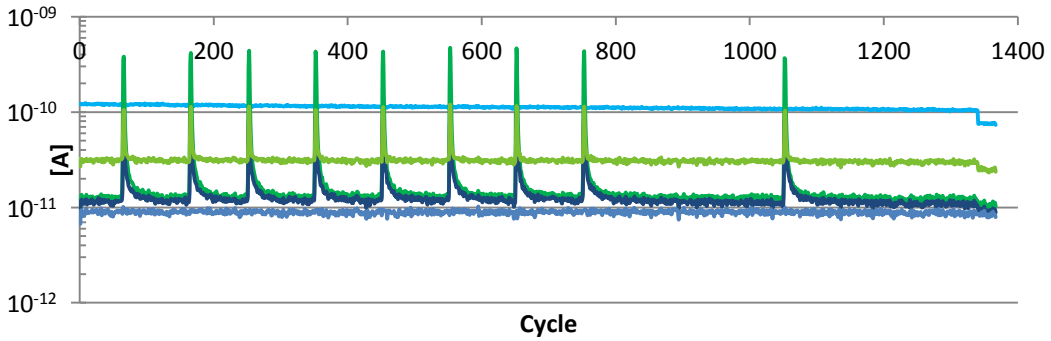

Figure 9. Mass spectrum of CH_4 formation for FeMn catalyst after MEA poisoning. Reaction conditions were T=300 °C at atmospheric pressure.

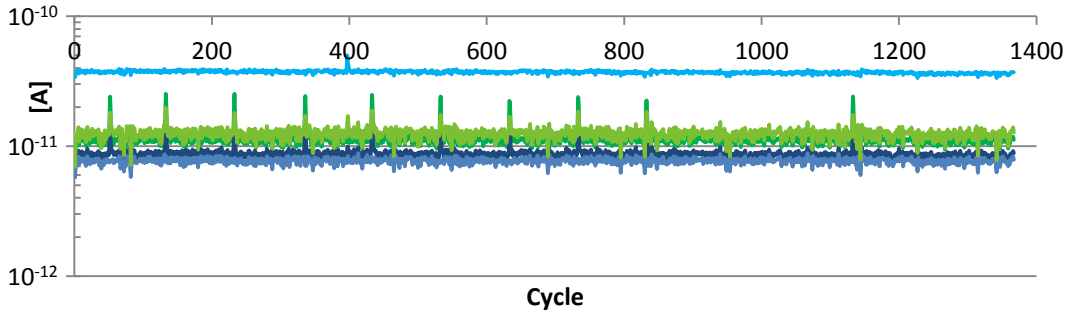

Figure 10. Mass spectrum of CH_4 formation for low α-Fe catalyst before MEA poisoning. Reaction conditions were T=300 °C at atmospheric pressure.

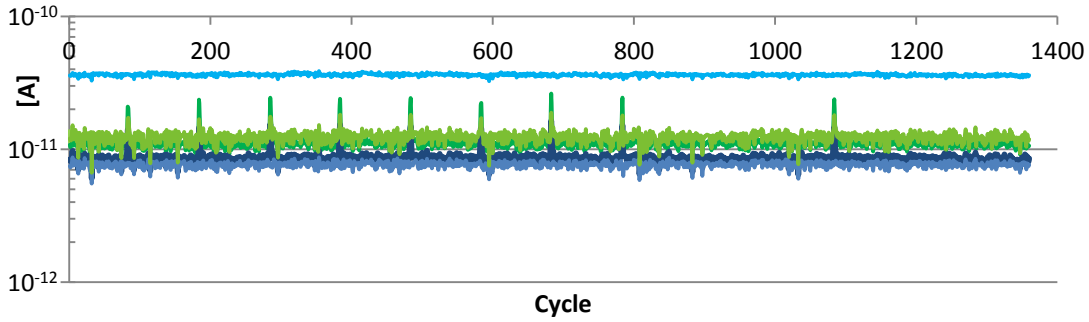

Figure 11. Mass spectrum of CH_4 formation for low α-Fe catalyst during MEA poisoning. Reaction conditions were T=300 °C at atmospheric pressure.

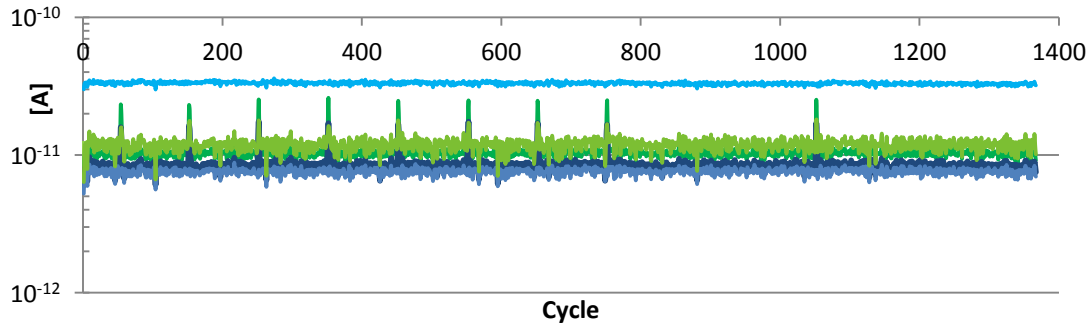

Figure 12. Mass spectrum of CH_4 formation for low α-Fe catalyst after MEA poisoning. Reaction conditions were T=300 °C at atmospheric pressure.